Ca' Foscari
University
of Venice

Corso di Laurea in

Chimica e
tecnologie
sostenibili
"ordinamento D.M.
270/2004"

Tesi di Laurea

# Electrochemical properties of carbon dots and their use as photocatalysts in C-O bond fragmentation

**Supervisor**
Prof. Alvise Perosa

**Assistant supervisor**
Dr. Emanuele Amadio

**Graduand**
Matteo Negrato
Matriculation Number 850575

**Academic Year**
2017 / 2018

# Abstract

Photocatalysis is emerging as a powerful synthetic tool that aims to use solar light to promote organic transformations by mimicking what plants do with photosynthesis. Over the last century, huge efforts have been made by researchers to discover photocatalysts that can be effectively triggered under the irradiation of suitable wavelengths. Among these, very recently carbon dots (CDs) have shown to be promising luminescent bio-based nanomaterials that can be used as sustainable and economical alternatives to the classical metal-based photocatalysts. These nanoparticles have been used in many different applications as nano-optoelectronic devices, sensors and nano-carriers. However, CDs have so far been generally under-explored in photochemical applications and predominantly in conjunction with other photosensitizers, semiconductors and metallic redox mediators to produce hydrogen, and for the conversion of carbon dioxide into small organic molecules.

In this thesis we describe the complete electrochemical characterization of a library of CDs by cyclic voltammetry and we test their efficiency in the photo-reductive cleavage of C-O bonds, by using picolinium esters as model substrates, without using any redox mediators.

The excellent photocatalytic performance, ease of synthesis and the use of renewable sources as precursors make these nanomaterials good candidates for the development of new metal-free and light-enhanced organic synthetic protocols.

# Sommario

Abstract ..... 2
1 Introduction ..... 8
2 What carbon dots are ..... 9
2.1 Nanodot types and nomenclature ..... 9
2.3 Semiconductors, quantum confinement effect, exiton binding energy ..... 10
2.3.1 Semiconductors ..... 11
2.3.2 Exciton binding energy and quantum confinement effect ..... 12
2.4 Synthesis and characterization of CDs ..... 14
2.4.1 Top-down synthesis ..... 14
2.4.2 Bottom-up synthesis ..... 15
2.4.3 Structural Characterization ..... 17
2.5 Optical properties of CDs ..... 20
2.5.1 Absorption ..... 20
2.5.2 Phololuminecesce (PL) and structural dependent mechanisms ..... 21
3 Photochemistry ..... 28
4 Photochemically releasable protecting group (PRPG) ..... 36
4.1 Case study: phenacyl esters ..... 36
4.2 Focus on N-Methyl-4-picolinium esters as model substrates ..... 38
5 Aim of the thesis ..... 39
6 Results and discussion: photocatalysis ..... 40
6.1 C-O bond photocleavage ..... 40
6.1.1 C-O cleavage of octanoic ester ..... 41
6.1.2 C-O cleavage of p-nitrobenzoic ester ..... 51
6.1.3 C-O cleavage of benzoic ester ..... 56
6.1.4 Comparison of substrates ..... 61
6.2 Electrochemical study ..... 63
6.3 Proposed photo-induced C-O bond cleavage mechanism ..... 77
8 Conclusions ..... 80
9 Acknowledgments ..... 81
10 Experimental part ..... 82
10.1 Synthesis and characterization of substrates ..... 82
10.1.1 Reagents ..... 82
10.1.2 Materials and instrumentation ..... 82
10.1.3 Synthesis and characterization of picolinium esters ..... 84

10.1.4 Protection of octanoic acid ..... 86
10.1.5 Protection of p-nitrobenzoic acid ..... 89
10.1.6 Protection of benzoic acid ..... 92
10.1.7 4-(hydroxymethyl)-1-methylpyridin-1-ium iodide synthesis ..... 95
10.1.8 1,4-dimethylpyridin-1-ium iodide synthesis ..... 96
10.2 Photodeprotection procedures ..... 97
10.3 Electrochemical procedures ..... 98
10.3.1 Reagents ..... 98
10.3.2 Instrumentations and electrodes for electrochemical experiments ..... 98
10.3.4 Sample preparation ..... 98
11 References ..... 99
**Appendix A: Supporting information** ..... **Errore. Il segnalibro non è definito.**
Protection of octanoic acid ..... **Errore. Il segnalibro non è definito.**
Spectrum $^{1}$H NMR **1a** ..... **Errore. Il segnalibro non è definito.**
Spectrum $^{13}$C NMR **1a** ..... **Errore. Il segnalibro non è definito.**
Spectrum $^{1}$H NMR **2a** ..... **Errore. Il segnalibro non è definito.**
Spectrum $^{13}$C NMR **2a** ..... **Errore. Il segnalibro non è definito.**
Spectrum GC/MS **2a** ..... **Errore. Il segnalibro non è definito.**
Spectrum $^{1}$H NMR **3a** ..... **Errore. Il segnalibro non è definito.**
Spectrum $^{13}$C NMR **3a** ..... **Errore. Il segnalibro non è definito.**
Spectrum $^{1}$H NMR **4a** ..... **Errore. Il segnalibro non è definito.**
Spectrum $^{13}$C NMR **4a** ..... **Errore. Il segnalibro non è definito.**
Spectrum $^{1}$H NMR **5a** ..... **Errore. Il segnalibro non è definito.**
Spectrum $^{13}$C NMR **5a** ..... **Errore. Il segnalibro non è definito.**
Protection of 4-nitrobenzoic acid ..... **Errore. Il segnalibro non è definito.**
Spectrum $^{1}$H NMR **1b** ..... **Errore. Il segnalibro non è definito.**
Spectrum $^{13}$C NMR **1b** ..... **Errore. Il segnalibro non è definito.**
Spectrum $^{1}$H NMR **2b** ..... **Errore. Il segnalibro non è definito.**
Spectrum $^{13}$C NMR **2b** ..... **Errore. Il segnalibro non è definito.**
Spectrum $^{1}$H NMR **3b** ..... **Errore. Il segnalibro non è definito.**
Spectrum $^{13}$C NMR **3b** ..... **Errore. Il segnalibro non è definito.**
Spectrum $^{1}$H NMR **4b** ..... **Errore. Il segnalibro non è definito.**
Spectrum $^{13}$C NMR **4b** ..... **Errore. Il segnalibro non è definito.**
Spectrum $^{1}$H NMR **5b** ..... **Errore. Il segnalibro non è definito.**

Spectrum $^{13}$C NMR **5b** ..... **Errore. Il segnalibro non è definito.**
Protection of benzoic acid..... **Errore. Il segnalibro non è definito.**
Spectrum $^{1}$H NMR **1c**..... **Errore. Il segnalibro non è definito.**
Spectrum $^{13}$C NMR **1c**..... **Errore. Il segnalibro non è definito.**
Spectrum $^{1}$H NMR **2c**..... **Errore. Il segnalibro non è definito.**
Spectrum $^{13}$C NMR **2c**..... **Errore. Il segnalibro non è definito.**
Spectrum $^{1}$H NMR **3c**..... **Errore. Il segnalibro non è definito.**
Spectrum $^{13}$C NMR **3c**..... **Errore. Il segnalibro non è definito.**
Spectrum $^{1}$H NMR **4c**..... **Errore. Il segnalibro non è definito.**
Spectrum $^{13}$C NMR **4c**..... **Errore. Il segnalibro non è definito.**
Spectrum $^{1}$H NMR **5c**..... **Errore. Il segnalibro non è definito.**
Spectrum $^{13}$C NMR **5c**..... **Errore. Il segnalibro non è definito.**
Common spectra ..... **Errore. Il segnalibro non è definito.**
Spectrum $^{1}$H NMR **6**..... **Errore. Il segnalibro non è definito.**
Spectrum $^{13}$C NMR **6**..... **Errore. Il segnalibro non è definito.**
4-(hydroxymethyl)-1-methylpyridin-1-ium iodide synthesis ..... **Errore. Il segnalibro non è definito.**
Spectrum $^{1}$H NMR **6**..... **Errore. Il segnalibro non è definito.**
Spectrum $^{1}$H NMR **7**..... **Errore. Il segnalibro non è definito.**
Spectrum $^{13}$C NMR **7**..... **Errore. Il segnalibro non è definito.**
1,4-dimethylpyridin-1-ium iodide synthesis ..... **Errore. Il segnalibro non è definito.**
Spectrum $^{1}$H NMR **8**..... **Errore. Il segnalibro non è definito.**
Spectrum $^{1}$H NMR **9**..... **Errore. Il segnalibro non è definito.**
Spectrum $^{13}$C NMR **9**..... **Errore. Il segnalibro non è definito.**
Photocatalysis test ..... **Errore. Il segnalibro non è definito.**
C-O cleavage of octanoic ester..... **Errore. Il segnalibro non è definito.**
Kinetic calculation ..... **Errore. Il segnalibro non è definito.**
Experiment 15.1 ..... **Errore. Il segnalibro non è definito.**
Experiment 15.2 ..... **Errore. Il segnalibro non è definito.**
Experiment 16.1 ..... **Errore. Il segnalibro non è definito.**
Experiment 16.2 ..... **Errore. Il segnalibro non è definito.**
Experiment 17.2 ..... **Errore. Il segnalibro non è definito.**
Experiment 17.3 ..... **Errore. Il segnalibro non è definito.**
Experiment 18.1 ..... **Errore. Il segnalibro non è definito.**
Experiment 18.2 ..... **Errore. Il segnalibro non è definito.**

Experiment 19.1 ..... **Errore. Il segnalibro non è definito.**
Experiment 20.1 ..... **Errore. Il segnalibro non è definito.**
Experiment 21.3 ..... **Errore. Il segnalibro non è definito.**
Experiment 22.1 ..... **Errore. Il segnalibro non è definito.**
Experiment 23.3 ..... **Errore. Il segnalibro non è definito.**
Experiment 24.1 ..... **Errore. Il segnalibro non è definito.**
Experiment 25.1 ..... **Errore. Il segnalibro non è definito.**
Experiment 25.2 ..... **Errore. Il segnalibro non è definito.**
Experiment 25.3 ..... **Errore. Il segnalibro non è definito.**
Experiment 25.4 ..... **Errore. Il segnalibro non è definito.**
Experiment 25.5 ..... **Errore. Il segnalibro non è definito.**
Experiment 27.1 ..... **Errore. Il segnalibro non è definito.**
Experiment 27.2 ..... **Errore. Il segnalibro non è definito.**
Experiment 27.3 ..... **Errore. Il segnalibro non è definito.**
Experiment 27.4 ..... **Errore. Il segnalibro non è definito.**
Experiment 26.2 ..... **Errore. Il segnalibro non è definito.**
Experiment 28.1 ..... **Errore. Il segnalibro non è definito.**
C-O cleavage of p-nitrobenzoic ester ..... **Errore. Il segnalibro non è definito.**
Kinetic calculation ..... **Errore. Il segnalibro non è definito.**
Experiment 29.1 ..... **Errore. Il segnalibro non è definito.**
Experiment 29.2 ..... **Errore. Il segnalibro non è definito.**
Quantification by gas chromatography..... **Errore. Il segnalibro non è definito.**
C-O cleavage of benzoic ester ..... **Errore. Il segnalibro non è definito.**
Kinetic calculation ..... **Errore. Il segnalibro non è definito.**
Experiment 29.3 ..... **Errore. Il segnalibro non è definito.**
Experiment 29.4 ..... **Errore. Il segnalibro non è definito.**
Quantification by gas chromatography..... **Errore. Il segnalibro non è definito.**
**Appendix B: Focus on the key photochemical concepts** ..... **Errore. Il segnalibro non è definito.**
B.1 Photophysical Processes ..... **Errore. Il segnalibro non è definito.**
B.2 Absorbance Maximum for Lowest Energy Absorption $\lambda_{max}$. ..... **Errore. Il segnalibro non è definito.**
B.3 Quantum Yield ..... **Errore. Il segnalibro non è definito.**
B.4 Lifetime of Fluorescence $\tau_f$ and Quantum Yield $\phi_f$: .... **Errore. Il segnalibro non è definito.**
B.5 Quantum Yield of Intersystem Crossing $\phi_{ISC}$ ..... **Errore. Il segnalibro non è definito.**

B.6 Photoinduced electron transfer PET: thermodynamics and electrochemistry concepts ..... **Errore. Il segnalibro non è definito.**

B.7 General schemes for photoredox catalysis..... **Errore. Il segnalibro non è definito.**

B.8 Singlet or Triplet Excited States ..... **Errore. Il segnalibro non è definito.**

B.9 Electron transfer kinetics ..... **Errore. Il segnalibro non è definito.**

**Appendix B: Focus on Electrochemical methods applied to CDs**..... **Errore. Il segnalibro non è definito.**

C.1 Cyclic voltammetry: electrochemical cell..... **Errore. Il segnalibro non è definito.**

C.2 Fermi Level and Absolute Potential ..... **Errore. Il segnalibro non è definito.**

C.3 Reference Electrodes ..... **Errore. Il segnalibro non è definito.**

C.4 Electrode processes ..... **Errore. Il segnalibro non è definito.**

C.5 Standard reduction potential..... **Errore. Il segnalibro non è definito.**

C.6 Nernst Equation ..... **Errore. Il segnalibro non è definito.**

C.7 Cyclic voltammetry: the response..... **Errore. Il segnalibro non è definito.**

C.8 Characteristic parameters..... **Errore. Il segnalibro non è definito.**

C.8 Liquid junction potentials..... **Errore. Il segnalibro non è definito.**

C.9 Convention ..... **Errore. Il segnalibro non è definito.**

C.10 Background limits..... **Errore. Il segnalibro non è definito.**

C.11 Overpotential ..... **Errore. Il segnalibro non è definito.**

C.12 HOMO LUMO calculation..... **Errore. Il segnalibro non è definito.**

C.13 Optical gap vs fundamental gap: electrochemistry vs UV/visible spectroscopy. . **Errore. Il segnalibro non è definito.**

# 1 Introduction

The challenge for green chemists is to develop new products, processes and services that achieve the social, economic and environmental goals. This needs to reduce the materials and energy requirements of chemical processes, minimise or eliminate the dispersion of harmful chemicals in the environment, maximise the use of renewable resources. Some of the challenges for chemists include the discovery and development of new synthetic pathways using alternative feedstocks or more selective chemistry, identifying sustainable reaction conditions and solvents for improved selectivity and energy minimisation and designing less toxic and inherently safer chemicals[1]. In this context the discovery of carbon dots (CDs) has attracted considerable interest for the innovative properties and benefits that this class of materials could bring. Their possible applications in the organic synthesis field range from the production of $H_2$[2,3,4] to the conversion of $CO_2$[4,5] into HCOOH, $CH_3COOH$, $CH_3OH$, $CH_2O$ and other organical small molecules. CDs may also have other applications, for example in biological, bioimaging, sensing, diodes, solar cells, photocatalysis and many others fields.[6]

In this thesis the objective is to study the optoelectronic properties and the photocatalytic reactivities of a library of CDs synthesized by the Perosa's group. The final purpose is to identify the key characteristics of these nanoparticles that could be ad hoc modulated for future green organic chemistry applications.

In the following issues, the fundamental concepts related to the CDs, along with photocatalysis (appendix B) and electrochemistry (Appendix C) will be exhaustively discussed for helping the readers to a better understanding of the real nature of these nanomaterials and their main properties.

# 2 What carbon dots are

Carbon dots are a newer class of carbon nanomaterials with excellent optoelectronic features. These nanoparticles are essentially composed by a mixture of molecular-like fluorophores, carbonaceous graphitic/amorphous-like cores tipically decorated with carboxylic, hydroxyl, and/or amine groups. Their size is in the order of 2-10 nm. For these characteristics, CDs have a high-water affinity and can therefore be dispersed in aqueous solutions. Despite those structural behaviours, the main interesting property of the CDs is the luminescence. The absorption of UV-visible light generates excited states which emit fluorescence through the so called "radiative" relaxation pathways.[7]

Over the last years, all these unique properties have conducted researchers to study these materials to better understand their behaviors and therefore to improve this field. However, since their discovery in the 2004 many names have been used to classify these nanomaterials (such as Carbon dots, Carbon Nano Dots, Graphene Quantum Dots, Carbon Quantum Dots, Polymer Dots, etc..) thus leading to misunderstandings. Therefore, hereafter their classification will be clarified.

## 2.1 Nanodot types and nomenclature

Nanodots is the most appropriate term for generalizing a class of nanometer-sized materials. Research on nanoparticles has produced an innumerable amount of these nano-compounds that differ in structure and properties. This brought the need to create a general nomenclature to distinguish and identify unequivocally the different existing types.

In the first publications dealing with carbon-based fluorescent nanodots, the term “carbon quantum dots” was assigned to all the emerging types of carbon fluorescent nanodots without providing a sufficiently detailed assessment of the requirements to be named “quantum dots”. In nanoscience the term “dot” is generally referred to nanometer-sized objects or particles while “quantum” alludes to the presence of carrier confinement by the reduced dimensions. The quantum confinement effect is observed when the size of the particle is too small to be comparable to the wavelength of the electron. As the size of a particle decrease until reach a nano scale the decrease in confining dimension makes the energy levels discrete and this

increase the band gap in semiconductor nanoparticles. So, the term "quantum dots" refers to types of nanodots with quantum confinement.

When the nanodots present quantum confinement and crystalline structure, we can distinguish between "Semiconductor Quantum Dot" (**SQDs**) made of metals with a core and a shell, the spherical quantum dots refereed as "Carbon Quantum Dots" (**CQDs**) and the π-conjugated single sheet referred as "Graphene Quantum Dots" (**GQDs**).

Amorphous quasi-spherical nanodots but also those with greater degree of graphitization that have exclusively molecular-like excited states and which usually lacks in quantum confinement, are refereed in other papers as carbon nanocluster, polymer dots or even carbon dots or C-dots, are classified "Carbon NanoDots" (**CNDs**).[8] Figure 1 shows nanodots and their classification.

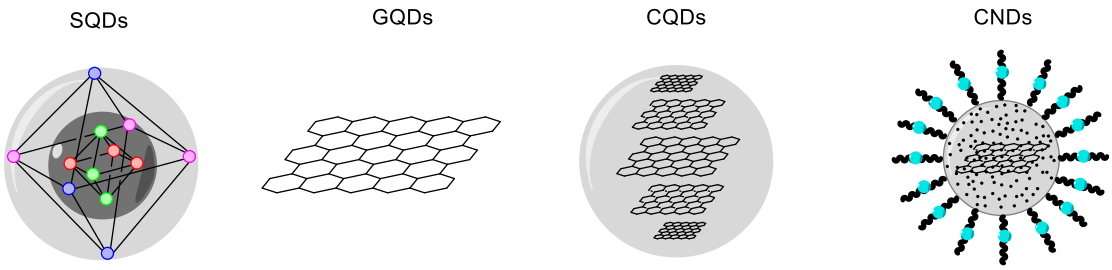


*Figure 1: Classification of fluorescent nanodots: SQDs (Semiconductor Quantum Dots), GQDs (Graphene Quantum Dots), CQDs (Carbon Quantum Dots) and CNDs (Carbon NanoDots).*

In this thesis, the term carbon dots (CDs) will be generically used to describe such of nanoparticles without consideration for their actual morphologies and presence or absence of quantum confinement effect.

## 2.3 Semiconductors, quantum confinement effect, exiton binding energy

By taking inspiration from the analogous well-known semiconductor materials, the quantum confinement effect together with both the intrinsic exiton binding energy will be illustrated in greater details. These knowledges will allow us to become familiar with such of phenomena which are central topics for the understanding of how CDs work.

### 2.3.1 Semiconductors

A semiconductor is a material with particular electrical conduction properties. It is defined as intrinsic if it is formed by a regular and ordered atomic structure while it is extrinsic if it contains atoms different from the ordered crystalline structure.[9]

Consider an extrinsic semiconductor that can be of type n or p depending on whether the defect incorporated in the crystal lattice leads to an additional free electron or an electronic hole in the structure of the material as shown in Figure 2:

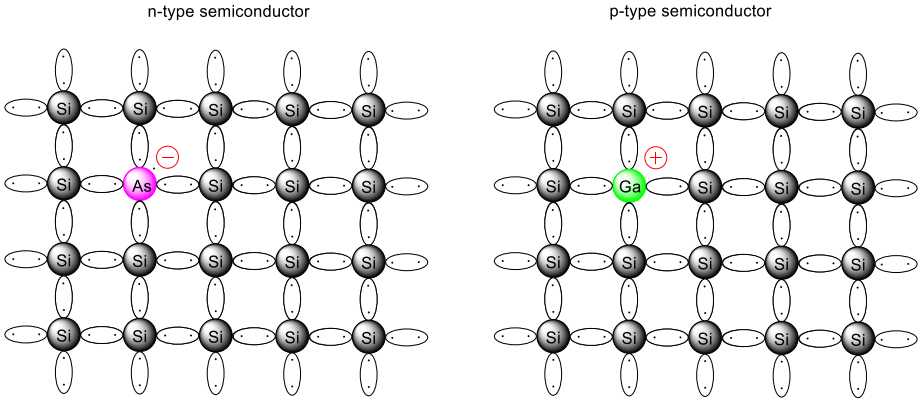


*Figure 2: n-type and p-type semiconductor.*

The lattice orbitals can be combined leading to the formation of valence band and conduction band. In intrinsic semiconductors in which there are no defects, these bands are separated by a gap. In extrinsic semiconductors. The presence of defect states also generates much narrower bands intemedies between the energy gap of the pure material. This is described in Figure 3:

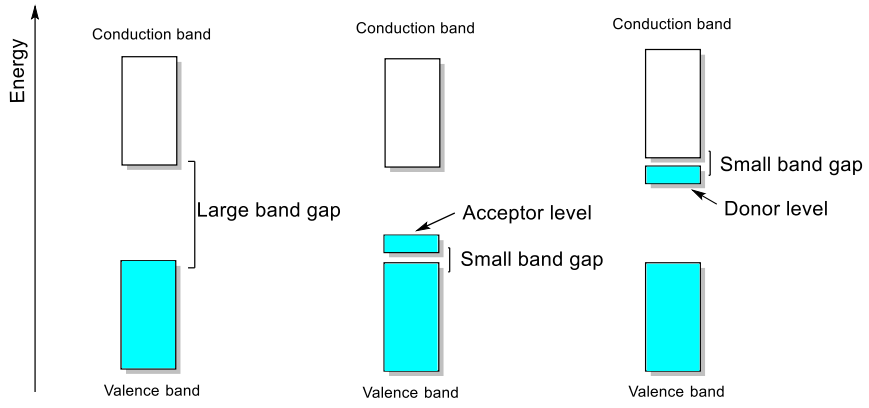


*Figure 3: intrinsic and extrinsic semiconductors.*

When electron pass in a conduction band leave a hole. A charge carrier in a semiconductor is either a positive hole or an electron that is able to conduct electricity.

### 2.3.2 Exciton binding energy and quantum confinement effect

Mobility and Exciton binding energy are important electrical properties of semiconductors and directly influence the efficiency of optoelectronic devices.[10] Mobility is a measure of the speed of a charge carrier as it moves through a conductive medium in the presence of an electric field. When a semiconductor interacts with a radiation of a suitable wavelength, the electrons in the valence band are energized to the conduction band leaving a hole. The band-gap in a material is the energy required to create an electron and a hole at rest (i.e., with zero kinetic energy) at a distance far enough apart that their Coulombic attraction is negligible. If one carrier approaches the other, they may form a bound electron-hole pair, i.e., an exciton, whose energy is a few meV lower than the band-gap. This is also valid in the mycoscopic world of nanoparticles. Strongly interacting electrons and holes form excitons with large binding energies. Exciton binding energy is a measure of the strength of interaction between an electron and a hole. In nanoparticles exciton can be regarded as particles trapped in a box so, the energies of the charge carriers are quantized. From the solution of the appropriate Schrödinger's quation emerges that the energy of the exciton decreases with increasing radius of box (Figure 4).[11,12,13]

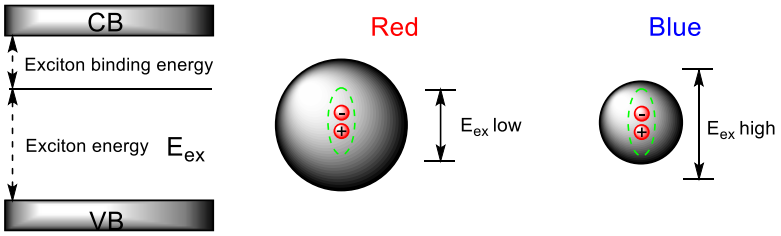


*Figure 4: exciton energy compare with size of nanoparticle.*

In conclusion the energy required to create mobile charge carriers and to induce electrical conductivity depends on the size of the particles. This effect is called quantum confinement effect.

The interaction between exciton binding energy and mobility determines the rate of exciton dissociation and thus the rate of radiative recombination.[10] To enhance the radiative rate, strong exciton binding and/or low mobility are preferred in light-emitting materials. When efficient charge extraction is required, weak binding and high mobility are necessary to suppress radiative recombination, which now represents a loss.

CDs can be seen in this sense as organic semiconductors in solution according to the degree of graphitization of the core. However, for our purposes this is of little interest to us. In this section we have only introduced the importance of the phenomena that govern the formation of excited electrons and holes and the energy states that are generated due to the size of the nanoparticles. In this sense, the term carbon dot for some nanoparticles may be inappropriate because even these nanoparticles could show the quantum confinement effect and therefore it would be more appropriate to define them as quantum dots with peculiar characteristics such as the absence of metals and a sustainable synthesis. However, in the literature we remember these nanoparticles obtained regardless of the degree of graphitization are generalized as carbon dots.

## 2.4 Synthesis and characterization of CDs

There are several synthetic procedures in the literature for these nanoparticles that can be generalized into two classes[14]:

### 2.4.1 Top-down synthesis

Exfoliation and oxidation of existing ordered carbon structures, including graphene (oxide) and graphite (oxide), etc. it's what characterizes Top-down synthesis. Chemical ablation, electrochemical carbonization, laser ablation are others examples of the methods used in the literature[6]. These types of procedure have the disadvantage of being expensive and give low yields.

In case of GQDs the precursors are graphene-based materials mainly, whereas CQDs can be prepared from other carbon nanomaterials with crystalline structure such as carbon nanotubes. CDs synthesised by top-down procedures usually contain high degrees of graphitisation and often require surface functionalisation, such as with poly-ethylene glycol diamine species, to impart photoluminescence. Figure 5 shows Top-down synthesis and the nanoparticles the can be produced.

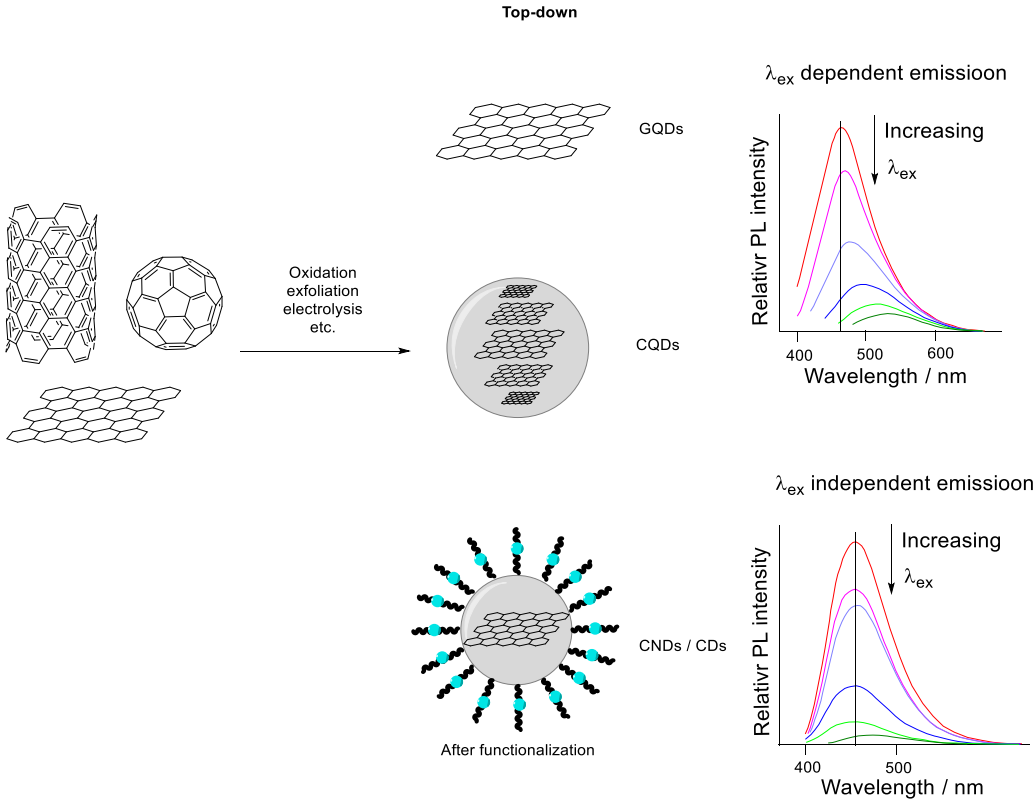


*Figure 5: Top-down synthesis.*

### 2.4.2 Bottom-up synthesis

Bottom-up methods involve the thermal decomposition of cheap organic molecular precursors such as carboxylic acid and hydroxyl containing molecules. Hydrothermal/solvothermal treatment, microwave irradiation, pyrolysis are the most used techniques.[6] These types of procedure have the advantage of being cheap, give high yields and substrates from renewable sources can be used.

An example is citric acid one of the first substrates used in the preparation of CDs can be pyrolysed or hydrothermally treated, resulting in the loss of small molecules ($CO_2$,$H_2O$) through dehydration and decarboxylation reactions and the build-up of a carbon core.[15]

CDs produced by bottom-up syntheses typically have diameters between 2–10 nm with different compositions of their carbon core, ranging from amorphous (a-CD) to graphitic (g-CD) depending on the temperature of decomposition employed. Generally, temperatures above 300 °C lead to significant graphitisation, whilst those below 300 °C result in amorphous particles.

Bottom-up CD syntheses can be further divided into two categories: Single source precursor (SSP) and Multi-component (MC) that lead to CDs with different structure and properties.

In the SSP heteroatom doping can be achieved by selecting a precursor in which all desired dopant elements are present. In doing so, heteroatom incorporation is directed into the core of the forming carbon nanoparticle. CDs synthesised from precursors rich in carboxylic acid display carboxylic acid functionalities at the surface.

In the MC approach, a precursor is decomposed in the presence of additional species containing heteroatoms such as N, P, B. In CDs synthesised by the MC approach, the heteroatom incorporation is thought to be localised largely at the CD surface, with surface functionalities consisting mainly of amide and/or amine functionalities, as well possibly carboxylic acids. These CDs are often referred to as ‘‘doped’’ or ‘‘surface passivated.

Optical properties of CDs show differences when synthesized under pressure in autoclave or at atmospheric pressure. In fact, these different approaches determine the reaction temperature which therefore influences the degree of graphitization of these particles. Figure 6 shows Bottom-up synthesis and the nanoparticles the can be produced.

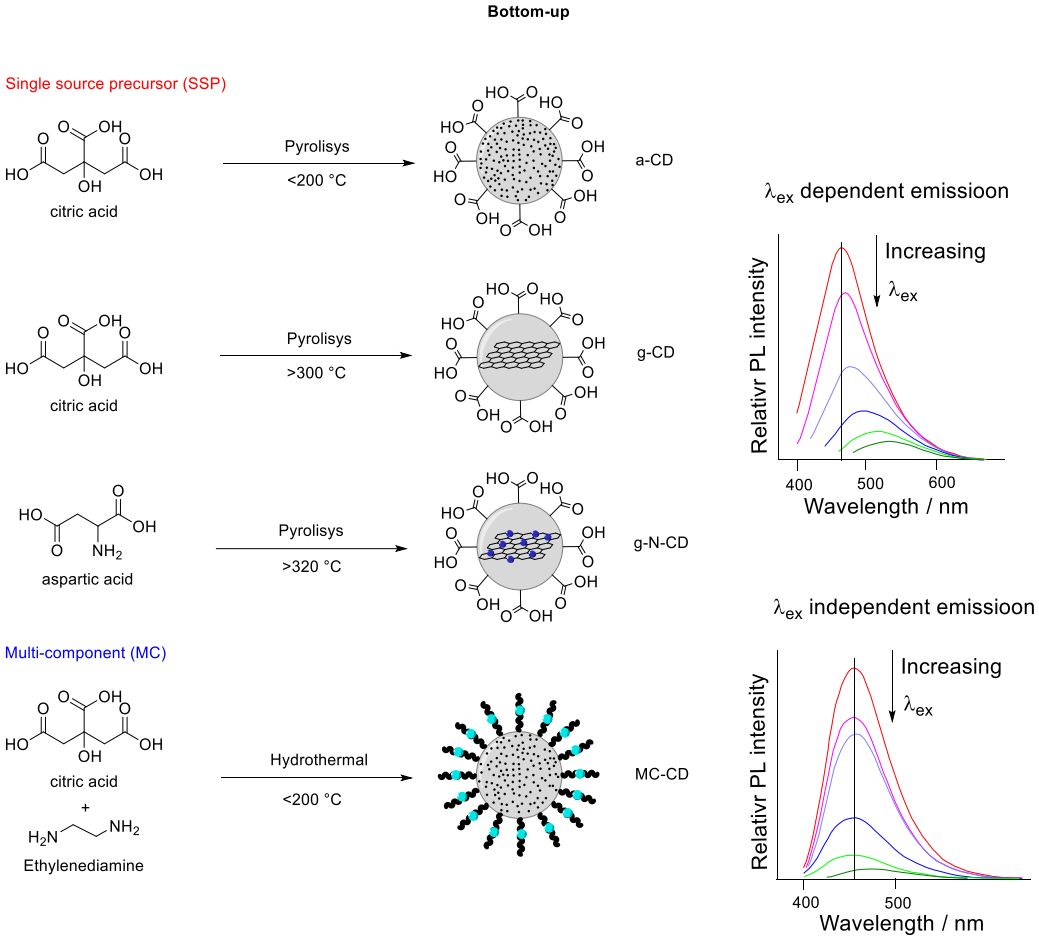


*Figure 6: Bottom-up synthesis*

Finally, to control the dimension of CDs the most commonly utilised procedure is dialysis but there are others such as chromatography, ultrafiltration and electrophoresis.

Despite this classification in the recent literature there are still doubts about the possible fluorescence mechanisms that can lead to a wrong classification of these nanoparticles. The method of synthesis in conjunction with the optical properties of these materials is the best way to classify these materials. In this thesis the nomenclature of the CDs follows the general lines indicated. The CDs obtained by pyrolysis of citric acid are named g-CDs, those obtained by hydrothermal synthesis a-CDs while the MC-CDs obtained from citric acid and ethylenediamine by pyrolysis or hydrothermal treatment are respectively designated g-N-CDs and a-N-CDs. For the latter two it is good to remember that temperature influences the nature of the core and the surface. Doping takes place mainly on the surface, what changes is the nature of the graphitic or amorphous core.

### 2.4.3 Structural Characterization

Several techniques have been used to characterize CDs, to have a better understanding of their structure and to study their physical properties[16].

Transmission electron microscopy (TEM) and High-resolution TEM (HRTEM) providing important information about particle morphology, size distribution, and crystalline organization. Figure 7 presents a TEM and HRTEM image of a Carbon-Dots, featuring the graphite lattice planes of the carbon core:

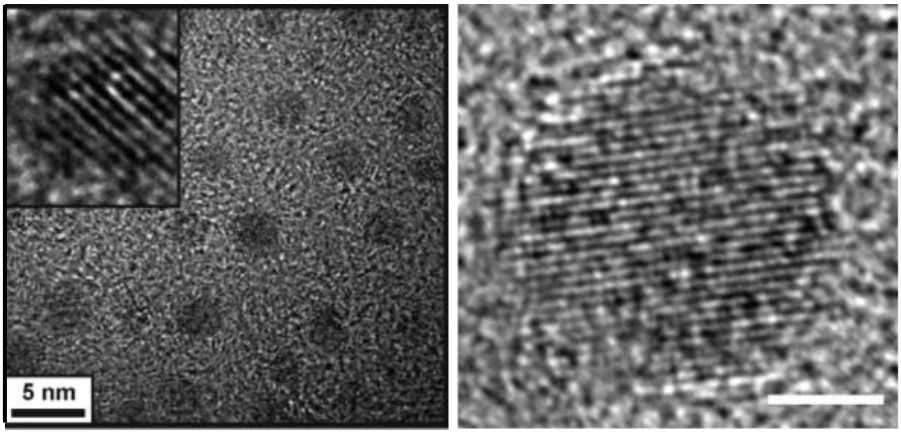


*Figure 7: TEM and High-resolution TEM (HRTEM).*

X-ray diffraction (XRD) provides information upon the unit cell dimensions and crystal spacing within the crystalline carbon cores. Figure 8 is a representative XRD pattern, showing a diffraction peak at around 20° reflecting the crystalline graphitic structure with a lattice spacing of 0.45 nm which is greater than bulk graphite (0.35 nm) indicating certain amorphous character of the synthesized Carbon-Dots

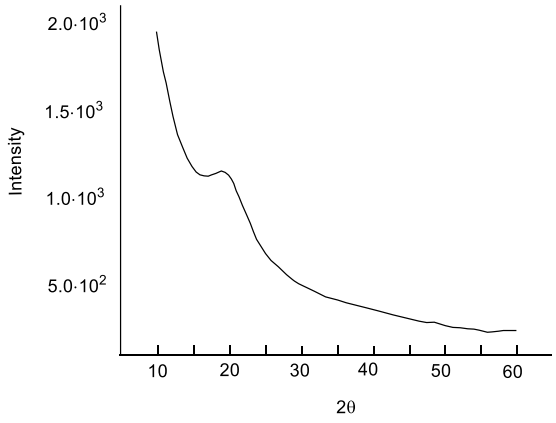


*Figure 8: X-ray diffraction (XRD).*

Raman scattering reveals the structural features of the carbon atoms within Carbon-Dots. Figure 9 shows typical Raman spectrum of Carbon-Dots. We can note two peaks corresponding to the D and G bands, respectively. The D band at around 1350 $cm^{-1}$ is ascribed to disordered $sp^3$ carbons, while the G band at around 1600 $cm^{-1}$ arises from the in-plane stretching vibration mode of crystalline graphite carbons. The ratio of the intensities ($I_D/I_G$) of the characteristic Raman bands can be used to study the structural properties such as degree of crystallinity and relative abundance of core carbon atoms versus surface atoms.

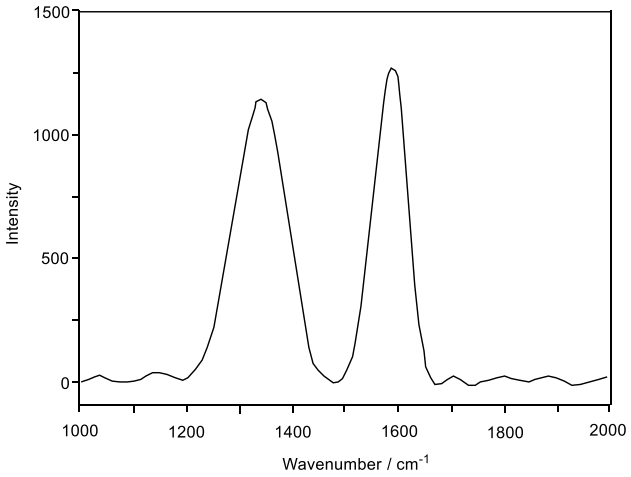


*Figure 9: Raman scattering.*

Fourier transform infrared (FTIR) spectroscopy shows functional units that derive from typical vibration bands. Figure 10 shows typical spectra.

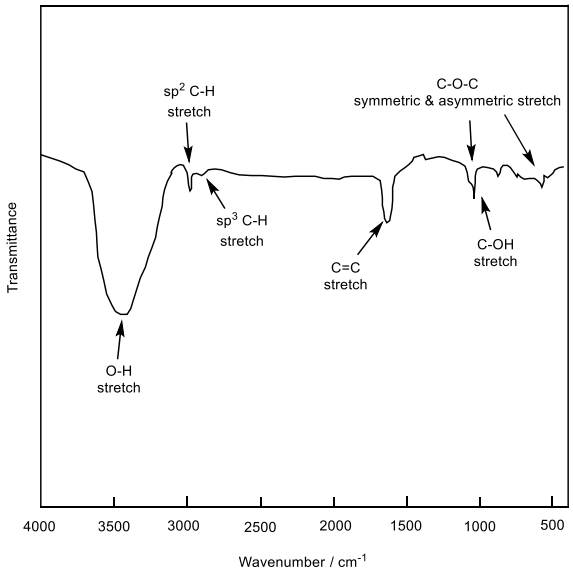


*Figure 10: Fourier transform infrared (FTIR) spectroscopy.*

X-ray photoelectron spectroscopy (XPS) provides information upon specific atomic units present upon Carbon-Dots's surface. An example of an XPS analysis is provided in Figure 11. The spectral analysis reveals the distinct nitrogen-, oxygen-, and carbon-bonded units displayed upon the Carbon-Dots's surface.

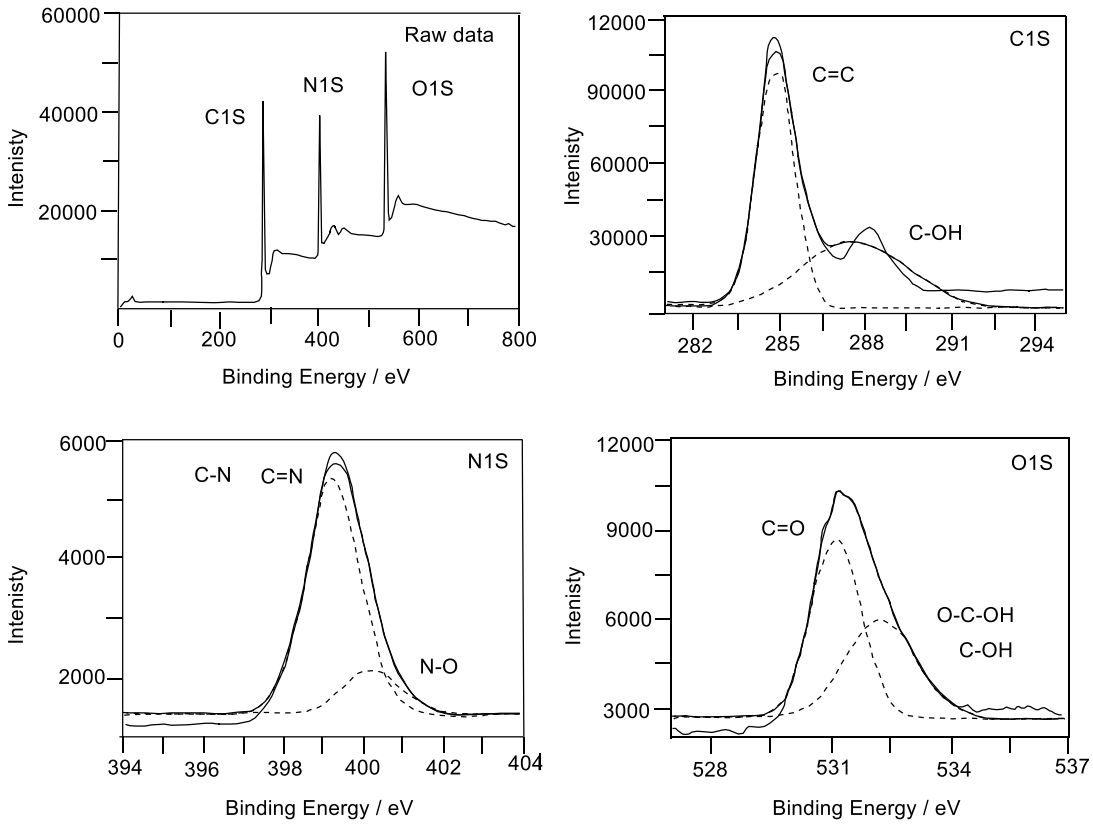


*Figure 11: X-ray photoelectron spectroscopy (XPS).*

$^{1}H$ and $^{13}C$ NMR spectroscopy can be another useful technique of characterization. $^{13}C$ NMR spectroscopy is useful for monitoring reaction progress and ensuring complete decomposition of the precursor compound during the synthesis. A large number of scans and high CD concentrations (200 mg/mL) are required to achieve sufficient signal to noise ratio. Two-dimensional NMR correlation experiments is used to get information on the size and diffusion coefficients of these nanoparticles.

## 2.5 Optical properties of CDs

### 2.5.1 Absorption

The origin of absorption in CDs derives from a variety of π– π* (C=C) and n– π*(C=O) transitions in the core and on the surface of the particles[14].

Carboxylic acid-terminated CDs, such as those synthesised by the SSP approach, typically have a broad UV-visible absorption profile, lacking clearly resolved features, whereas CDs synthesised by MC procedures, show an additional characteristic peak at approximately 355 nm for the n–π*(amide) transition. CDs with higher levels of graphitisation display much higher absorption than amorphous CDs, due to the greater number of π – π*(C=C) transitions present. Amorphous CDs synthesised by multi-component procedures are increasingly thought to result from highly emissive amide-containing molecular-like fluorophores corresponding to the well-defined absorption observed in the UV-visible spectrum. Figure 12 shows some characteristic absorption spectra.

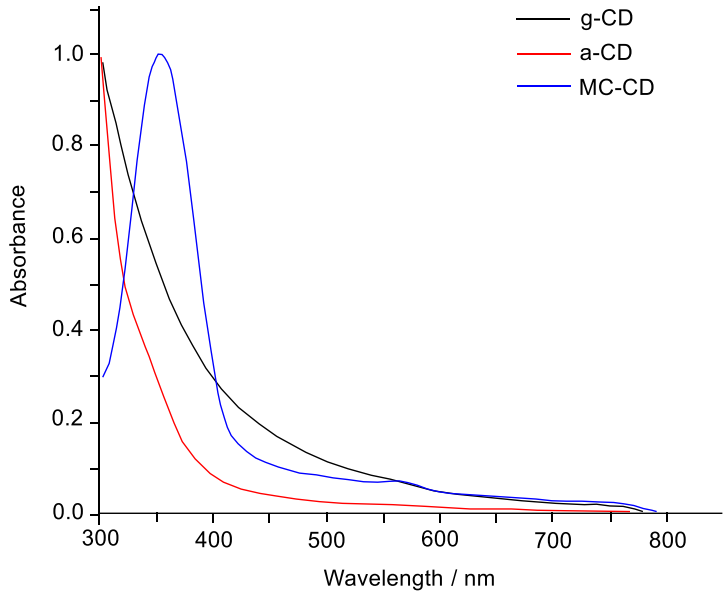


*Figure 12: Characteristic absorption spectra for g-CD, a-CD, MC-CD.*

CDs synthesised by the SSP approach typically display excitation wavelength-dependent emission properties, and CDs synthesised by the MC approach generally results in excitation wavelength independent emission probably due to the presence of these fluorophores as described (see Figures 5, 6 for a better understanding). Typically, quantum yields of fluorescence (ϕ) for SSP CDs are lower then 10%, indicating that there exists a number of non-radiative recombination pathways while quantum yields for MC/CDs are around 50%.

### 2.5.2 Phololuminecesce (PL) and structural dependent mechanisms

Although the exact mechanism which generates the light absorption and emission for CDs is still an open issue, the more reasonable hypotheses attribute such of properties to the morphologies as well as the chemical/physical properties for the CDs. Summarizing, three are the possible origin of PL[8]:

1) The first is the quantum confinement effect, which is determined by both the degrees of π conjugation and size of the carbon core. This type of PL, which arises from a band-edge recombination (Figure 13.a), is commonly observed in the homologous "metal based" Quantum Dots, and confer to the here discussed carbon-based nanoparticles a size-dependent, excitation-independent, and a very narrow emission band.
2) The second type of emission is generated by the surface states, which are determined by surface defects, functional groups, and surface passivation of the carbogenic core. In this case the superficial defects entrap the photoexcited electrons and/or holes in the bandgap thus generating PL with lower energy. The resulting PL is a combination of the first two type of mechanisms (Figure 13.b) leading to an excitation-dependent luminescence which is however strongly affected by the synthetic procedure used.
3) The third is the molecule state type which is associated to the presence of fluorophores on the CDs composition. In this case, neither quantum confinement or surface defect effects exist, and the luminescence is solely a consequence of the superposition of several “molecular” type emissions (Figure 13.c). PL is therefore size-independent, excitation-dependent and exhibits a very broad emission band.

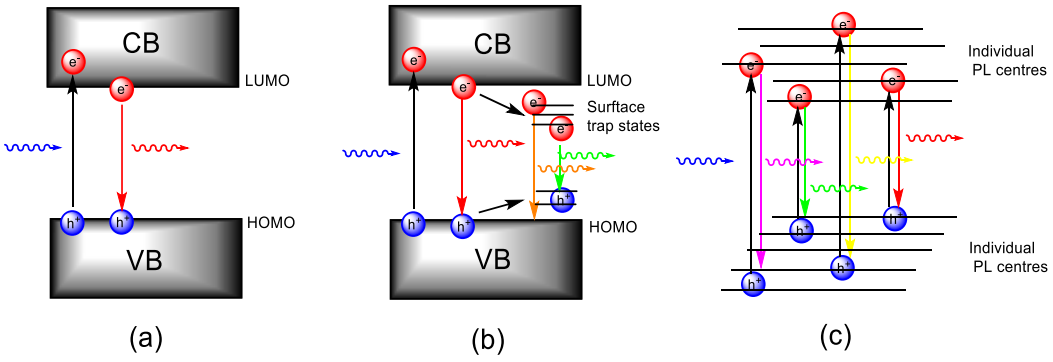


*Figure 13: Scheme of the different photoluminescence mechanisms.*

The photoluminescence properties of the carbon dots are strictly correlated to their intrinsic structure and consequently to the synthetic procedure used. Despite the difficulties to determine the actual origin of luminescence and to further classify the CDs considering their exact morphology, in general the first two PL mechanisms are invoked for “graphitic-like” GQDs and CQDs synthetized *via* both top-down or harsh bottom-up approaches (*i.e.* pyrolysis) while the third for “amorphous-like” CNDs prepared through soft hydro/solvothermal bottom-up treatments.

Herein, recent studies on the PL properties of CDs will be discussed. Generally, it is not possible to isolate the quantum confinement effect from that of surface or molecular states that are “intrinsic” properties of CDs, but it is possible to understand the effect of the individual contributions they have.

Zhang and co-workers in 2016 have prepared different sized CDs *via* gel electrophoresis of the crude nanoparticles prepared through a photo-Fenton reaction of graphene oxide.[17] They demonstrate that the PL of CDs depend on both the nanoparticles size, according to the quantum confinement effect, and by the peripheral carboxylic groups. More importantly, it has been revealed that for small sized CDs prevails the surface status effect on the PL with the contribution of carbon skeleton which appears only when exciting the nanomaterial at longer wavelengths. While for the large sized CDs the effect of the graphitic core is dominant to their PL leading to an emission wavelength which increases with size (minor energy gap). The latter phenomenon can only be explained with the quantum confinement effect (Figure 14).

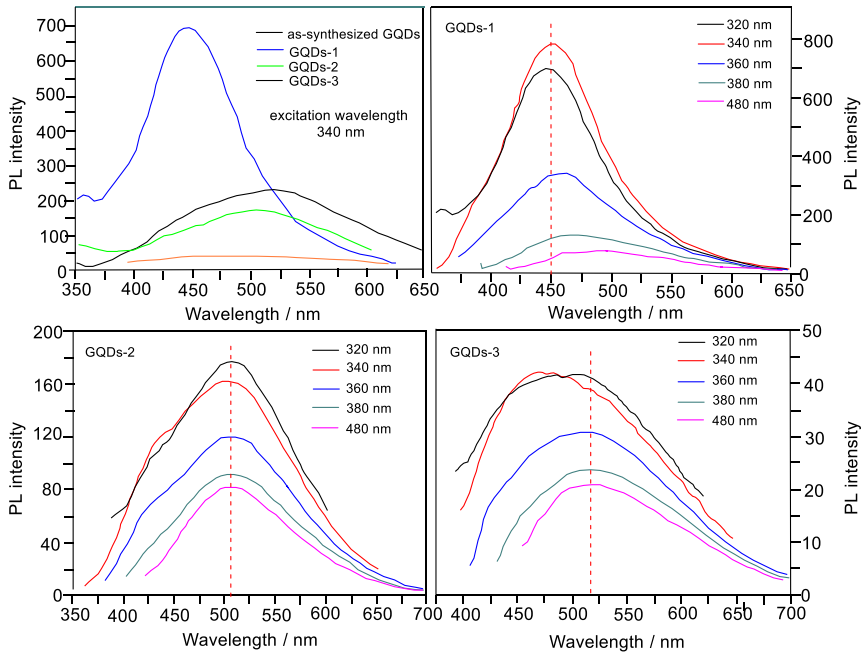


*Figure 14: PL properties of the GQDs separated by gel electrophoresis. Size order: GQDs-1< GQDs-2<GQDs-3 (wider particles distribution).*

Considering the effect on the PL of the superficial CDs decorations, many other studies have appeared in the last years. In the context, Ding and co worker in 2016 using Urea and p-phenylenediamines as precursors prepared equal-sized CDs from blue to red with an excitation-indipendent luminescence emission spectra.[18] The observed color changes were found to depend on the degree of superficial oxidation structures rather than the particle size. In more details, the observed red shift in their emission peaks from 440 to 625 nm was ascribed to a gradual reduction in their band gaps with the increasing incorporation of oxygen species into their surface structures (Figure 15).

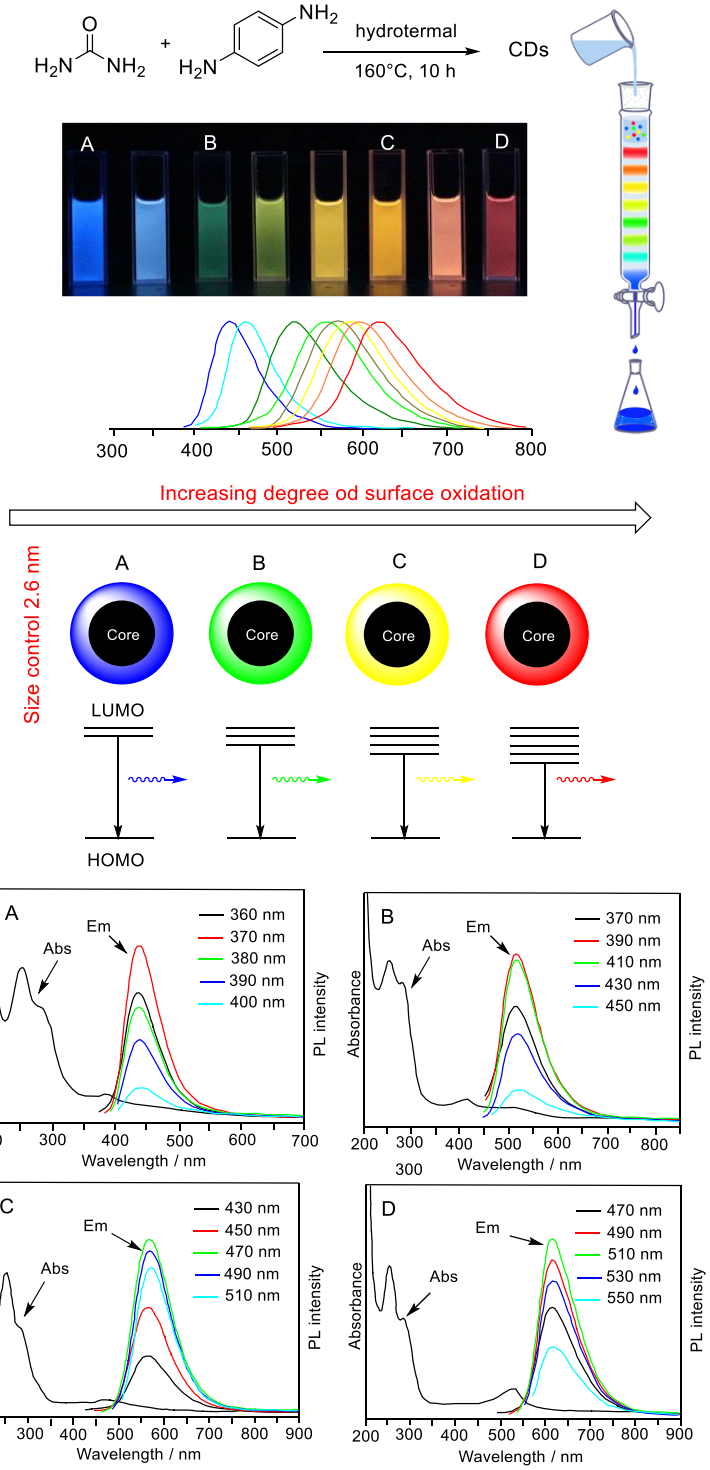


*Figure 15: effect of increasing the degree of oxidation on the surface of the CD.*

Regarding the third molecular state effect of the PL on the CDs, an unequivocal demonstration was given by Song *et al*. in 2015 which was able to isolate and to characterize the molecular fluorophore "imidazo[1,2-a]pyridine-7-carboxylicacid,1,2,3,5-tetrahydro-5-oxo" (IPCA) demonstrating that its absorption and emission spectra were identical to the one of the synthetized CDs (Figure 16).[15] The fluorophore resulted to be the main emitting species in the as synthetized CDs. IPCA was then used in hydrothermal synthesis at two different temperatures, confirming how the temperature influences the degree of graphitization.

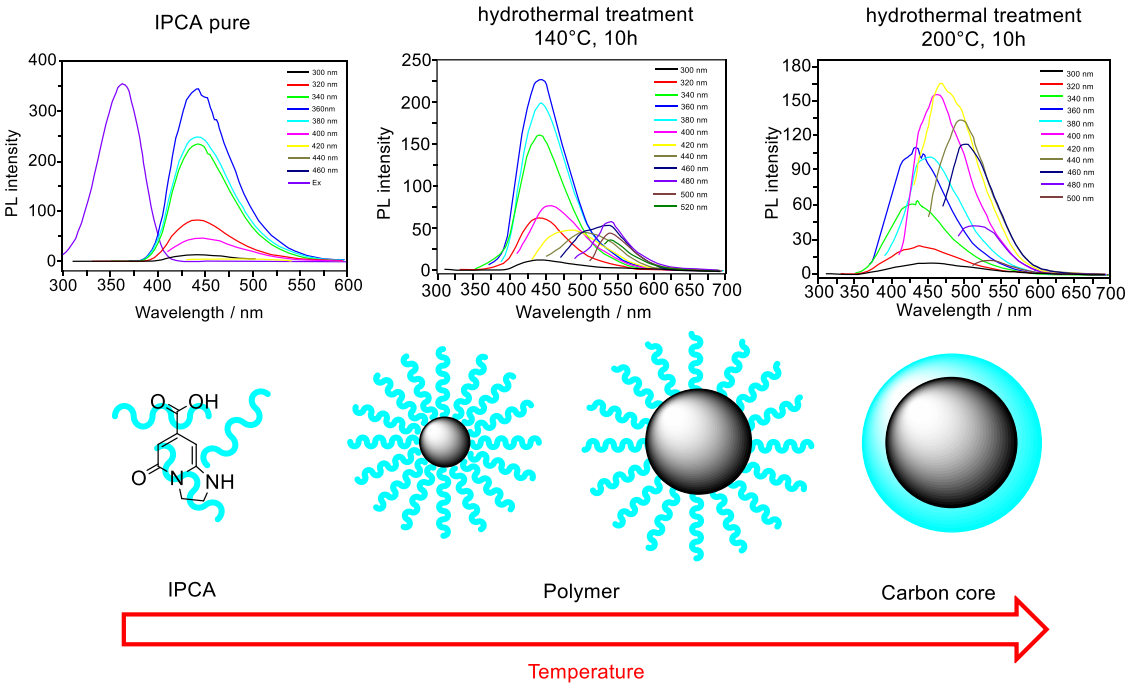


*Figure 16: hydrothermal treatment of IPCA.*

An additional very recent hypothesis on the origin of the PL behavior of the CDs and on the specific role played by the different component was made by Fang *et al*. [19] They suggested that the PL of CDs are the results of a cooperative effects between the graphitic carbon core, the defect states and the molecular fluorophore. The authors used citric acid and amino group-containing molecules as precursors to prepare CDs having luminescent pyridine-derivatives. CDs and free pyridine-derivatives were separated by a dialysis treatment. The PL behavior of the fluorophore molecules agreed with the one of the original CDs solution. with, however, a higher QY and a less evident excitation-dependent behavior. Combining these outcomes with an accurate optical study the authors proposed a hypothetical PL mechanism in which fluorophores, defect states and carbon core play a different role.

Under the irradiation of UV light in the range from 280 to 380 nm, the electrons in the π orbitals of the luminescent conjugation units can be excited to the π* orbitals (Process a). Then some of the excited electrons in the π* orbitals may recombine with the holes in the π orbitals directly, emitting the PL signal centered at 420-440 nm, which can be referred as the intrinsic emission like the band-edge emission observed in QDs (Process b). The other excited electrons in the π orbitals may be trapped by the defect states of energies lower than in the π* orbitals (Process c) before they are finally recombining with the holes in the π orbitals. Meanwhile, some electrons may be excited and trapped directly by the defect states (Process d) and relax through either radiative (Process e) or nonradiative (Process f) ways. The PL signal from the radiative relaxation is the defect emission, which is also observed in QDs. Therefore, when the excitation wavelength is in the range of 280-380 nm, the CD produce both intrinsic PL and defect PL signal. When the excitation wavelength is longer than 380 nm, the energy of which is less than that needed for the π-π* transition, the electrons can only be excited to the defect states. Accordingly, only the defect emission can be observed. It should be mentioned that both the intrinsic emission and defect emission of the CDs would be partially quenched by the graphitic cores a phenomenon called FRET effect (Process g). Due to the effects of the defect states and the graphitic cores, the PLQYs of the CDs are usually much lower than those of the corresponding pyridine-derivatives. Figure 17 shows the mechanism proposed.

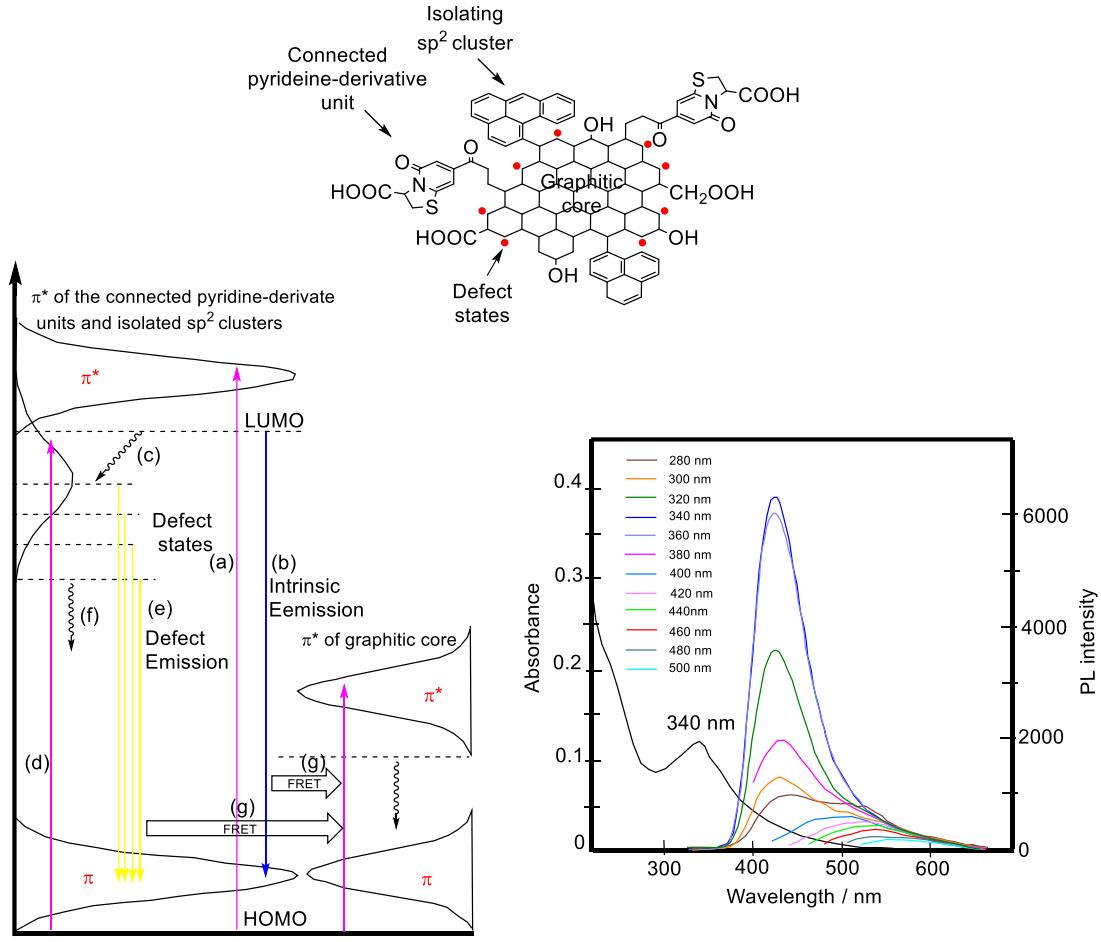


*Figure 17: PL mechanism.*

In conclusion, while the PL spectra depends on both molecular fluorophores and defect states, the magnitude of QY is mainly affected by the graphitic core of the CDs.

Overall, even if this latter PL mechanism is satisfactory from an intuitive level, many other issues (such as role of the carbon core size and the structural morphologies of the CD, i.e. amorphous or crystalline) were not effectively addressed. Therefore, a real understanding on the mechanisms of fluorescence of these nano-systems remain unresolved to date.

# 3 Photochemistry

Solar energy that reaches Earth's surface is composed of radiations with a wavelength ranging from infrared to ultraviolet (Figure 18). The intensity of these radiation is maximum in the visibie region. [20]

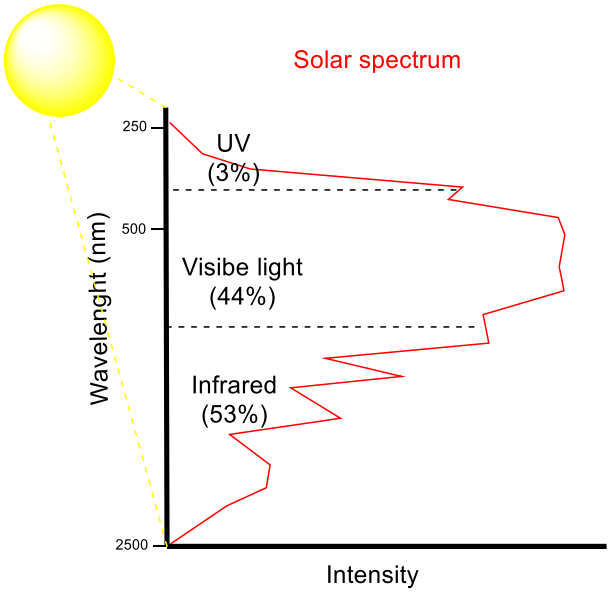


*Figure 18: solar energy that reaches Earth's surface.*

Now imagine a chemical industry that could synthesize chemicals in the same manner that plants do by using sunlight as a safe, inexpensive, abundant, and renewable source of chemical potential. [21] Natural photosynthesis takes place in two phases: i) the light-dependent phase in which ATP and NADH are produced, and ii) the Calvin cycle in which ATP and NADH are consumed in the carbon fixation phase to produce organic compounds (Figure 19.a).[22] Photocatalysis mimics both the photosystem II (photo-oxidations) and the photosystem I (photo-reductions) of the light dependent phase (Figure 19.b).

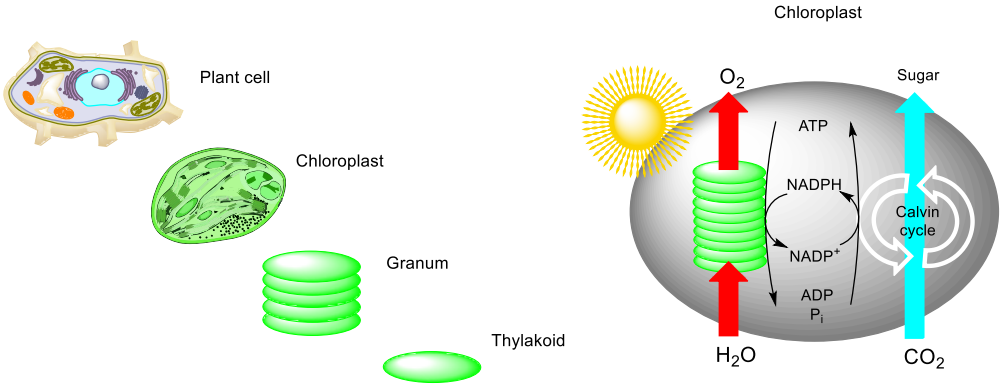


(a)

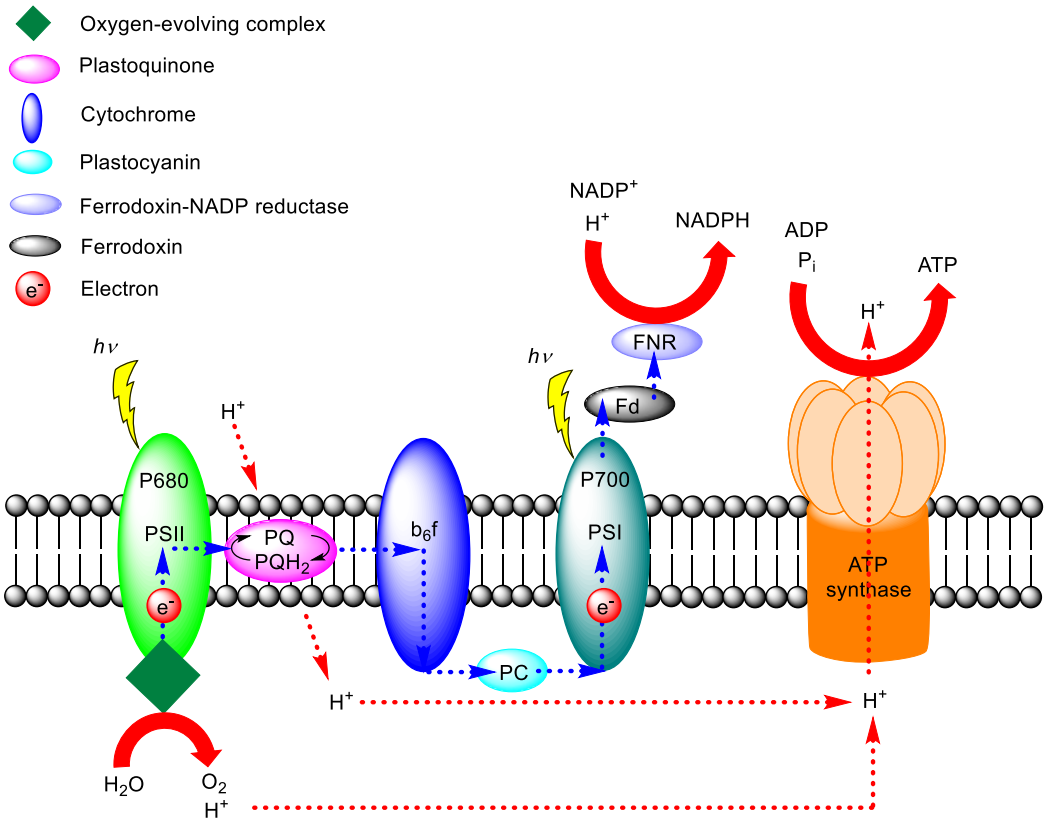


(b)

*Figure 19: Natural photosynthesis.*

By mimicking the natural photosynthesis many photo-devices have been developed over the last decades. Among these, the metal based photosensitizers (such as the Ru-bpy systems) and the photovoltaic systems DSC (dye-sensitised solar cells) or DSP (dye-sensitised photocatalysis) resulted to be the most interesting examples for the conversion of sunlight into chemicals or electricity. [23]

Transition metal chromophores, such as the well explored $Ru(bpy)_3^{2+}$, are used to convert visible light into useful chemicals for synthetic purposes. As an example, $Ru(bpy)_3^{2+}$ exhibits a strong broad absorbance in the visible range that results in the production of a long-lived excited state suitable for triggher organic transformations via electron transfer (ET). As schematized in Figure 20, upon absorption of a photon in the visible region an electron in one of the photocatalyst's metal-centered $t_{2g}$ orbitals is excited to a ligand-centered π* orbital. This transition is called a metal to ligand charge transfer (MLCT) and results in a species in which the metal has effectively been oxidized to a Ru(III) oxidation state and the ligand framework has undergone a single-electron reduction. The initially occupied singlet MLCT state undergoes rapid intersystem crossing (ISC) to give the lowest-energy triplet MLCT state. This triplet state is the long-lived photoexcited species that are involved in single-electron transfer. The photoexcited specie has the remarkable property of being both more oxidizing and more reducing than the groundstate.[24]

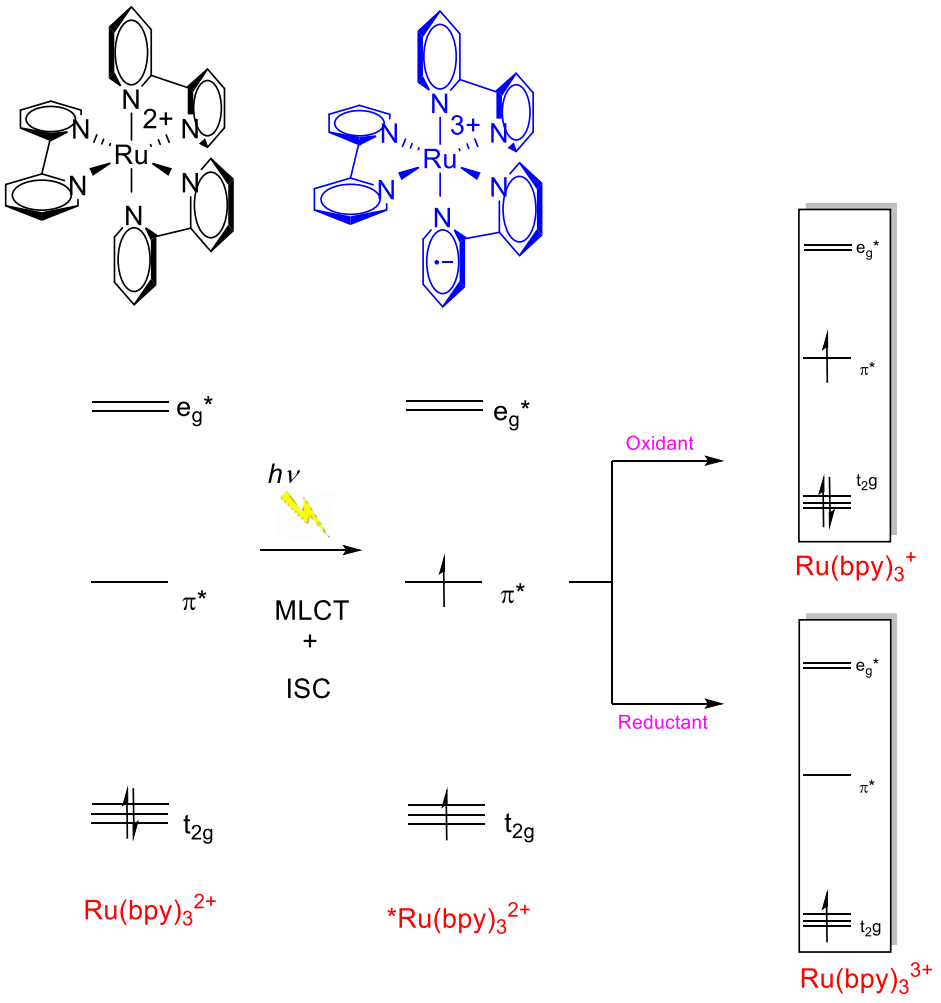


Figure 20: excitation mechanism of $Ru(bpy)_3^{2+}$.

In the context of organic synthesis, the photoexcited $Ru^*(bpy)_3^{2+}$ can promote both i) one-electron reduction of a variety of electron-deficient substrates ($D \rightarrow D^{\cdot+}$) or ii) one-electron oxidation of electron rich substrates ($A \rightarrow A^{\cdot-}$). Alternatively, $^*Ru(bpy)_3^{2+}$ can directly transfer energy to a suitable organic substrate ($S \rightarrow {}^*S$). The resulting electronically excited organic compound (*S) reacts quite differently than it would in the ground state. In Figure 21 these mechanisms are shown.

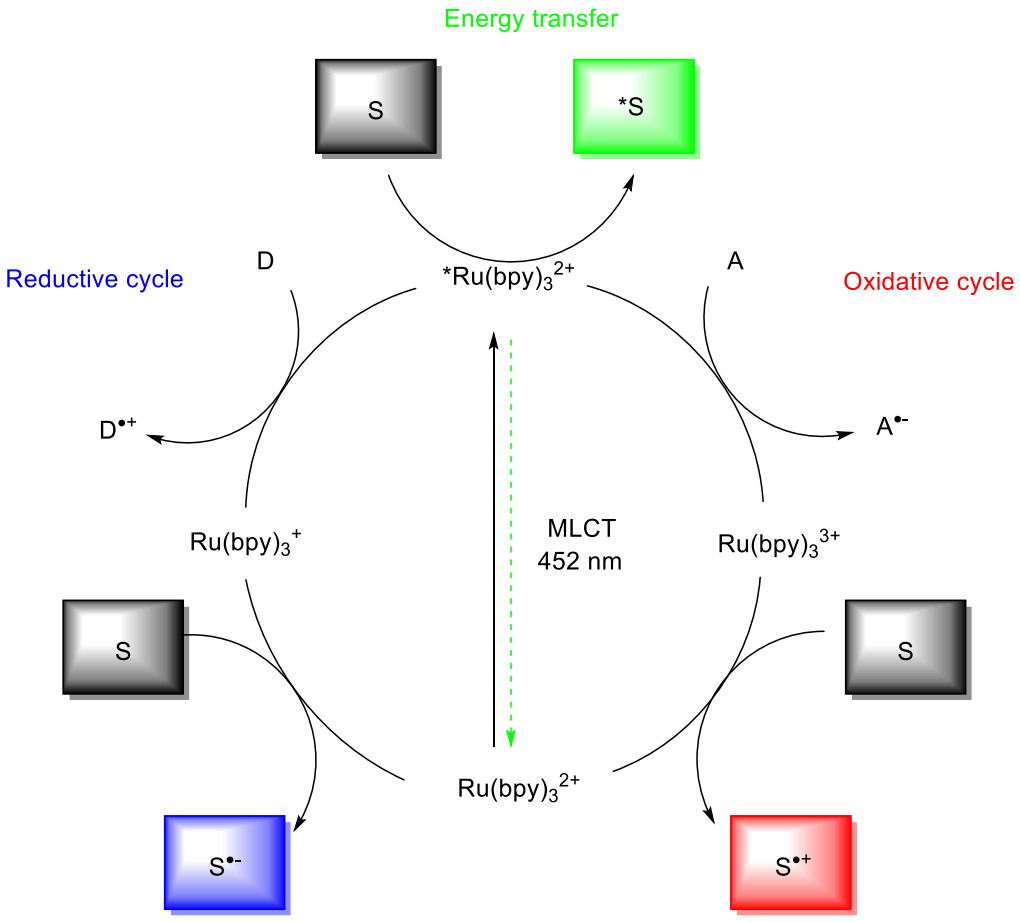


*Figure 21: electron transfer by $Ru(bpy)_3^{2+}$.*

In a typical DSC (dye-sensitised solar cells) setup, a red-ox cycle is formed between the electrons (photogenerated by the dye and collected at a $TiO_2$ photoanode) and holes (filled by the reduced species of a redox mediator ($M/M^-$)). The key features of this type of solar cell are the efficiency of dye in absorbing sunlight and the electron injection into the conduction band (CB) of the semiconductor. Figure 22 shows a DSC system.

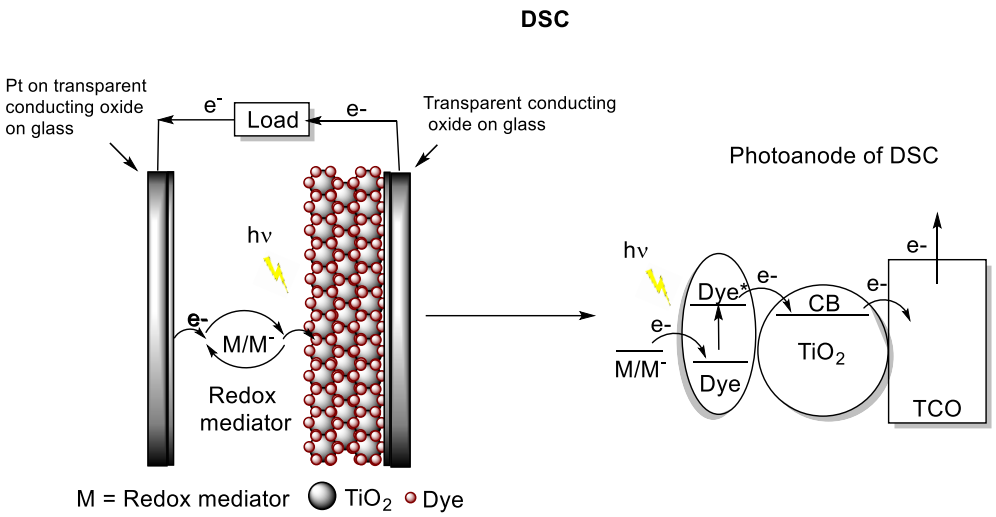


Figure 22: dye-sensitised solar cells (DSCs).

DSP (dye-sensitised photocatalysis) builds upon the excellent dye-semiconductor interface, but electrons are transferred to an electrocatalyst for fuel production instead of generating electricity. Electrons from the photoexcited dye are transferred to a $H_2$ evolution catalyst ($cat_{red}$) via the conduction band of $TiO_2$, while the oxidised dye should be regenerated (directly or indirectly) by a water oxidation catalyst ($cat_{ox}$) to close the fuel-making cycle. Figure 23 shows a DSP system.

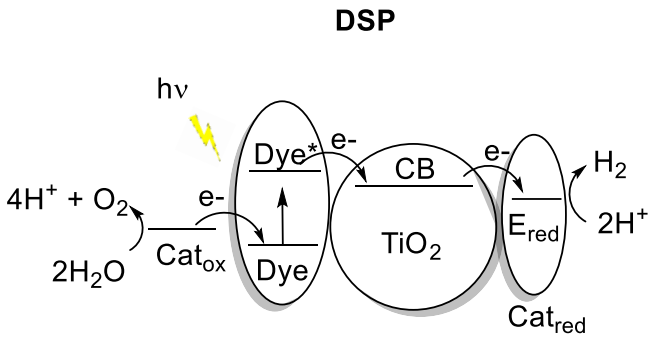


Figure 23: dye-sensitised photocatalysis (DSP)

Figure 24 shows the scale of the times in which the electronic transfer and recombination of electrons and holes takes place in a DSP. From this figure we can see that: i) the chemical reactivity requires the longest time scale (pathway 4) to respect to the others electron transfer events (pathway 2, 3, 5 and 6). Furthermore, iii) the time required for the recombination of the electrons with the holes is much slower when the electron is in the conduction band (pathway 8) while it is almost immediate if the electron is in the orbital with the highest energy of the dye (pathway 7).

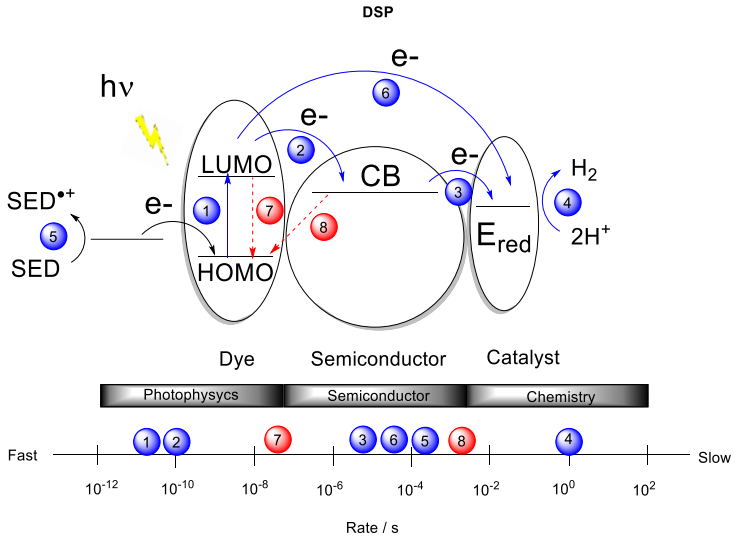


Figure 24: kinetics in DSP system.

If we now compare the DSP system with natural photosynthesis, the recombination of electrons with the holes becomes increasingly slow passing through the system of complexes and enzymes of the photosystem II. This is shown in Figure 25

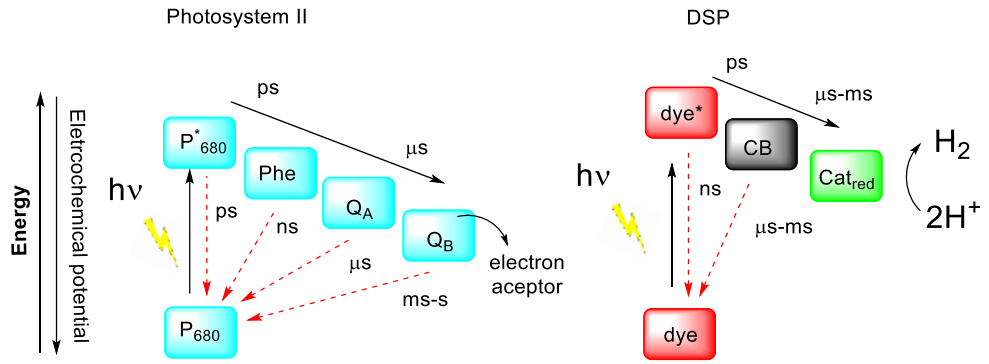


*Figure 25: comparison between the DSP system and natural photosynthesis.*

It becomes clear from this example how delaying the recombination of electrons with holes is a key feature in these systems.

In this context, the novelty is that the CDs have the magnificent property of absorbing light thus performing photo-electron transfer (PET) to a substrate that will undergo chemical reactions (Figure 26). Therefore, these nanomaterials can be effectively used as sustainable and metal free alternative to the here above discussed photosystems.

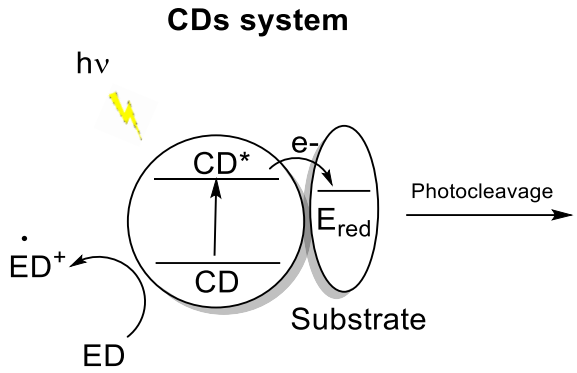


*Figure 26: CD as a photosensitizer*

Thus, it becomes clear that when we consider the CD system as a photosensitiser, the very high rate with which we recombine electrons and holes are one of the factors limiting the reaction because it competes with bimolecular diffusion kinetics. Figure 27 describe CD system.

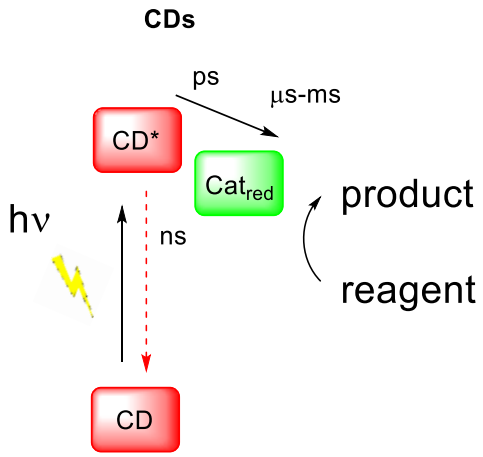


*Figure 27: CD system. Recombination rate is the limiting step.*

However, it has been observed that the addition of a sacrificial electron donor decreases the electrons and holes recombination rate by filling the hole left free after the excitation of the CD. This has been observed by Benjamin C. M. and co-worker who have studied CD/NiP (metal catalyst) system producing hydrogen when illuminated at a suitable wavelength[25]. Herein the CDs will be used as photocatalyst for promoting light triggered C-O cleavage reactions. The choice of substrate, mechanisms and reaction conditions will be described with more detail in the following sections.

To deeper understand the fundamentals of photocatalysis (fluorescence and phosphorescence mechanisms, lifetime of excited states, quantum yield) and the thermodynamics and electrochemistry concepts of the electronic transfer kinetics see the Appendix B and C.

# 4 Photochemically releasable protecting group (PRPG)

A protecting group is a molecule that can be linked and subsequently detached to a functional group to protect its reactivity during a synthesis.[26] A photochemically releasable protecting group acts as any other protecting group except for the release which is due to light exposure[27]. Several features are desirable in a PRPG including: i) high yields in protection and high yield/quantum yield in deprotection, ii) readily separated by products, iii) the group should be removable with light wavelengths that are not also absorbed by the substrate with reduction in quantum yield or adverse reactions and finally, iv) the protecting group should be stable in the absence of light. For these challenges, rather than a universal protecting group, many PG have been developed for solve specific synthetic problems.

Photo- induced electron transfer event triggers the PRPG release. In general, the deprotection reaction mechanism involves the light excitation of a photosensitizer (PS → PS*) which in turn, by reacting with the PRPG, forms the correspondent radical/cation ($PRPG^{+\cdot}$) or radical/anion ($PRPG^{-\cdot}$). Such radical pairs may then undergo or back electron transfers or the desiderd deprotection following radical cleavages (Figure 28).

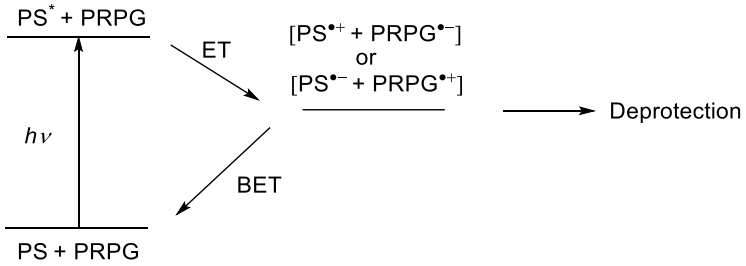


*Figure 28: photo- induced electron transfer reactions.*

## 4.1 Case study: phenacyl esters

Examples in literature are useful for understanding what happens in the system we are going to study. Among these, worth of notice is the deprotection of phenacyl esters to restore acid functionality *via* a photo-induced pathway as reviewed by Falvey and Sundararajan.[27] Accordinghly to the above mentioned general mechanisms, the light excited state of the sensitizer (PS*) donates an electron to the phenacyl ester creating the anion-radical pair. Rapid elimination of the carboxylate anion generates the phenacyl radical and the by-product, acetophenone, formed via a second net H atom transfer. The mechanism of reductively-sensitized phenacyl deprotection is given in Figure 29.

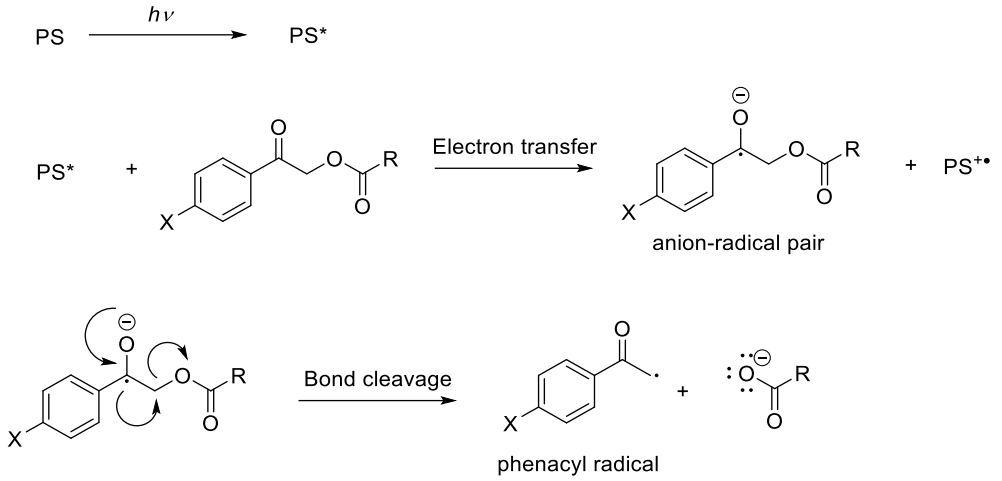


*Figure 29: Phenacyl esters deprotection.*

A series of para-substituted phenacyl esters having both electron donor or electro withdrawing groups were photocleaved and an inverse and unexpected correlation between the ease of reduction and the breaking of the C-O bond were observed. Such substituent effect was rationalized though thermodynamic considerations, as schematized in Figure 30, and with the reasonable assumption that the C–O bond strengths do not vary significantly with para substitution. The more easily reduced esters (low $\Delta G_{red}$) will have a lower driving force for bond scission (low $\Delta G_{BB}$) and conversely esters with the more negative reduction potentials (high $\Delta G_{red}$) will have the highest driving force (high $\Delta G_{BB}$) for bond scission.

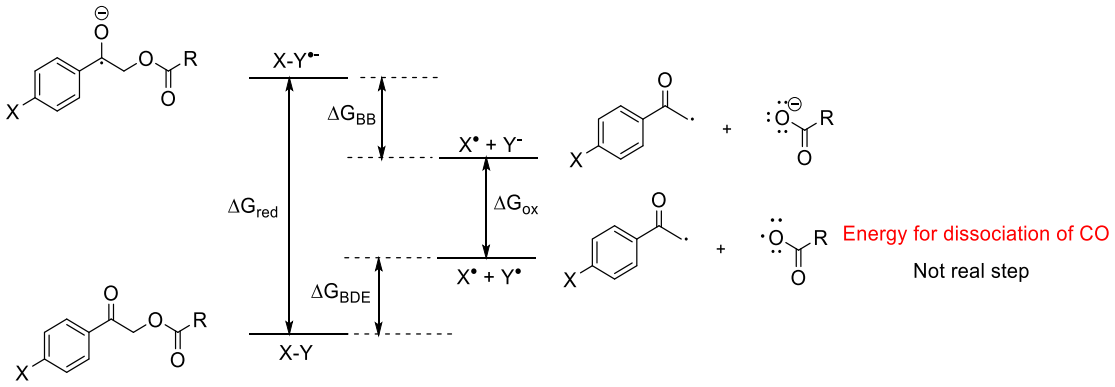


*Figure 30: The free energy change in the bond-breaking of C-O. ΔGred=Gibbs free energy for reduction; $\Delta G_{BB}$=Gibbs free energy for bond-breaking; $\Delta G_{ox}$=Gibbs free energy for oxidation; $\Delta G_{BDE}$=Gibbs free energy for bond dissociation energy.*

## 4.2 Focus on N-Methyl-4-picolinium esters as model substrates

In this thesis the photodeprotection of N-Methyl-4-picolinium esters is studied. The general reaction is shown in Figure 31.

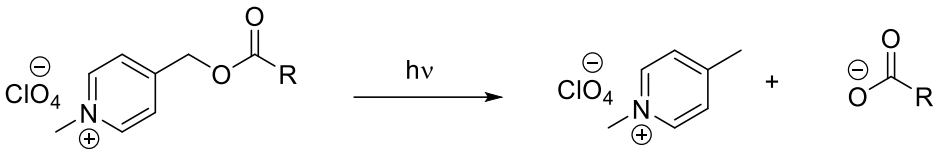


*Figure 31: general reaction for photodeprotection of N-Methyl-4-picolinium esters.*

The importance of the perchlorate as counterion makes that the compound does not absorb in the UV-visible region thus avoiding direct photolysis, which occurs instead in the presence of other counterions such as iodide[28]. This importance was demonstrated by Kunsberg and co workers. Although the perchlorate salts absorb only at low wavelengths (<320 nm), it was found that the iodide salts absorb between 350 and 450 nm. This is attributed to a charge-transfer absorption of the picolinium/iodide ion pair. Irradiation of such charge- transfer bands creates a species that is a caged radical pair consisting of radical and iodine atom. Therefore, photolysis of these salts would lead to fragmentation of the C-O bond (Figure 32).

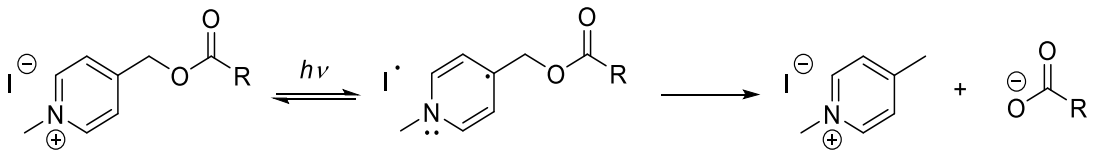


*Figure 32: charge-transfer absorption.*

In any case, the photodeprotation mechanism is reported in Figure 33.

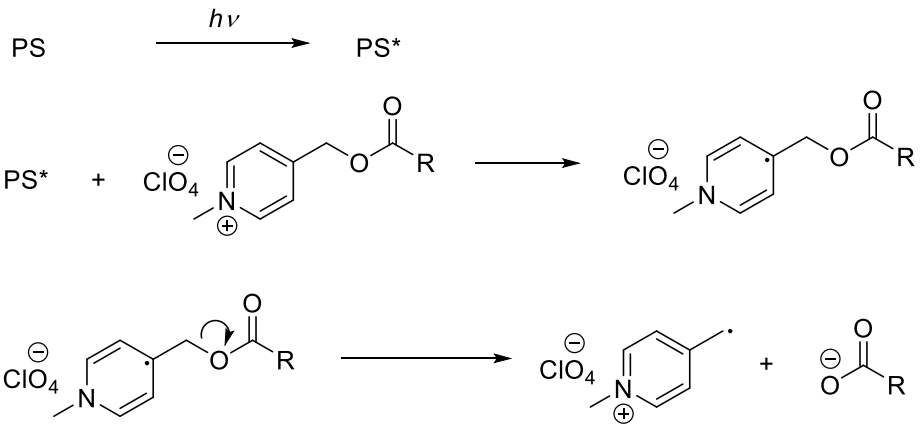


*Figure 33: photodeprotation mechanism.*

# 5 Aim of the thesis

In this thesis a library of CDs having different structural/morfological features are used as photosenitizers for promote light induced photo-reductive cleavage of C-O bonds, by using picolinium esters as model PRPG substrates. With this aim, starting from commercially available octanoic acid, benzoic acid, p-nitrobenzoic acid and 4-(Hydroxymethyl)pyridine three model substrates were synthethised by using a four-step procedure as indicated in Figure 34.

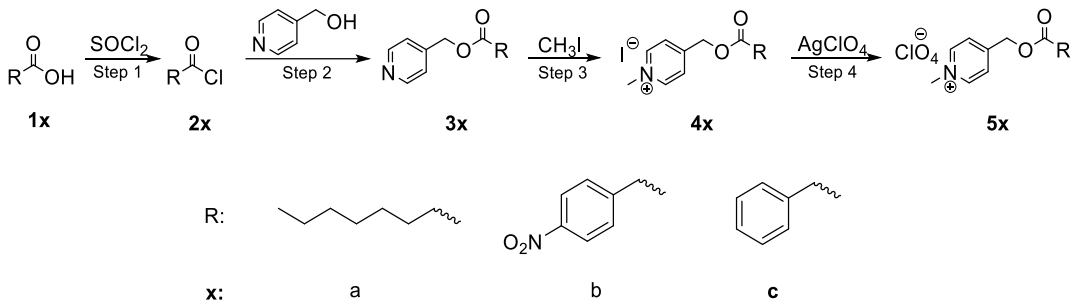


*Figure 34: general scheme for protection reaction.*

For analytical purposes the theoretical photocleavage (7 an 9) products were also prepared following the one step procedure reported in Figure 35.


*Figure 35: theoretical products deriving from the photoclavage.*

Using the PRPG **5a-c** as models, the C-O bond breaking reaction were optimized and the effects of type of CDs, concentration of CDs, concentration of the sacrificial donor, oxygen and light source were investigated. The reactivities were carried out performing photocatalysis in an NMR tube and following the reaction profiles (*via* NMR) at different light exposure times as described in the experimental section.

Furthermore, the electrochemical properties of both the CDs and the substrates **5a-c** were studied through cyclic voltammetry measurements.

The photoreactivities and electrochemical data were then rationalized considering both the HOMO-LUMO gap of the CDs and the reduction potentials of the esters. From the overall experimental evidence, a new revised photo-cleavage mechanism was proposed.

# 6 Results and discussion: photocatalysis

## 6.1 C-O bond photocleavage

In this section we report all the data obtained from the photodeprotection reactions of the carboxylic acids used. Contextually, the photodeprotection of the ester (**5**) yields to the formation of the desired acid (**1**) and 1,4-dimethylpyridin-1-ium (**9**). As a side reactivity, **1** and the 4-(hydroxymethyl)-1-methylpyridin-1-ium (**7**) could be formed by no light dependent hydrolysis. In Figure 36 the reactions products and their labelling are reported.

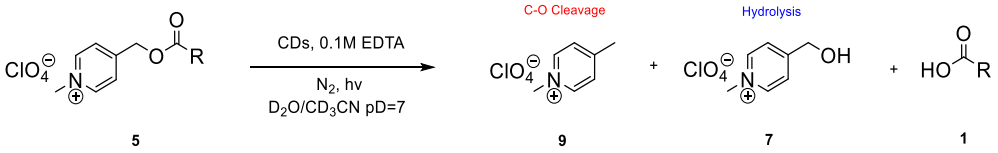


*Figure 36: general scheme for the photodeprotection reaction.*

In the following sections and in the additional supporting information the results of all the tests performed are described and discussed in detail.

### 6.1.1 C-O cleavage of octanoic ester

Figure 37 shows the general scheme for the photodeprotection reaction of octanoic acid.

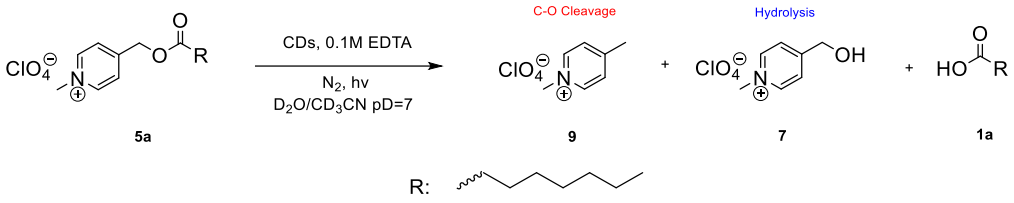


*Fgure* 37: Scheme of photodeprotection reaction of octanoic acid.

In Figure 38 the spectra of the reaction 27.4 at t=0 and t=48 hours are shown along with the one of the products **9**, **7**, **1a**. The formation of octanoic acid **1a** can be monitored by using the triplet **a**. The singlet **b** allowed to investigate the formation of the hydrolysis byproduct **7**. The formation of the cleavage product **9** can be followed by doublet **c**. In order to evaluate the conversion of the substrate **5a** the integration of doublet **d**, singlet **e**, or triplet **f** was measured. Each signal and the corresponding nucleus are shown in the figure. The terminal protons of both octanoic acid **1a** and substrate **5a** fall at the same chemical shift and are used as internal standard **std**.

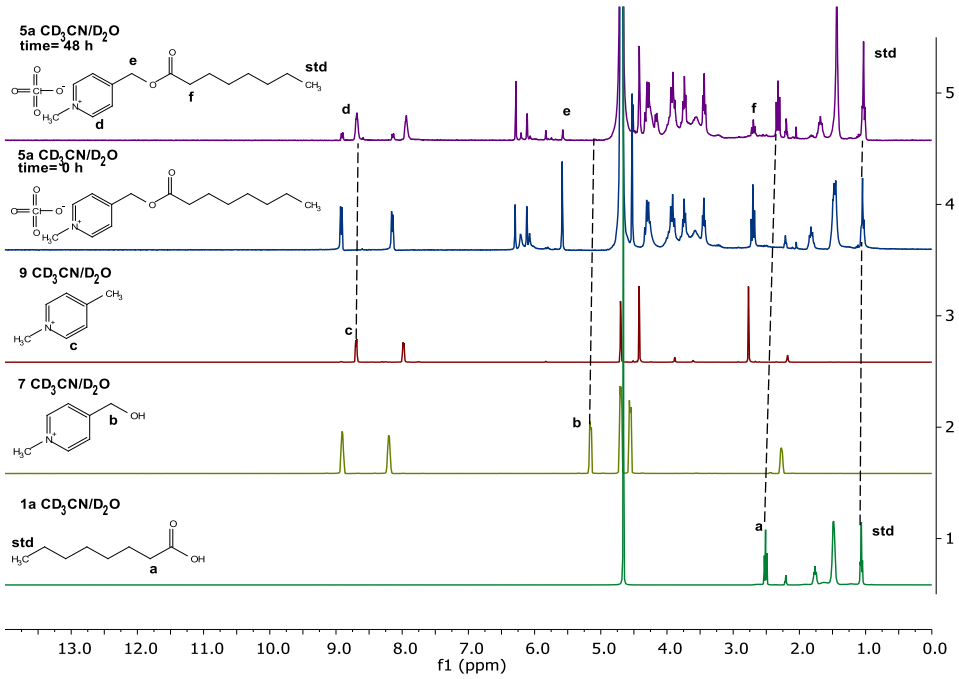


*Figure 38: [1]H NMR characteristic signals to follow the C-O cleavage. Experiment 27.4.*

The use of the above indicated signals has therefore allowed to show in a graph the trend of the starting substrate concentrations **5a** and C-O cleavage and hydrolysis products **1a**, **7**, **9**. In Figure 39 the evolution of the photocatalytic reaction is shown along with the concentrations profile of **5a, 1a**, **7**, **9** and the overall mass balance.

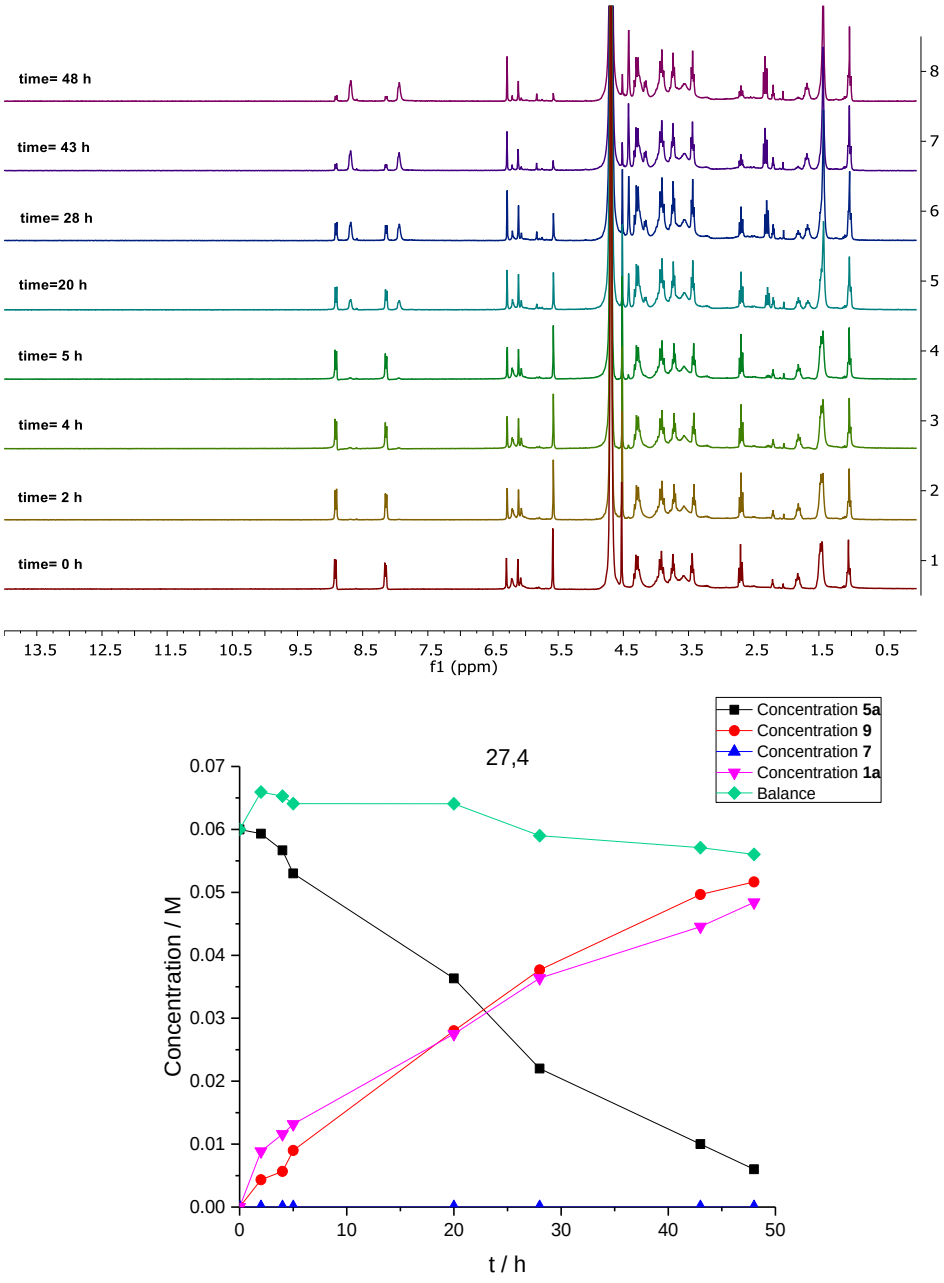


*Figure 39: $^{1}$H NMR evolution and relative concentration profiles for the photodeprotection of octanoic acid. Experiment 27.4.*

A $^{13}C$ NMR spectra comparison between **1a**, **7**, **9** and at the end of the reaction were also performed to further analyze the evolution of the reaction (Figure 40). After 48 hours of exposure the photocleavage product **9** could be identify by the signal **c**. Moreover, the side product **7** was also been detected due to the presence of the characteristic signals **a** and **b**. The latters are of slight entity confirming the low degree of hydrolysis, therefore the photodeprotection of the acid results to be the main reaction. Other characteristic signals of **1a**, **7,** and **9** are not reliable, consequently they were not taken in consideration.

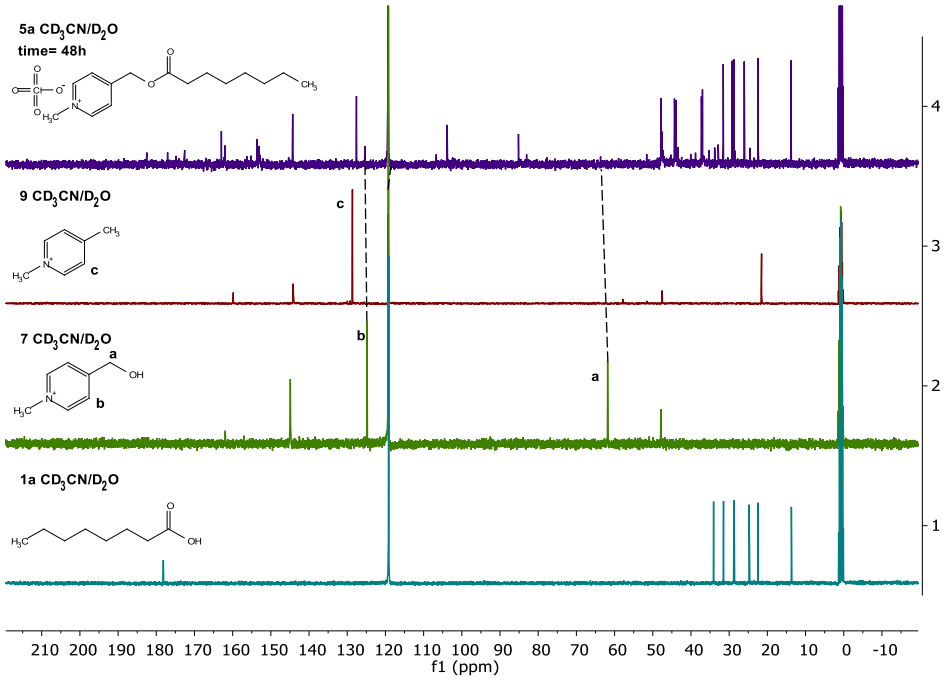


*Figure 40: $^{13}C$ NMR characteristic signals to follow the C-O cleavage. Experiment 27.4*

In supporting informations the procedure for the calculation of concentration profiles and deprotection products were describes in more detail.

Different type of CDs, concentrations, sacrificial donor, effect of the light, oxygen and the comparison with a common photosensitizer such as $Ru(Bpy)_3^{2+}$ were studied and the results are reported hereafter.

#### *6.1.1.1 Tests on different types of CDs*

First, we tested the different CDs as photocatalysts in the photodeprotection reaction of octanoic acid. All tests were performed using 20 mg/ml of CDs, 0.1 M EDTA as sacrificial donor, under nitrogen, using the same light source and pD=7 for 48 hours (defined hereafter as "standard conditions"). The results are shown in Table 1. Experiments 15-18 were performed in duplicate and average results are reported.

| **Exp n°** | **Cat** | **Cat** | **EDTA** | **hv** | **t** | **Conversion 5a** | **Yield ratio 9/7/1a** | **Selectivity C-O Cleavage** |
|---|---|---|---|---|---|---|---|---|
| | | (mg/ml) | (M) | | (h) | (%) | (%) | (%) |
| 15.1, 15.2 | g-CDs | 20 | 0.1 | UV | 48 | 53 | 49/3/52 | 93 |
| 16.1, 16.2 | a-CDs | 20 | 0.1 | UV | 48 | 15 | 12/0/15 | 100 |
| 17.1, 17.2 | g-N-CDs | 20 | 0.1 | UV | 48 | 43 | 32/0/25 | 100 |
| 18.1, 18.2 | a-N-CDs | 20 | 0.1 | UV | 48 | 63 | 61/0/63 | 100 |
| 19.1 | a-Glu | 20 | 0.1 | UV | 48 | 66 | 63/0/66 | 100 |
| 20.1 | g-Glu | 20 | 0.1 | UV | 48 | 53 | 53/0/53 | 100 |
| 21.3 | g-N-Glu | 20 | 0.1 | UV | 48 | 52 | 51/9/58 | 86 |
| 22.1 | a-Fru | 20 | 0.1 | UV | 48 | 43 | 37/5/43 | 89 |
| 21.3 | g-N-Glu | 20 | 0.1 | UV | 48 | 45 | 37/5/49 | 88 |
| 24.1 | g-N-Fru | 20 | 0.1 | UV | 48 | 30 | 30/0/30 | 100 |

*Table 1: tests on a CDs library.*

From the table it is possible to notice that in all the tests hydrolysis is minimal. The selectivity of C-O cleavage is instead variable from 85% to 100%. Since the produced octanoic acid **1a** can derive both from photodeprotection as well as from hydrolysis, the photodeprotection efficiency is estimated from the yield of compound **9**. From the table it thus emerges that the order of reactivity and effectiveness for photocatalytic photodeprotection reaction with the CDs follows the order: a-CDs < g-N-Fru-CDs ≈ g-N-CDs < g-N-Glu-CDs ≈ a-Fru-CDs < g-CDs < g-N-Glu-CDs ≈ g-Glu-CDs < a-N-CDs ≈ a-Glu-CDs. The a-N-CDs were selected as a model catalyst for the further studies.

### *6.1.1.2 Effect of concentration*

The effect of the amount of CDs on photocatalysis was then investigated. Table 2 reports the results obtained performing the reaction using different quantities of a-N-CDs and in standard conditions.

| **Exp n°** | **Cat** | **Cat** | **EDTA** | **hv** | **t** | **Conversion 1** | **Yield ratio 9/7/1a** | **Selectivity C-O Cleavage** |
|---|---|---|---|---|---|---|---|---|
| | | (mg/ml) | (M) | | (h) | (%) | (%) | (%) |
| 25.3 | a-N-CDs | 0 | 0.1 | UV | 48 | 13 | 9/16/13 | 60 |
| 27.1 | a-N-CDs | 1 | 0.1 | UV | 48 | 35 | 20/01/31 | 93 |
| 27.2 | a-N-CDs | 5 | 0.1 | UV | 48 | 36 | 24/01/38 | 96 |
| 25.1 | a-N-CDs | 10 | 0.1 | UV | 48 | 58 | 49/1/59 | 99 |
| 18.1, 18.2 | a-N-CDs | 20 | 0.1 | UV | 48 | 63 | 61/0/63 | 100 |

*Table 2: effect of the concentration on the deprotection of octanoic acid.*

From the table it is possible to observe that performing the reaction without CDs led to almost no photodeprotection while hydrolysis increased. Varying the amount of CDs from 1 mg/ml to 20 mg/ml, there is a noticeable increase in photodeprotection yield. In all cases hydrolysis is limited. This behavior is explained by the fact that a greater amount of CDs increase the probability of electronic transfer between the excited state and the substrate to be deprotected.

### *6.1.1.3 Effect of the sacrificial donor*

The effect of the sacrificial donor was studied by comparing two tests in the presence and absence of EDTA in standard condition, the results are shown in Table 3.

| Exp n° | Cat | Cat | EDTA | hv | t | Conversion 1 | Yield ratio 9/7/1a | Selectivity C-O Cleavage |
|---|---|---|---|---|---|---|---|---|
| | | (mg/ml) | (M) | | (h) | (%) | (%) | (%) |
| 18.1, 18.2 | a-N-CDs | 20 | 0.1 | UV | 48 | 63 | 61/0/63 | 100 |
| 25.2 | a-N-CDs | 20 | x | UV | 48 | 52 | 49/1/60 | 98 |

*Table 3: effet of the sacrificial donor.*

It is evident how the presence of the sacrifical donor increases the efficiency of the photodeprotection reaction. The presence of EDTA disfavour the recombination of the exciton by donating an electron to the hole, thus increasing the lifetime of the excited state. Consequently, the higher is the lifetime of the excited state the higher is the probability of electron transfer. Surprisingly, even in the absence of sacrificial donor the photodeprotection took place. A reasonable explanation relies either on the ability of CDs themselves to donate an electron to the holes increasing the lifetime of their excited state, or to the single CDs possessing the necessary lifetime to perform the photo electron transfer (PET).

### *6.1.1.4 Effect of the concentration in the absence of a sacrificial donor*

Since the same CDs works equally in the photodeprotection reaction in the absence of EDTA we have tried to force the conditions and in particular to increase the amount of CDs within the limits of dispersion. These tests were performed in the absence of EDTA, under nitrogen, using the same light source, pD=7 and with different amounts of CDs and the results are shown in Table 4.

| **Exp n°** | **Cat** | **Cat** | **EDTA** | **hv** | **t** | **Conversion 1** | **Yield ratio 9/7/1a** | **Selectivity C-O Cleavage** |
|---|---|---|---|---|---|---|---|---|
| | | (mg/ml) | (M) | | (h) | (%) | (%) | (%) |
| 25.2 | a-N-CDs | 20 | x | UV | 48 | 52 | 49/1/60 | 98 |
| 27.3 | a-N-CDs | 50 | x | UV | 48 | 73 | 66/0/68 | 100 |
| 27.4 | a-N-CDs | 100 | x | UV | 48 | 90 | 86/0/81 | 100 |

*Table 4: effect of the concentration in the absence of a sacrificial donor.*

From the table emerged that by increasing the concentration of 20 mg/ml to 100 mg/ml the efficiency of photodeprotection increases considerably with a 100% selectivity. These results are very promising considering that only CDs can be used to perform the reaction. Once again, the greater amount of CDs increases the probability of electron transfer.

### *6.1.1.5 Effect of oxygen*

The reaction was then tested also under air in order to evaluate the necessity of the inert condition. The effects of the presence of oxygen were observed by comparing two testperformed in standard condition in presence or absence of oxygen. After 48 hours the solution prepared under air exhibit a brown color. The photoreduction results are shown in Table 5.

| Exp n° | Cat | Cat | EDTA | hv | t | Conversion 1 | Yield ratio 9/7/1a | Selectivity C-O Cleavage |
|---|---|---|---|---|---|---|---|---|
| | | (mg/ml) | (M) | | (h) | (%) | (%) | (%) |
| 18.1, 18.2 | a-N-CDs | 20 | 0.1 | UV | 48 | 63 | 61/0/63 | 100 |
| 25.5 | a-N-CDs | 20 | 0.1 | UV | 48 | 74 | 61/7/72 | 90 |

*Table 5: effect of oxygen. 25.5 was performed in oxygen presence.*

As shown in the table the presence of oxygen does not affect the efficiency of photodeprotection, however it is possible to notice an increase in hydrolysis which leads to lower selectivity. This behaviour can be explained by the formation of radical species such as the superoxide ion $O^{2-\cdot}$ which could favor the hydrolysis reaction. In any case, hydrolysis is limited compared to photodeprotection.

### *6.1.1.6 Effect of light*

In order to evaluate the effect of the UV light to trigger the reaction different tests were performed. In more detail, the reaction was performed in standard conditions using two different light sources, UV and visible, and in dark condition. The results are shown in Table 6.

| Exp n° | Cat | Cat | EDTA | hv | t | Conversion 1 | Yield ratio 9/7/1a | Selectivity C-O Cleavage |
|---|---|---|---|---|---|---|---|---|
| | | (mg/ml) | (M) | | (h) | (%) | (%) | (%) |
| 18.1, 18.2 | a-N-CDs | 20 | 0.1 | UV | 48 | 63 | 61/0/63 | 100 |
| 25.4 | a-N-CDs | 20 | 0.1 | x | 48 | 0 | 0/0/0 | 0 |
| 28.1 | a-N-CDs | 20 | 0.1 | Vis | 48 | 7 | 6/0/7 | 100 |

*Table 6: effect of the light source.*

In absence of a light source the photodeprotection reaction does not occur indicating the main role of light. The best result was obtained employing a UV source, while when a visible light is used, photodeprotection is much less efficient. This is due to the maximum absorption wavelength of CDs that exhibits greater absorption intensity in the UV zone.

#### *6.1.1.7 Comparison with $Ru(bpy)_3^{2+}$*

Finally, we performed the photodeprotection reaction replacing CDs with $Ru(bpy)_3^{2+}$ a standard photosensitizer for photocatalysis. The comparison was made using the least possible amount of Ru while for the CDs we taken into account the stoichiometric test (with the higher amount of CDs and without EDTA) and the catalytic (stardand conditions). Due to the maximum absorption wavelength the Ru catalysed reaction was performed under visible light, while for the CDs a UV source was employed, the results are shown in Table 7.

| **Exp n°** | **Cat** | **Cat** | **EDTA** | **hv** | **t** | **Conversion 1** | **Yield ratio 9/7/1a** | **Selectivity C-O Cleavage** |
|---|---|---|---|---|---|---|---|---|
| | | (mg/ml) | (M) | | (h) | (%) | (%) | (%) |
| 18.1, 18.2 | a-N-CDs | 20 | 0.1 | UV | 48 | 63 | 61/0/63 | 100 |
| 27.4 | a-N-CDs | 100 | x | UV | 48 | 90 | 86/0/81 | 100 |
| 26.2 | $Ru(bpy)_3^{2+}$ | 5 % mol | 0.1 | Vis | 48 | 100 | 97/3/100 | 97 |

*Table 7: comparison of photodeprotation between $Ru(bpy)_3^{2+}$ and CDs.*

From the table it is clear that for both tests the hydrolysis is almost absent and the selectivity of the C-O cleavage is 100%. Surprisingly, the photo-reactivity of the here developed CDs, both under catalytic or "stoichiometric" conditions, are comparable to the one observed by using the well known and extensively used ruthenium complex. Even if when using higher quantity of CDs, the ease of synthesis from renewable sources, the non-toxic properties and the low cost of these nanomaterials compete with the effectiveness of metal complexes. Instead, $Ru(bpy)_3^{2+}$ complex has the greatest disadvantage of being extremely expensive, containing the metal and therefore not usable in green optics, difficult to recover and unstable over time.

#### *6.1.1.8 Conclusions for the photodeprotection of octanoic acid*

In conclusion we studied the effect on the deprotection of octanoic acid for a CDs library, and with the best performer CDs, the effects of light, concentrations, sacrificial donor and oxygen on photocatalysis were investigated. Finally, we compared this system with one of the most common and efficient metal complexes used in photocatalysis. The results obtained are completely encouraging. The photodeprotection reaction of octanoic acid is the starting point for the controlled of C-O bonds cleavage.

### 6.1.2 C-O cleavage of p-nitrobenzoic ester

Figure 41 shows the general scheme for the photodeprotection reaction of p-nitrobenzoic acid.

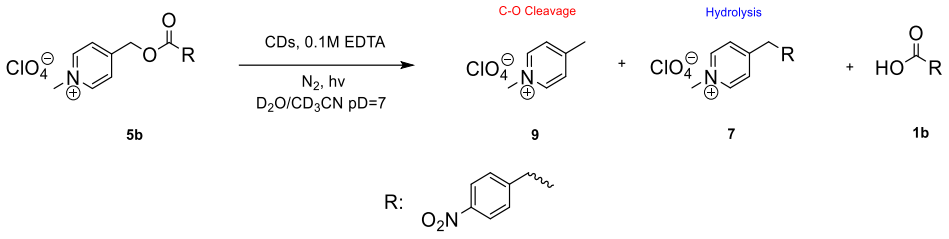


*Fgure* 41: Scheme of photodeprotection reaction of p-nitrobenzoic acid.

In Figure 42 the spectra of the reaction 29.1 at t=0 and t=48 hours are shown along with the one of the products **9**, **7**, **1b**. The formation of p-nitrobenzoic acid **1b** can be monitored by using the doublet **a**. The singlet **b** allowed to investigate the formation of hydrolysis product **7**. The formation of the cleavage product **9** can instead be followed by singlet **c**. In order to evaluate conversion of the substrate **5b** the integration of doublet **d** or singlet **e** were measured. Each signal and the corresponding nucleus are shown in the figure. The terminal protons of ethyl acetate are used as internal standard **std** in concenration of 0.006M.

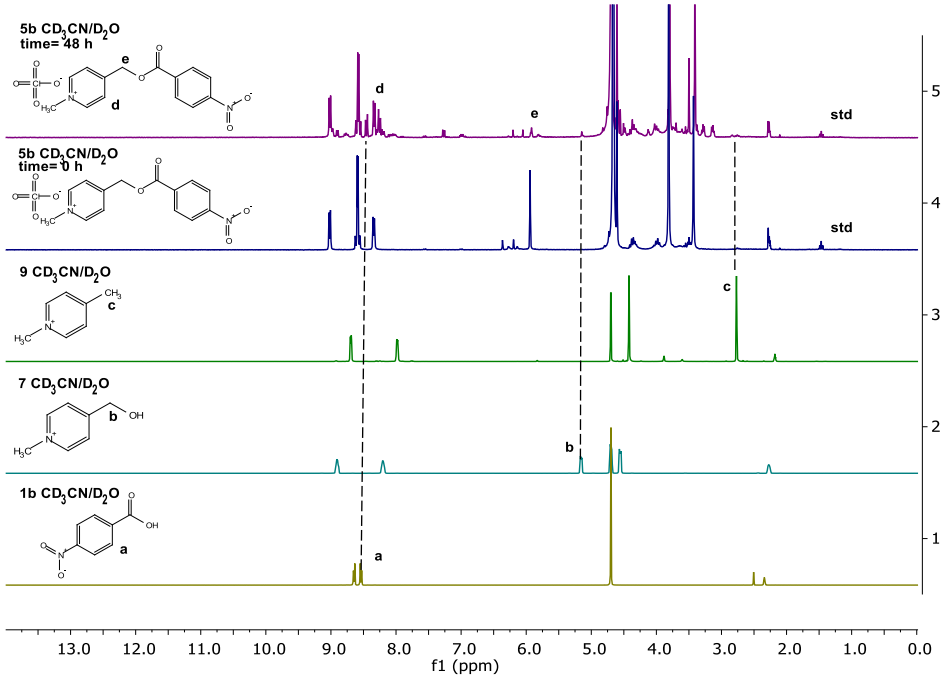


*Figure 42: [1]H NMR characteristic signals to follow the C-O cleavage. Experiment 29.1.*

The use of the above indicated signals has therefore allowed to show in a graph the trend of the starting substrate concentrations **5b** and CO cleavage and hydrolysis products **1b**, **7**, **9**. In Figure 43 the evolution of the photocatalytic reaction is shown along with the concentrations profile of **5b**, **1b**, **7**, **9**, and the overall mass balance.

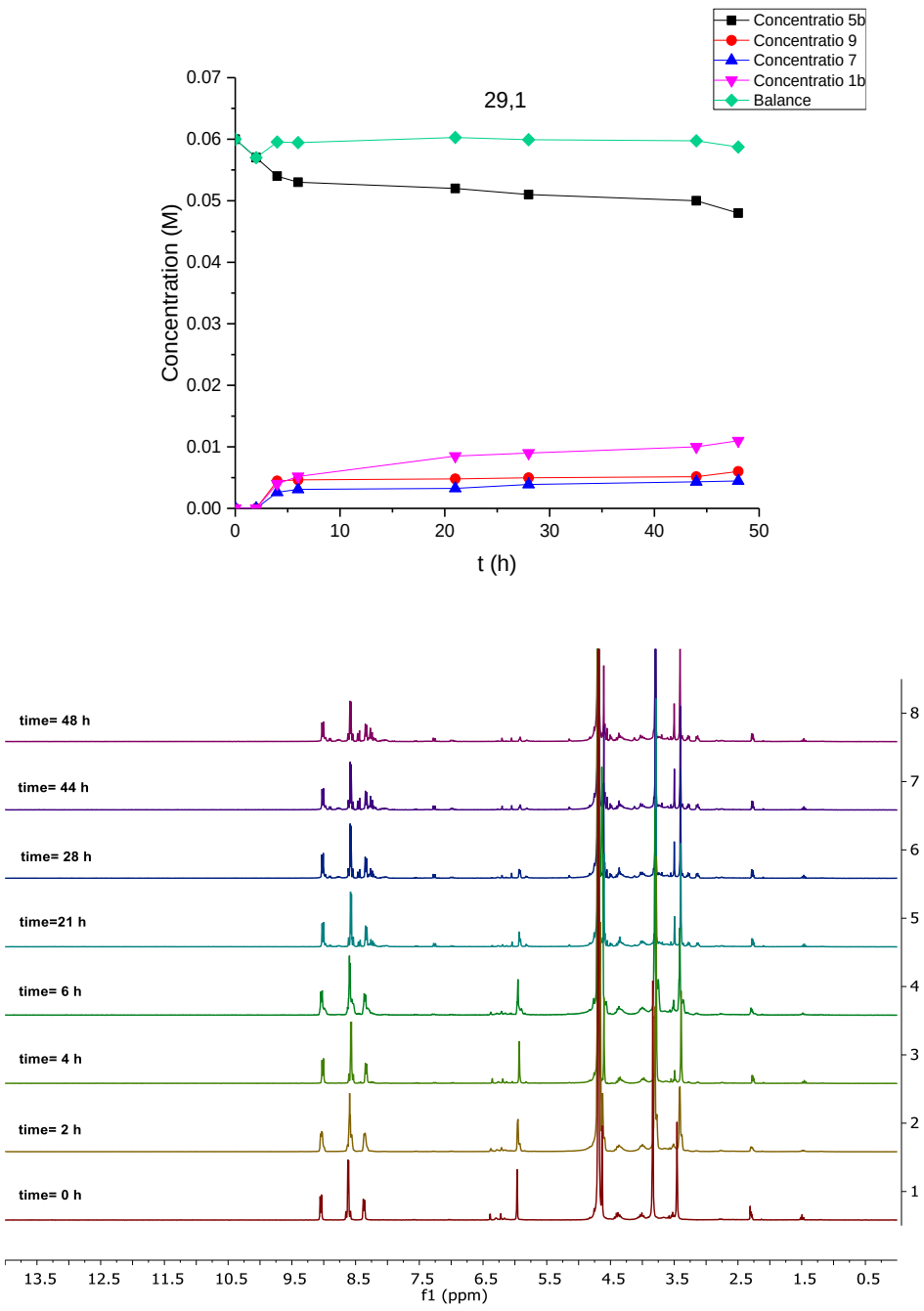


*Figure 43: Spectrum $^{1}H$ NMR evolution over time and relative concentration profiles for the photodeprotection of p-nitrobenzoic acid. Experiment 29.1.*

A $^{13}C$ NMR spectra comparison between **1b**, **7**, **9** and at the end of the reaction were also performed to further analyze the evolution of the reaction (Figure 44). After 48 hours of exposure, no characteristic signals of the product **9** were noticed, in particular, the one associated with carbon **b**. Contrariwise, for the side product **7** the signal of carbon **a** was present although weak. These results agree with the $^{1}H$ NMR spectra which provide a slight amount of both hydrolysis and photodeprotection. The low amount of cleavage products **9** and hydrolysis **7** led to hardly observable signals in the $^{13}C$ NMR spectra. Other characteristic signals of **1b**, **7** and **9**, are not reliable, consequentialy they were not taken in consideration.

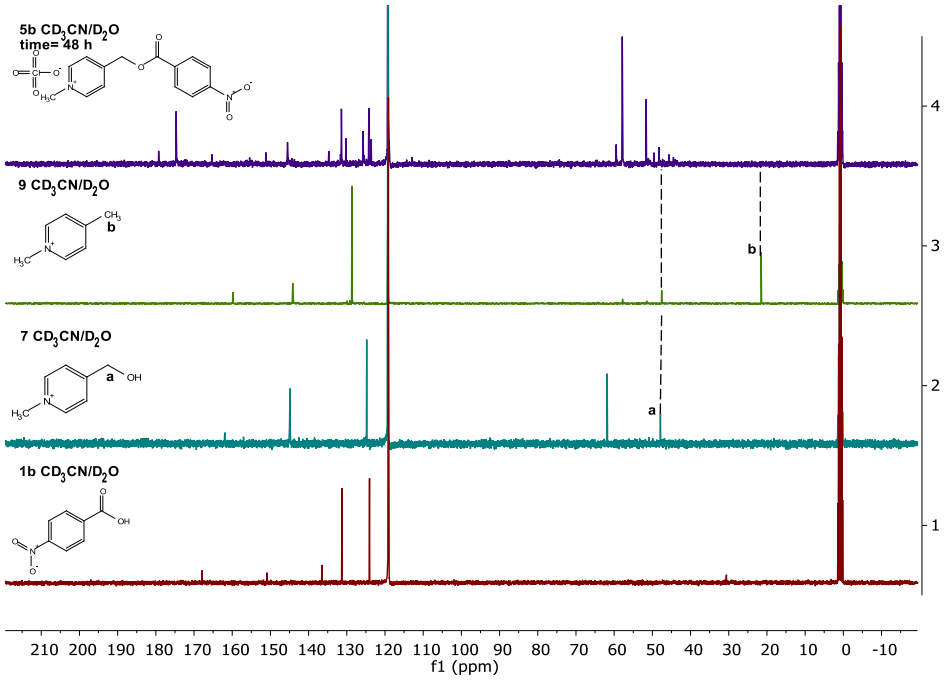


*Figure 44: $^{13}C$ NMR characteristic signals to follow the C-O cleavage. Experiment 29.1.*

In supporting informations the procedure for the calculation of concentration profiles and deprotection products were describes in more detail.

### *6.1.2.1 Specific tests*

The photodeprotation reaction of p-nitrobenzoic acid was studied both in stoichiometric condition, with higherer amount of CDs and without EDTA, and standard conditions. Table 8 shows the results of these studies.

| Exp n° | Cat | Cat | EDTA | hv | t | Conversion 5b | Yield ratio 9/7/1b | Selectivity C-O Cleavage |
|---|---|---|---|---|---|---|---|---|
| | | (mg/ml) | (M) | | (h) | (%) | (%) | (%) |
| 29.1 | a-N-CDs | 20 | 0.1 | UV | 48 | 20 | 10/7/18 | 57 |
| 29.2 | a-N-CDs | 100 | x | UV | 48 | 28 | 0/25/27 | 0 |

*Table 8: results for the photodeprotection of p-nitrobenzoic acid.*

From the table it is possible to observe that for both tests there is a considerable hydrolysis highlighted by the presence of product **7**. Moreover, in the absence of the EDTA, the photodeprotection reaction and so product **9** is absent despite the presence of a large quantity of CDs. Therefore, EDTA has a key role in photodeprotection, once again increasing the lifetime of excited states by delaying the recombination of the exciton.

### *6.1.2.2 Quantification by GC*

Since the NMR signal of the acid formed may be of a questionable nature, the presence of the latter has been revealed also by gaschromatography analysis. The quantification was made by constructing a calibration curve of p-nitrobenzoic acid using 0.006M biphenyl as internal standard. GC injection of the unknown sample was made at the end of photocatalysis without treatment. In Figure 45 the calibration curve is shown with the respective equation.

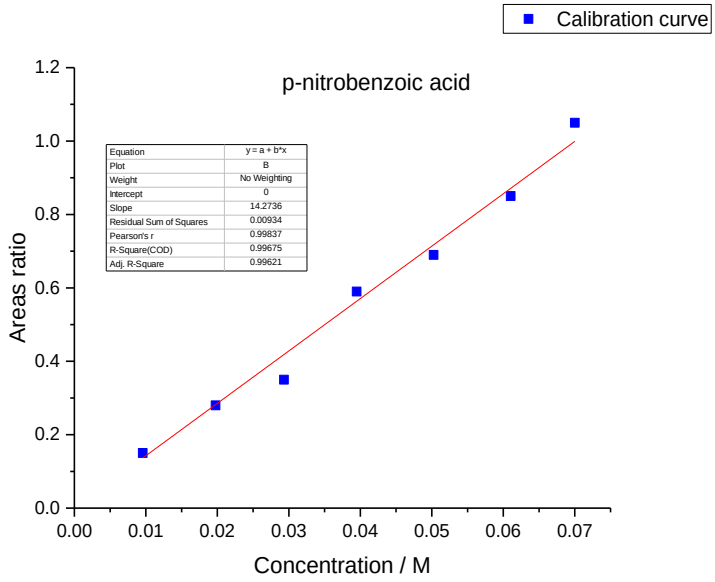


*Figure 45: calibration curve for the quantification of p-nitrobenzoic acid.*

The quantifications of the acid at the end of the photocatalysis tests are reported in Table 9

| **Exp n°** | **Cat** | **Cat** | **EDTA** | **hv** | **t** | **Concentration 1b** | **Yield 1b** |
|---|---|---|---|---|---|---|---|
| | | (mg/ml) | (M) | | (h) | (M) | (%) |
| 29.1 | a-N-CDs | 20 | 0.1 | UV | 48 | 0.012 | 20 |
| 29.2 | a-N-CDs | 100 | x | UV | 48 | 0.019 | 31 |

*Table 9: quantification of p-nitrobenzoic acid by GC.*

The table shows how the as described quantification led to results comparable to the one obtained by the NMR.

### 6.1.3 C-O cleavage of benzoic ester

Figure 46 shows the general scheme for the photodeprotection reaction of benzoic acid.

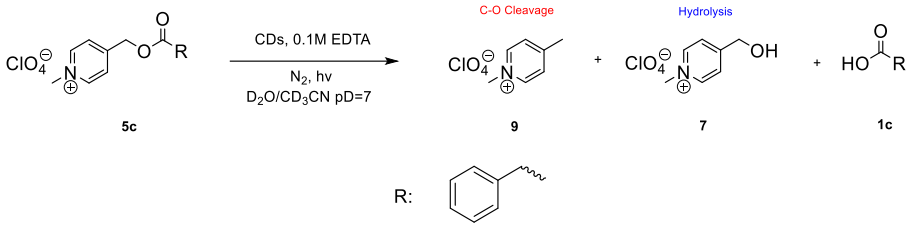


*Fgure* 46: Scheme of photodeprotection reaction of benzoic acid.

In Figure 47 the spectra of the reaction 29.3 at t=0 and t=48 hours are shown along with the one of the products **9**, **7**, **1c**. The formation of benzoic acid **1c** results impossible to follow. The singlet **a** allowed to investigate the formation of the hydrolysis byproduct **7**. The formation of the cleavage product **9** can be followed by singlet **b**. In order to evaluate the conversion of the substrate **5c** the integration of singlet **c** was measured. Each signal and the corresponding nucleus are shown in the figure. The terminal protons of ethyl acetate are used as internal standard **std** in concenration of 0.006M.

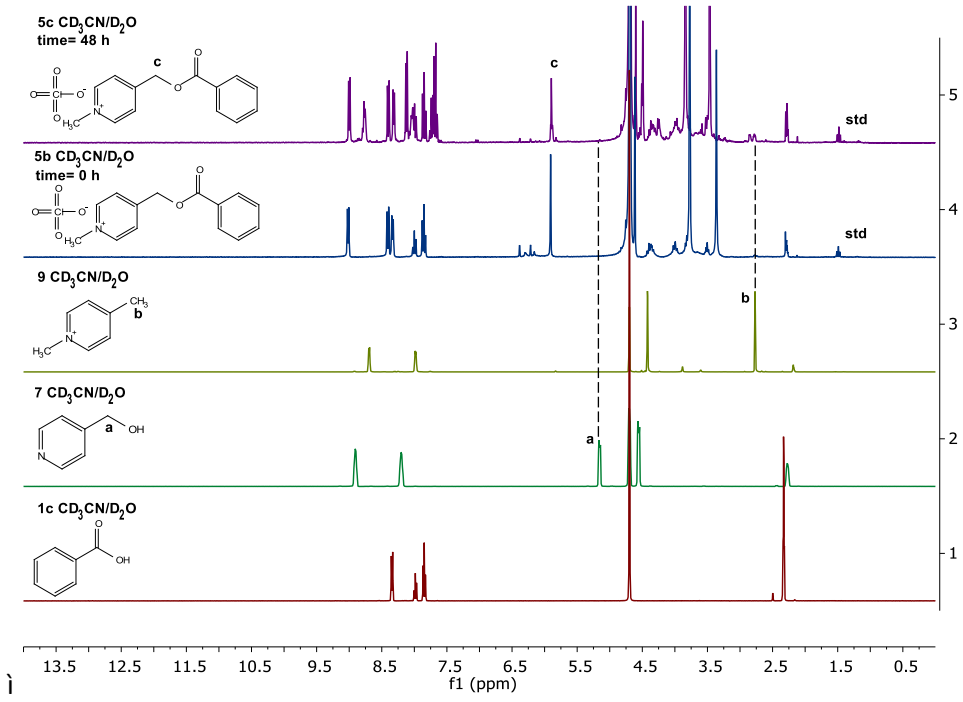


*Figure 47: [1]H NMR characteristic signals to follow the C-O cleavage. Experiment 29.3.*

The use of the above indicated signals has therefore allowed to show in a graph the trend of the starting substrate concentrations **5c** and C-O cleavage and hydrolysis products **7**, **9**. The concentration profile of benxoic acid **1c** is not reported because it is not possible to follow a characteristic signal, therefore the mass balance is not reported. In Figure 48 the evolution of the photocatalytic reaction is shown along with the concentrations profile of **5c**, **7**, **9**.

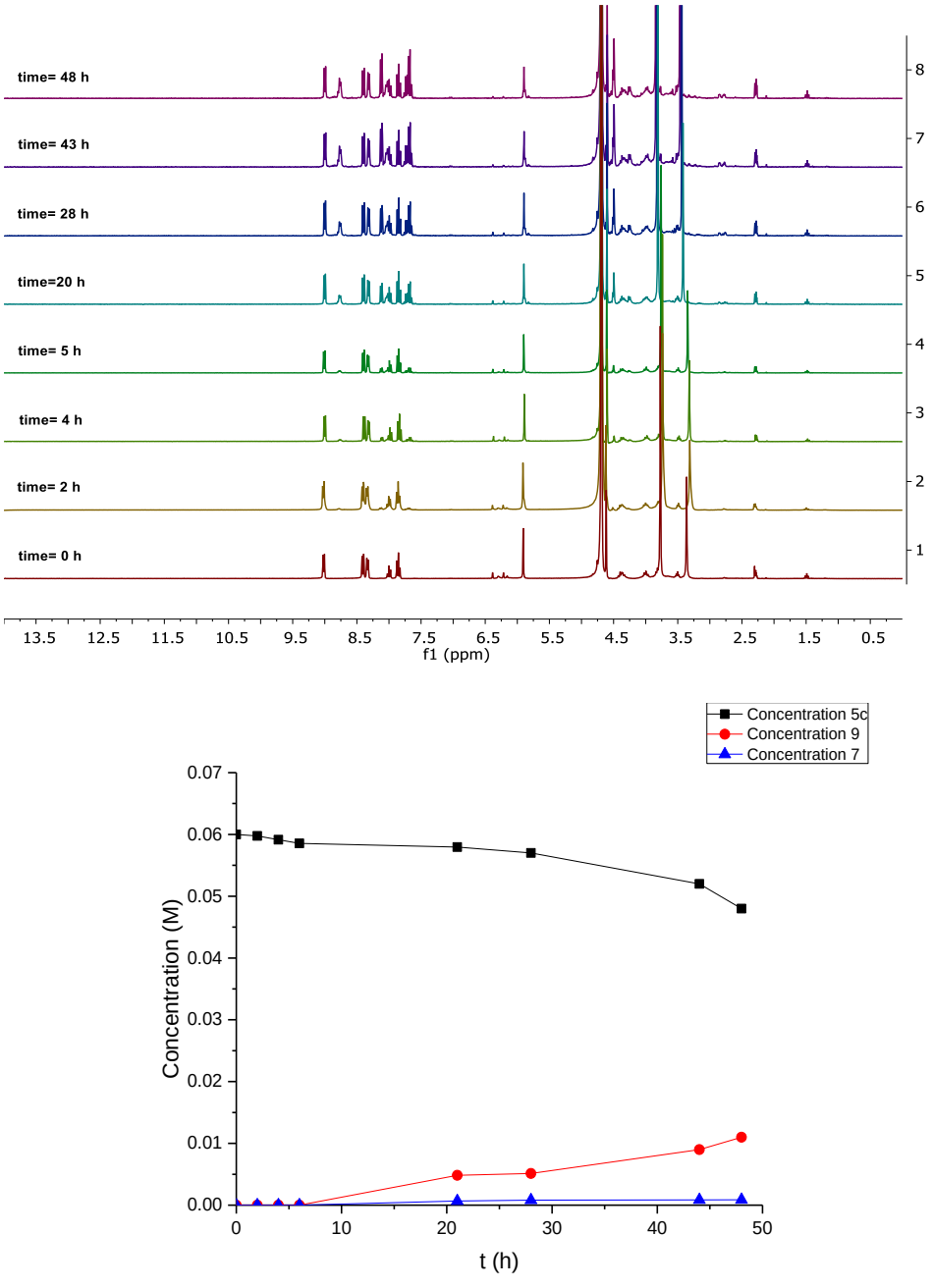


*Figure 48: Spectrum $^{1}H$ NMR evolution over time and relative concentration profiles for the photodeprotection of benzoic acid. Experiment 29.3.*

A $^{13}C$ NMR spectra comparison between **1c**, **7**, **9** and at the end of the reaction were also performed to further analyze the evolution of the reaction (Figure 49). After exposure to 48 hours there are no characteristic signals of the photocleavage product **9** in particular, the one associated with carbon **b**. Contrariwise, for the side product **7** the signal of carbon **a** was present although weak. These results agree with the $^{1}H$ NMR spectra which provide a slight amount of both hydrolysis and photodeprotection. The low amount of cleavage products **9** and hydrolysis **7** are such that they are hardly observable in the $^{13}C$ NMR spectra. Other characteristic signals of the benzoic acid **1c**, of the hydrolysis product **7** and of the photodeprotection byproduct **9**, are ambiguous to be recognized, therefore we limit ourselves to considering only the most reliable signals.

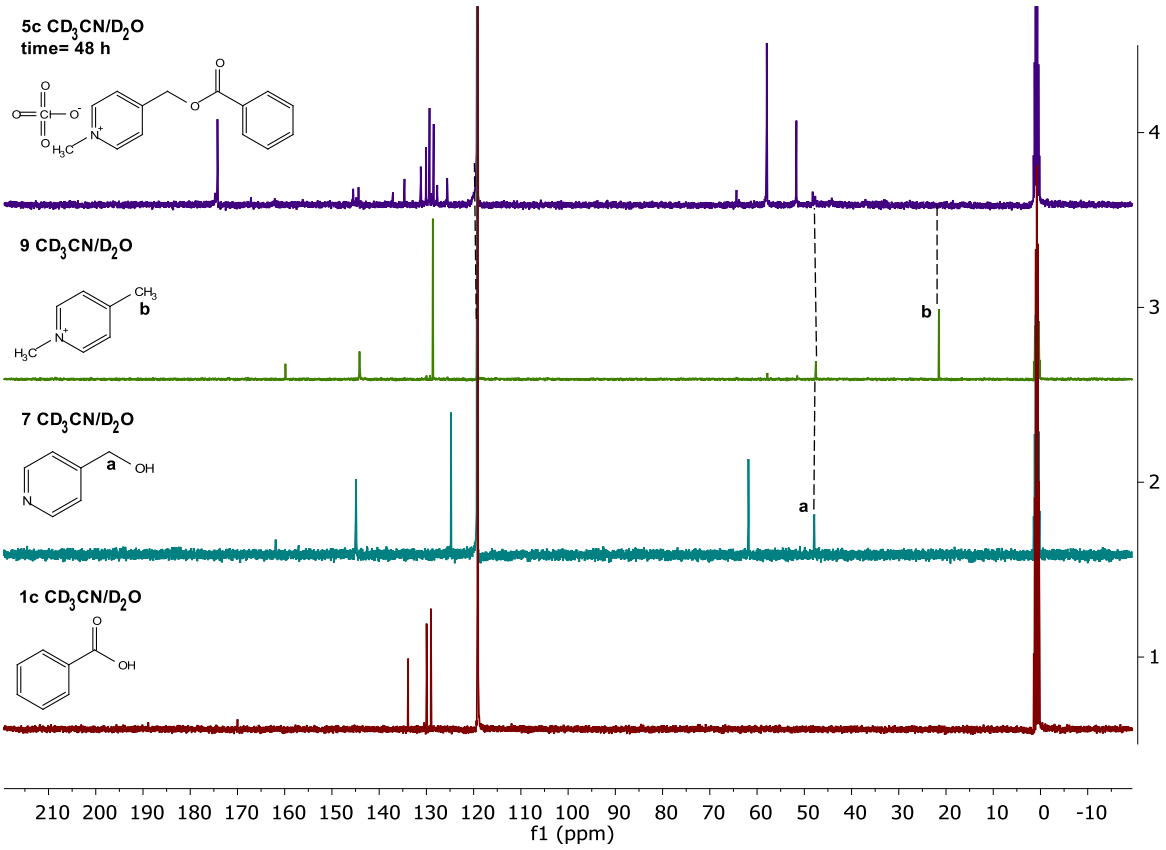


*Figure 49: $^{13}C$ NMR characteristic signals to follow the CO cleavage. Experiment 27.4*

In supporting informations the procedure for the calculation of concentration profiles and deprotection products were describes in more detail.

### *6.1.3.1 Specific tests*

The photodeprotation reaction of benzoic acid was studied both in stoichiometric condition, with higherer amount of CDs and without EDTA, and standard conditions. Table 10 shows the results.

| Exp n° | Cat | Cat | EDTA | hv | t | Conversion 5c | Yield ratio 9/7/1c | Selectivity C-O Cleavage |
|---|---|---|---|---|---|---|---|---|
| | | (mg/ml) | (M) | | (h) | (%) | (%) | (%) |
| 29.3 | a-N-CDs | 20 | 0.1 | UV | 48 | 20 | 18/1/- | 33 |
| 29.4 | a-N-CDs | 100 | x | UV | 48 | 61 | 4/0/- | 100 |

*Table 10: results for the photodeprotection of benzoic acid.*

From the table it is possible to observe that for both tests hydrolysis is totally absent. Moreover, in the absence of the EDTA sacrificial donor, the photodeprotection reaction and so the formation of product **9** is really low despite the presence of a large quantity of CDs. Therefore, EDTA has a key role in photodeprotection, once again increasing the lifetime of excited states by delaying the recombination of the exciton. In this case it was not possible to quantify the presence of acid **1c**. In the test in the absence of EDTA it is also possible to notice a conversion of the substrate **5c** high, which however leads to undetected secondary products.

### *6.1.3.2 Quantification by GC*

As the formation of benzoic acid can not be followed by NMR it has been confirmed by gaschromatography. The quantification was made by constructing a calibration curve using biphenyl as internal standard in 0.006M concentration. GC injection of the unknown sample was made at the end of photocatalysis without treatment. In Figure 50 the calibration curve is shown with the respective equation.

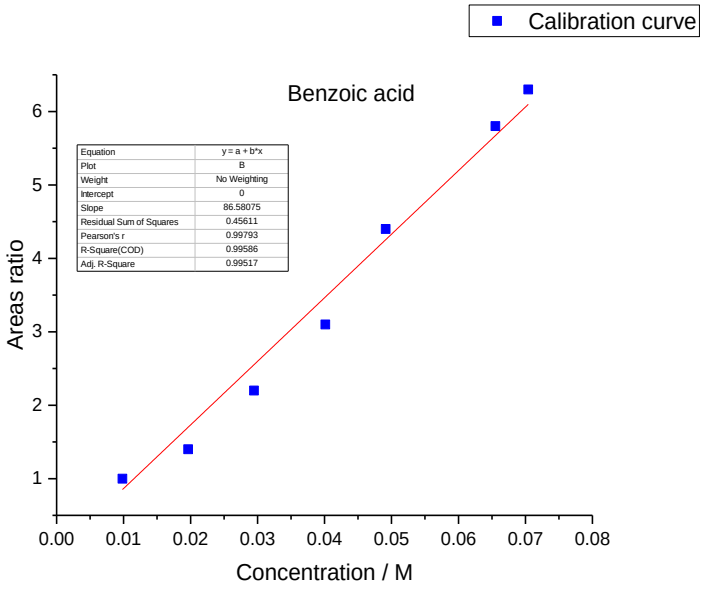


*Figure 50: calibration curve for the quantification of benzoic acid.*

The quantification of the acid at the end of the photocatalysis tests is reported in Table 11

| Exp n° | Cat | Cat | EDTA | hv | t | Concentration 1c | Yield 1c |
|---|---|---|---|---|---|---|---|
| | | (mg/ml) | (M) | | (h) | (M) | (%) |
| 29.1 | a-N-CDs | 20 | 0.1 | UV | 48 | 0.013 | 21 |
| 29.2 | a-N-CDs | 100 | x | UV | 48 | 0.003 | 4 |

*Table 11: quantification of benzoic acid by GC.*

The table shows how the quantification of the acid by gaschromatography results in total agreement with the sum of the products of hydrolysis and cleavage by NMR.

### 6.1.4 Comparison of substrates

The photodeprotection of **5a**, **5b** and **5c** were compared in both catalytic and stoichiometric conditions. In Table 12 we report the comparison.

| Exp n° | Sub | Cat | EDTA | hv | t | Conversion 5 | Yield ratio 9/7/1 | Selectivity C-O Cleavage |
|---|---|---|---|---|---|---|---|---|
| | | (mg/ml) | (M) | | (h) | (%) | (%) | (%) |
| 18.1, 18.2 | 5a | 20 | 0.1 | UV | 48 | 63 | 61/0/63 | 100 |
| 29.1 | 5b | 20 | 0.1 | UV | 48 | 20 | 10/7/18 | 57 |
| 29.3 | 5c | 20 | 0.1 | UV | 48 | 20 | 18/1/21* | 33 |
| 27.4 | 5a | 100 | x | UV | 48 | 90 | 86/0/81 | 100 |
| 29.2 | 5b | 100 | x | UV | 48 | 28 | 0/25/27 | 0 |
| 29.4 | 5c | 100 | x | UV | 48 | 61 | 4/0/4* | 100 |

*Table 12: comparison of reactivity between substrates. All photocatalysis was performed in the presence of a-N-CDs. The apex * indicates that the data were obtained by GC.*

In both the conditions tested the reactivity order was **5b** <**5c** <**5a**. However, for the photodeprotection of the substrate **5a** there is an increase in the efficiency employing a large excess of CDs, while for the substrates **5b** and **5c**, the absence of EDTA limits the photodeprotection reaction. In these cases, the absence of EDTA once again favor the recombination of the exciton limiting the electronic transfer. Instead, for the substrate **5a** the absence of EDTA is not a limiting factor as the electronic transfer is fast enough to avoid the recombination of the exciton.

The reactivity order of **5a**, **5b**, **5c** towards photocleavage can only be explained if we consider the substrate reduction potentials. These potentials will be studied in greater detail in the section dedicated to electrochemical methods. As an anticipation the substrates that have a higher reduction potential and are therefore easier to reduce (lower $\Delta G_{Red}$) will be the ones that will face a more difficult breaking of the C-O bond (lower $\Delta G_{Cleavage}$) and viceversa. This can be better understood by looking at Figure 51.

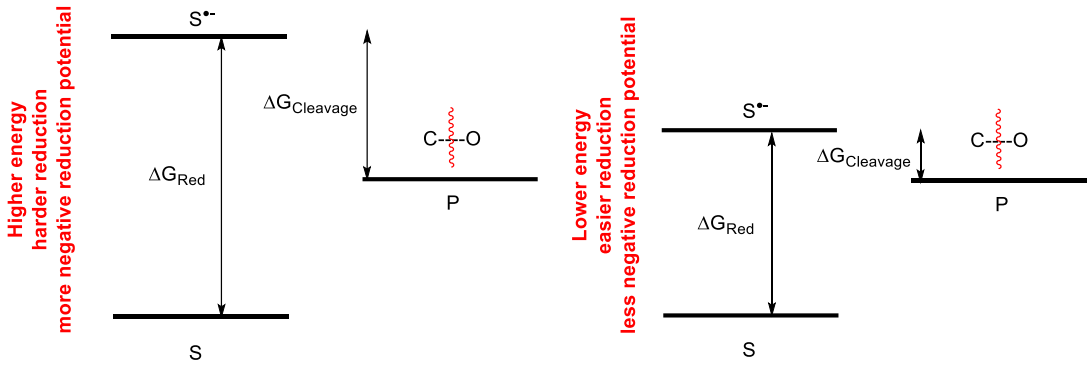


*Figures 51: CO cleavage rationalization.*

In conclusion, the C-O reactivity of the substrates is not only influenced by the reduction potentials of the latter but also by the lifetime of the excited states of the CDs and therefore by the rate of exciton recombination, by the reduction potentials of the CDs, by the kinetics of electronic transfer, from the diffusion of the CDs themselves and the substrates. The concomitance of these effects leads to the observed reactivity.

## 6.2 Electrochemical study

To fully understand the electrochemical characterization, the reader is advised to check Appendix C.

Preliminary, cyclic voltammetric measurements were performed in the background electrolyte, i.e., DMF + 0.1 M tetrabutylammonium perchlorate (TBAP), in order to establish the potential window in wich CDs can be investigated.

Figure 52 shows typical ciclyc voltammograms (CVs) recorded at 100 mV/s, starting from 0.0 V vs. Ag/AgCl and scanning the potential both in the cathodic (left) and anodic directions (right). As can been seen, small features are evident before the background discharge, wich occurs at about -2.7 V and 1.8 V in the chatodic and anodic regions, respectively. The small features recorded within the latter two limits, are probably due to impurities present in the electrolyte; the peak at about -2.2 V is related to trace water present in the solvent, due to humidity of the enviroment. Since, as reported in experimental, the CDs are not soluble in pure DMF, 200 µL of mili-Q water were used to disperse CDs in the medium.

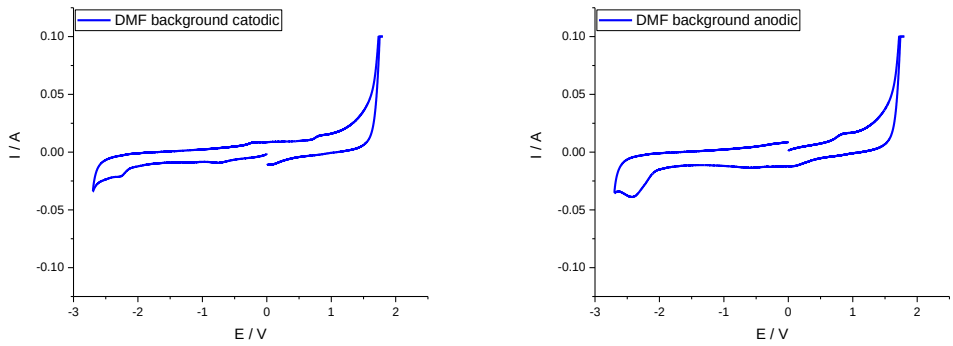


*Figure 52: cyclic voltammetry, scan rate 100mV/s, catodic direction (left), anodic direction (right) glassy carbon working electrode, Ag/AgCl/KCl saturated reference, platinum counter electrode.*

The effect of the water content on the CVs was therefore also investigated. Figure 53 shows CVs obtained either running the scan in the negative (left) or positive (right) direction, after adding to the medium 200 and 400 µl of water. As is evident, the peak at -2.3 V increases by increasing the water content. Instead, no sensible changes occur for other features, including the background discharge limits.

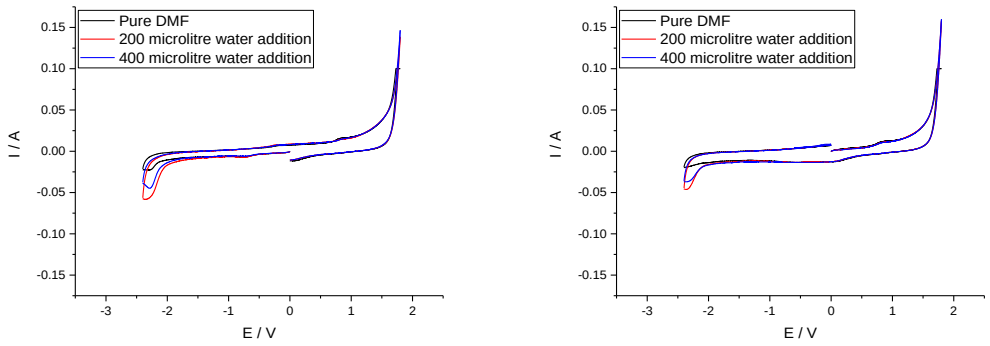


*Figure 53: cyclic voltammetry, scan rate 100mV/s, catodic direction (left), anodic direction (right), glassy carbon working electrode, Ag/AgCl/KCl saturated reference, platinum counter electrode.*

These results indicate that the potential window available to evaluate the CDs redox properties is quite wide and it ranges from about -2.3 V to 1.7 V.

In order to abtain potential data, unaffected by the actual reference electrode employed, the Ferrocene/Ferrocenium ($Fc/Fc^{+}$) system was used as an internal reference system. Figure 54 shows a serie of CVs obtained at different scan rates in DMF solution containing 5 mM Fc. The expected revesible anodic/cathodic pattern[29] is recorded; the halfway potential ($E_{1/2}$), calculated by Equation 1 (see Appendix C), is 0.492 (± 0.012) V.

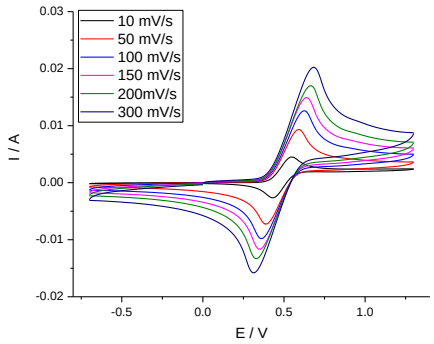


*Figure 54: cyclic voltammetry of ferrocene, different scan rate, anodic direction, glassy carbon working electrode, Ag/AgCl/KCl saturated reference, platinum counter electrode.*

In Figure 55 it is shown how the $E_{1/2}$ value of Fc/ $Fc^+$ is used to determine the potential values of CDs and ester substrates in order to obtain homogeneous and directly comparable potential data.

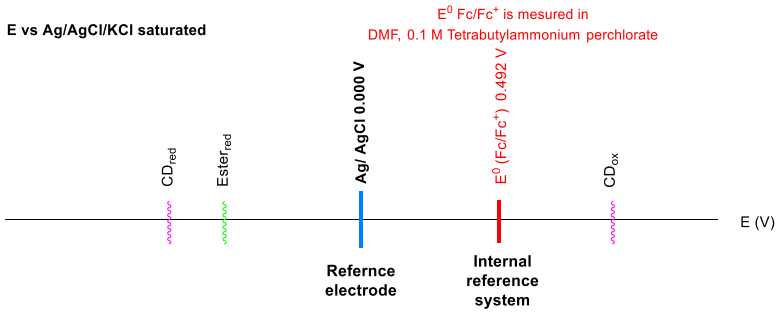


*Figure 55: Internal reference system Fc/Fc⁺.*

In the presence of CDs the voltammetric pictures become as is shown in Figure 56. It refers to typical CVs obtained in DMF solutions containing 25 mg/ml each of the four CDs, scanning the potential in both the cathodic (left) and anodic (right) region.

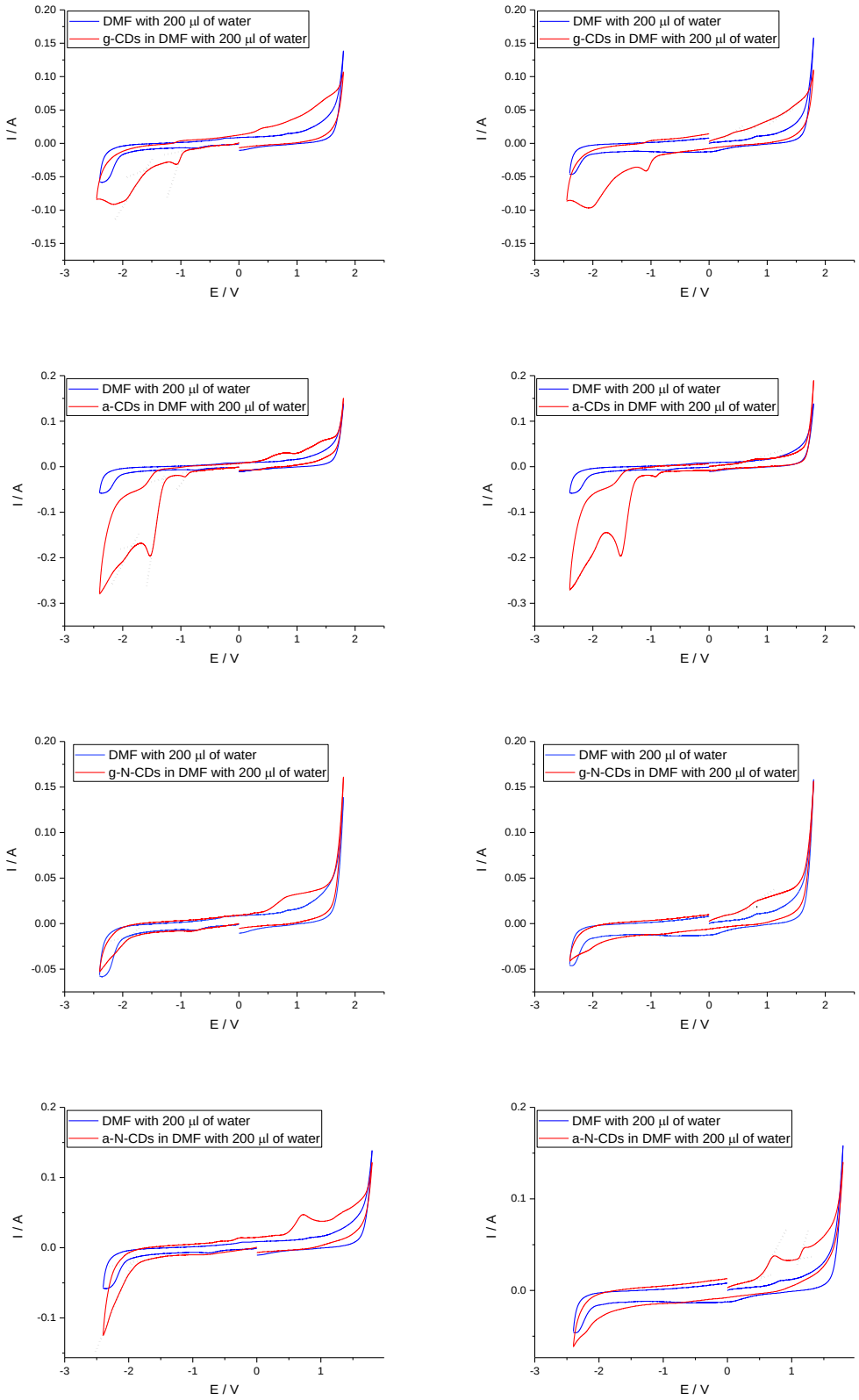


*Figure 56: CVs of different CDs in DMF with 200 µl of water, scan rate 100mV/s, chatodic direction (left)anodic direction (right), glassy carbon working electrode, Ag/AgCl/KCl saturated reference, platinum counter electrode. Black dashed line shows the onset potentials for reduction and oxidation.*

As can be seen, the number of processes recorded changes for each CDs. This suggests that the redox sites involved depend on the characteristics (chemical or structural) of CDs. Examples of electrode processes that could take place are schematized in Figure 57.a for a generic oxidation process. It must be considered that a second or third electrode process, following the first step, can be related to products formed after a homogeneous chemical reaction (Figure 57.b-c).

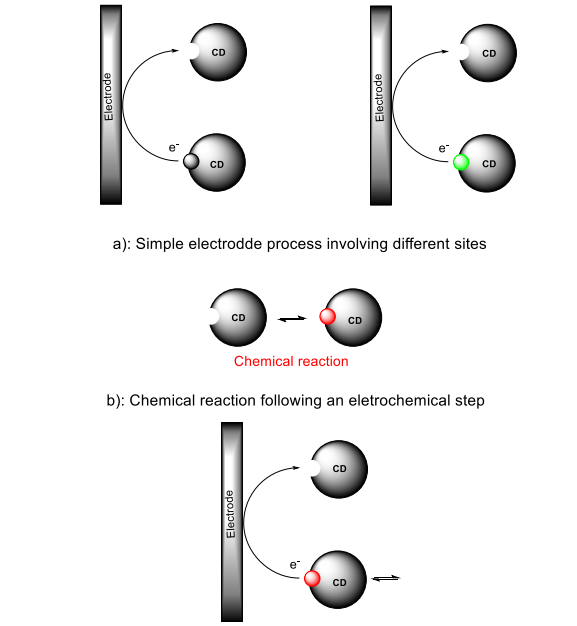


*Figure 57: possible electrode process for CDs.*

A similar scheme can be drown for reduction processes.[30]

At this stage, we are unable to establish wich of the previouos mechanism applies. Eventually, a more thorought investigation would be required. This was beyond the aim of this work. In this study, infact, main information to be obtained from CVs was the evaluation of the onset potentials of the various processes, wich in turn allows to evaluate the HOMO LUMO energies by using Equations 2.a and 2.b (see appendix C).

As for the evaluation of onset potentials, Figure 56 (dotted lines) shows examples of how they were obtained. Further details are provided in Apenidx C. Tables 13 and 14 show the values thus determined for either the reduction or oxidation processes; for a sake of clarity they are referred against the Ag/AgCl and $Fc/Fc^+$ system. The corresponding HOMO, LUMO values are included in the same tables.

$E_{onset, red}$ for CDs and LUMO energy level

| CDs | $E_{onset, red}$ (V) vs Ag/AgCl | $E_{onset, red}$ (V) vs Fc/Fc+ | E LUMO (eV) |
|---|---|---|---|
| g-CD | -0.97 | -1.46 | -3.6 |
| | -1.60 | -2.09 | -3.0 |
| a-CD | -0.85 | -1.34 | -3.8 |
| | -1.30 | -1.79 | -3.3 |
| | -1.83 | -2.33 | -2.8 |
| g-N-CD | -1.87 | -2.36 | -2.7 |
| a-N-CD | -1.94 | -2.43 | -2.7 |

*Table 13: $E_{onset, red}$ for CDs and LUMO energy level.*

$E_{onset, ox}$ for CDs and HOMO energy level

| CDs | $E_{onset, ox}$ a (V) vs Ag/AgCl | $E_{onset, ox}$ a (V) vs Fc/Fc+ | E HOMO (eV) |
|---|---|---|---|
| g-CD | 0.35 | -0.14 | -5.0 |
| | 0.69 | 0.20 | -5.3 |
| | 1.27 | 0.77 | -5.9 |
| a-CD | 0.52 | 0.03 | -5.1 |
| g-N-CD | 0.56 | 0.06 | -5.2 |
| a-N-CD | 0.53 | 0.03 | -5.1 |
| | 1.12 | 0.62 | -5.7 |

*Table 14: $E_{onset, ox}$ for CDs and HOMO energy level.*

A voltammetric investigation was also performed on the substrates **5a**, **5b**, **5c,** which were employed in the photocatalitic investigation of the C-O cleavage. Also in this case, from the CVs, the onset potentials can be obtained. These informations can be useful to further assess the reactivity of the a-N-CDs toward the investigated esters.

Figure 58 shows typical CVs recorded at 100 mV/s in the DMF solution containing 10 mM each of the investigated esters. In these experiments, the direct scan was performed only in the chatodic region, as in the anodic one no process worth to be considered was recorded.

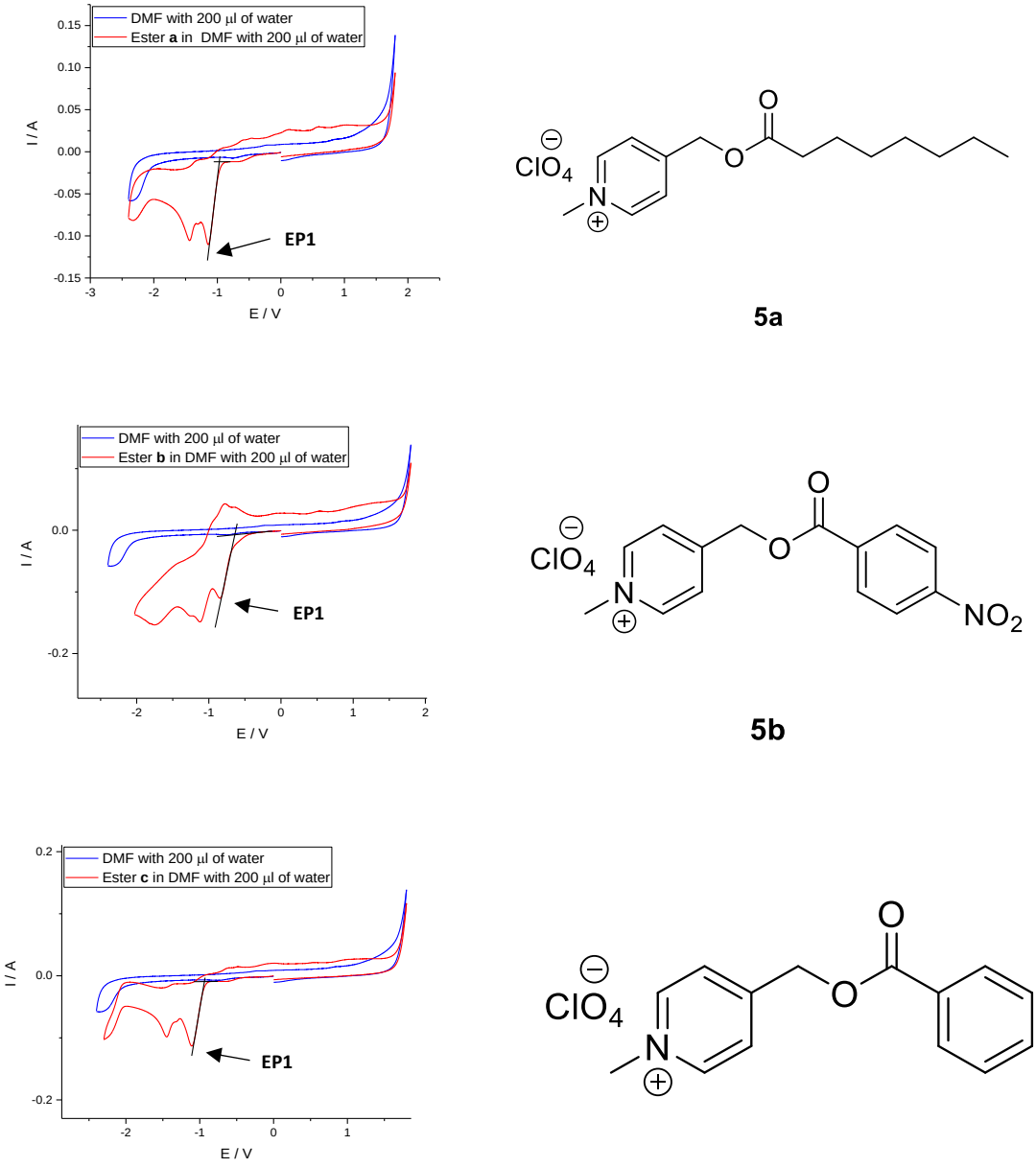


*Figure 58: cyclic voltammetry of different ester in DMF with 200 µl of water, scan rate 100mV/s, catodic direction glassy carbon working electrode, Ag/AgCl/KCl saturated reference, platinum counter electrode. Black line shows the onset potential for reduction.*

From the CVs, it is evident that the electrochemisty of the compounds is rather complex; in all cases, al least two main peacks were recorded. As for the first peack (EP1), it is likely (also from literature data [31, 32]) that it belongs to the reduction of the C=O moiety of the ester group. This hypothesis is supported by considering the peack potential values shown in Table 15 (again against both vs Ag/AgCl and $Fc/Fc^+$), from where it results that EP1, from the less to the more negative, follows the order **5b**, **5c**, **5a**. This is congruent whit the expected stability of a radical anion formed upon injection of an electron on the ester group. Infact, the electron of the radical anion in **5b** can be delocalized over the nitrobenzene group and therefore results quite stable. Its high stability is also proved by the appearance, upon scan reversal, of a peack at -0.9 V (see Figure 58), due to the oxidation of the radical anion. [27, 30, 31, 33]. Similarly, the radical anion, which can be formed from the reduction of **5c**, can be stabilized, tough to a lesser extent, by the benzene group. No similar groups are present in **5a**, able to provide delocalization of the electron, and consequently stability to the radical anion. In any case the CVs of either **5a** and **5c**, didn't provide any oxidation peack upun scan reversal. (see Figure 58.a.c).

EP1 for substrtes

| Substrate | EP1 (V) vs Ag/AgCl | EP1 (V) vs $Fc/Fc^+$ |
|---|---|---|
| 5a | -1.144 | -1.636 |
| 5b | -0.834 | -1.326 |
| 5c | -1.090 | -1.582 |

*Table 15: EP1 for substrates.*

As for as other peaks is concerned, considering the structrure of the molecules, it can be hypothesized that those at about -1.4 V for both **5a** and **5c** are due to the reduction of the piridine formed at the electrode surface after the C-O cleavage occurring on the first reduction process. Instead, because of the higher stability of the radical anion of **5b**, the peak at -1.8 V is due to the reduction of the piridine group still bound to the molecule. The other two processes occurring at about -1.1 V and -1.2 V can be due to the further reduction of radical anion and to the $NO_2$ goup respectively. The occurrence of such kind of processes in organic solvents are well know in the literature[34]. The above hypothesis to be fully proved would require a more detailed investigation; this however is beyond the aim of this thesis.

The onset potentials relevant to the first peak, which is of interest for our purposes, are shown in Table 16 along with the LUMO energy values obtained by using Equations 2.a and 2.b (see appendix C).

| $E_{onset, red}$ for substrate and LUMO energy level | | | |
|---|---|---|---|
| Substrate | $E_{onset, red}$ (V) vs Ag/AgCl | $E_{onset, red}$ c (V) vs Fc/Fc+ | E LUMO (eV) |
| 5a | -0.97 | -1.46 | -3.6 |
| 5b | -0.65 | -1.14 | -4.0 |
| 5c | -0.94 | -1.43 | -3.7 |

*Table 16: $E_{onset, red}$, $E_{onset, ox}$ for CDs and substrate 5a, 5b, 5c and HOMO-LUMO energy levels calculated.*

In order to compare all information gathered in the previous electrochemicall experiments for CDs and esters, onset potentials values against $Fc/Fc^+$ are displayed in Figure 59 both for the reduction (red colour) and oxidation (blue colour) processes.

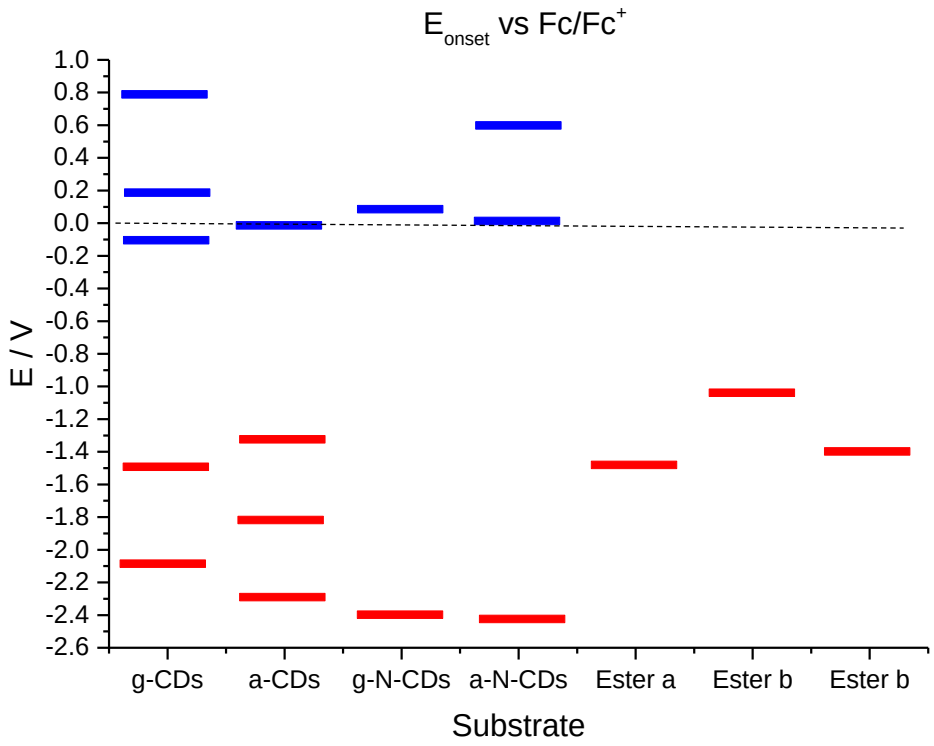


*Figure 59: onset potential for each redox process due to CDs and esters.*

A similar picture summarizing HOMO (red colour) and LUMO (blue color) energy levels obtained from the above onset potentials is displayed in Figure 60. Of course, the two pictures provide same information; however, in what follows, only the energy levels will be considered.

Moreover, as discussed in the photocalysis section, the reactivity of CDs was tested only towards **5a**; the reactivity order found is the following a-N-CDs> g-CDs> g-N-CDs> a-CDs.

Assuming that each onset potentials is due to a different redox site, the HOMO-LUMO gap could explain the reactivity of CDs toward **5a**. Considering the gaps displaied in Figure 60, the above reactivity agrees with the maximum HOMO-LUMO gap found from the electrochemical processes occurring at the most negative and positive potentials. However, although CDs are able to either oxidized or reduced the substrate, only the reduction process prevails.

Considering in more detail the reactivity of the a-N-CDs toward **5a**, **5b** and **5c**, it is evident that the easier is the reducibility of the substrate, the lower is the extent of the C-O cleavage. This reasoning can be better understood by recalling Figure 51 (pag 62). Overall, the reduction potentials of the substrates **5a**, **5b**, **5c** are in fully agreement with the reactivity order observed in the photocatalysis.

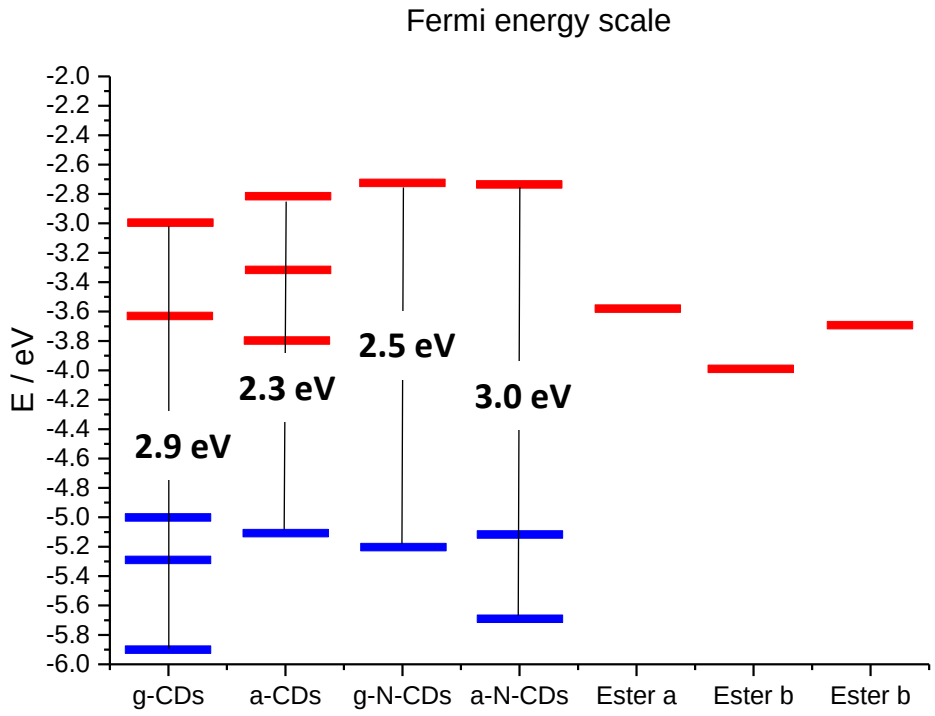


*Figure 60: energy orbitals of each process due to CDs and esters.*

The CDs HOMO-LUMO energies obtain by voltammetry were compared with those obtained by spectroscopy.

In Figure 61 the Uv/visible spectra, normalized by the maximum absorbance, for each CDs are shown. For g-CDs and a-CDs the spectra do not display any specific feature; a continuous increase of the absorbance is observed as soon as the wavelength became lower than about 600 nm. Conversely, for g-N-CDs and a-N-CDs a maximum at about 350 nm is recorded. These results indicate that, contrary to the case of the undoped CDs, the N doped CDs contain specific fluorophore on their surface. The onset wavelength in this case was obtained following the procedure suggested in reference[35], and schematized in Figure 61 with full black line.

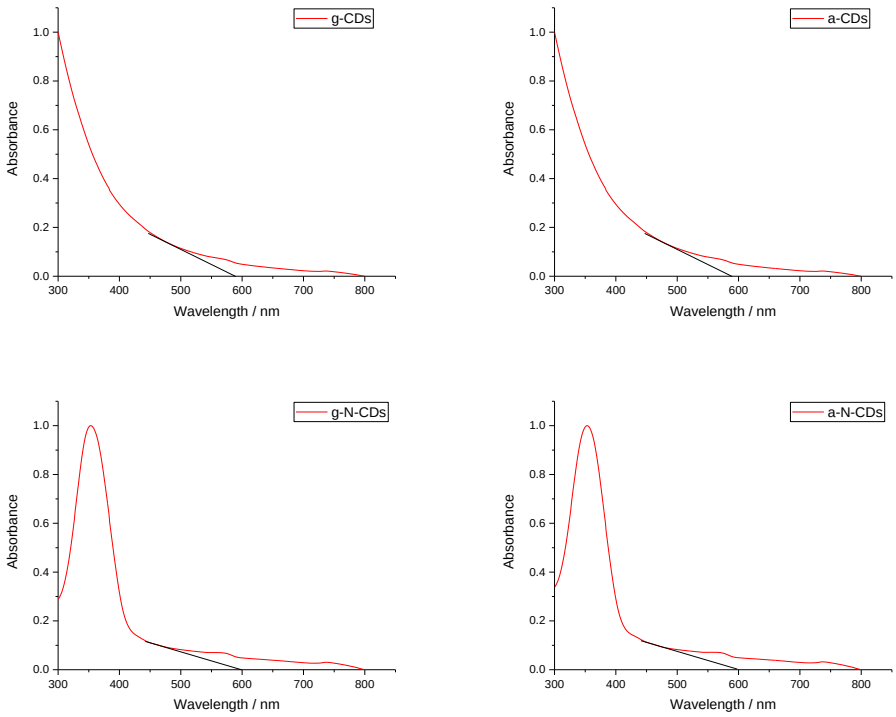


Figure 61: UV/visible spectra of CDs.

Optical gaps were than calculated using the Planck Equation:

$$\Delta E = h\frac{c}{\lambda} \qquad \text{Equation 3}$$

Where

$\Delta E$ is the band gap in eV

$h$ is the Planck costant ($4.13566751691 \cdot 10^{-15}$ eV·s)

$c$ is the the speed of light ($3 \cdot 10^{8}$ m/s)

$\lambda$ is in this case the onset wavelength of absorption (m)

Table 17 compares extreme HOMO-LUMO gap obtained by voltammetry with those obtained by spectroscopy.

| CDs | HOMO (eV) | LUMO (eV) | HOMO-LUMO gap | Optical gap(eV) |
|---|---|---|---|---|
| g-CD | -5.9 | -3.0 | 2.9 | 2.2 |
| a-CD | -5.1 | -2.8 | 2.3 | 2.2 |
| g-N-CD | -5.2 | -2.7 | 2.5 | 2.1 |
| a-N-CD | -5.7 | -2.7 | 3.0 | 2.1 |

Table 17: extreme HOMO LUMO gap and confront with optical gap.

As is evident the optical gaps are in all cases lower then those obtained by voltammetry, and their differences in some cases are quite high. However, the above electrochemical gaps fall within values reported in the literature for similar CDs. [36]

As for the discrepances found between optical and electrochmical gaps, they can be in part due to the assumptions made above for their evaluation. However, an explanation can be found considering the issue related to what extent spectroscopic and electrochemical data provide same information on HOMO-LUMO energy levels (see appendix C). Infact, if we consider the phenomena occurring in a spectroscopic or eletrcochemical experiment, it is clear that they are different. [37]

In voltammetric experiment, the generated species, for example in reduction, involves the addition of an electron to CDs with respect to the initial situation (see Figure 62.a). On the other hand, when CDs absorbs light, the electron from the ground state is promoted to an excited state (Figure 62.b). In this case, the CDs mantain same number of electrons. These considerations lead to the conclusion that the HOMO-LUMO energies evaluated by voltammetry are different for those obtained by UV/visible spectroscopy. Nevertheless, as also shown in this thesis, the two approaches can be used is some circumstances to obtain information which leads to same conclusion.

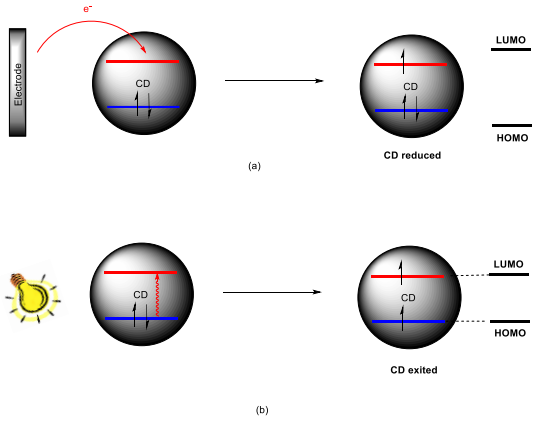


*Figure 62: Reduction vs excitation of CD: a) CDs reduction; b) CDs excitation.*

The experimental reactivity found in this work agrees with the energie gaps found by voltammetry. Infact, the electrochemical experiments can be regarded as the sum of two processes as displayed in Figure 63. In this case, CDs once excited by a suitable wavelength, can undergo a redox process thanks to sacrificial compounds (electron donors or acceptors). This overall process provides a final product in the same electronic state as that obtainable by electrochemistry.

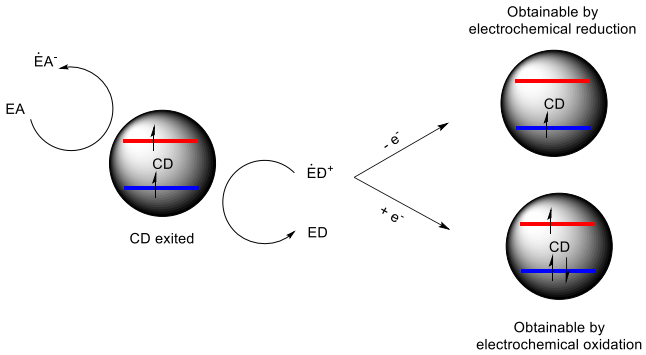


*Figure 63: photocatalysis vs electrochemistry.*

In conclusion four CDs (g-CDs, g-N-CDs, a-CDs, a-N-CDs) was selected to investigate their electrochemical properties by voltammetry. From CVs results, HOMO-LUMO gap for each CDs was calculated proving that this gap affects the reactivity order of CDs towards **5a**.

The same voltammetric study was performed on substrates **5a**, **5b**, **5c** highlighting that the reactivity order with a-N-CDs depends on their reduction potentials. The lower the reduction potential of substrates the higher is the C-O cleavage entity. These results are in accord with the reactivity order observed in the photocleavage test.

Summarizing, the C-O photocleavage depends on CDs HOMO-LUMO gap and the LUMO energy of the picolinium esters.

Considering the overall result it appears that, CDs that absorb at higher frequencies (UV region) are more efficient to promote photocleavage. This implies spending a considerable amount of energy. On the other hand, CDs that promote the same reaction at higher wavelengths, although less efficiently from the cleavage point of view, it allows employing more available wavelengths.

## 6.3 Proposed photo-induced C-O bond cleavage mechanism

From all these observations on the electrochemical behaviour, the photocatalytic results along with literature studies, some general conclusion on the photodeprotection mechanism could be advanced.

Considering the photodeprotection mechanism already discussed for the phenacyl and N-Methyl-4-Picolinium esters, some steps should be rationalized with the data herein collected.

Experimental evidences of direct Photolysis of Phenacyl Protecting Groups obtained by laser flash photolysis by Banerjee and Falvey[38] demonstrate that the initial step of this process is an hydrogen atom transfer from the solvent to the phenacyl carbonyl group. Since phenacyl esters and N-Methyl-4-picolinium esters, posses a similar carboxylic group as shown in Figure 64 the hydrogen transfer occur to this moiety.

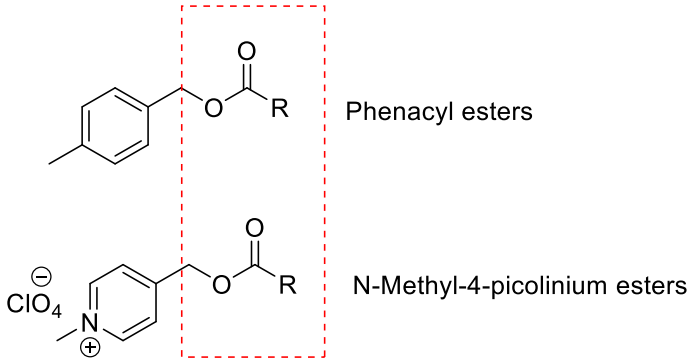


*Figure 64: common feature of Phenacyl esters and N-Methyl-4-picolinium esters.*

In Figure 65 a new photodeprotection mexhanism is proposed. The mechanism consists of six steps. In the first step the photosensitizer is excited. In the second step the ester undergoes protonation to the carboxylic group. In the third step the electron transfer from the photosensitizer to the the positively charged carbonyl carbon occur. This electron ends up on an anti-bonding orbital which weakens the C-O bond. This step was supported by the observed reduction peaks in the CVs analysis of 5a, 5b and 5c. In the fourth step there is the homolysis of the C-O bond which has been weakened. As shown in Figure 65 (in the brackets) both the radical species formed are stabilized by various resonsance structure. In the fifth step the methyl pyridine extracts a hydrogen atom from the solvent generating a hydroxyl radical that could combines with another onel in the sixth step to form hydrogen peroxide.

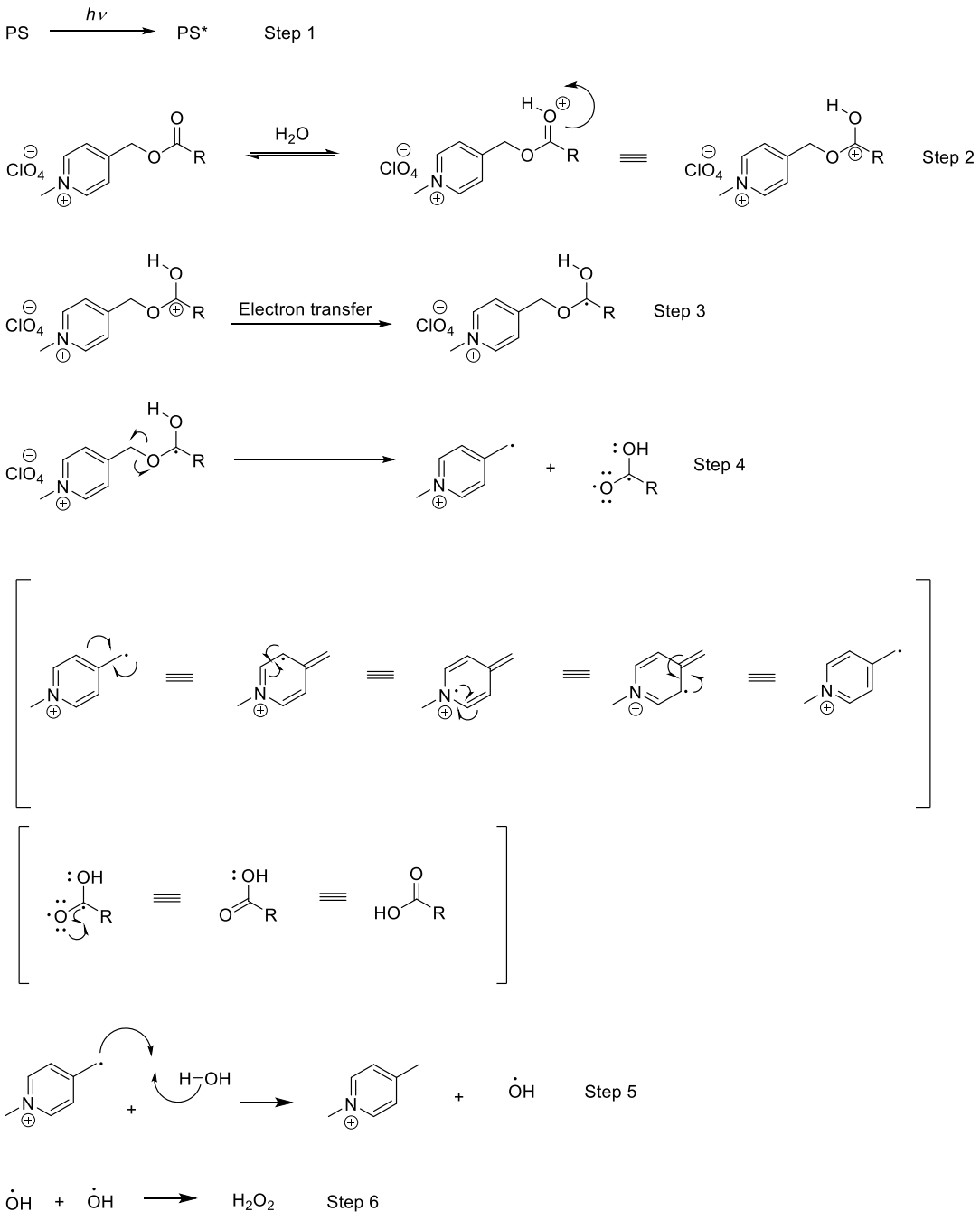


*Figure 65: proposed mechanism.*

CDs can be employed as photosensitizer in the above described mechanism. In this case, CDs can perform an electron tranfer through the process described in Figure 66.

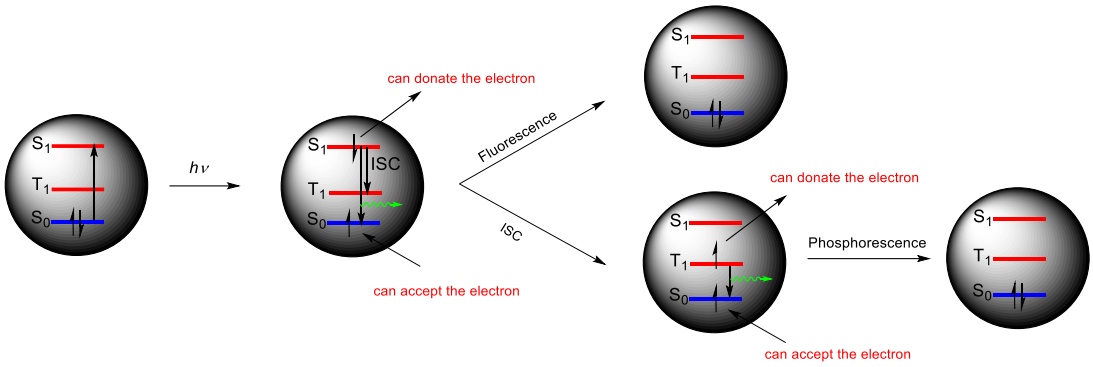


*Figure 66: CD activation.*

CDs absorb the light and, the electron from the fundamental state $S_0$ is excited to the state $S_1$. In this state CDs can either donate or accept an electron, relax to give fluorescence or give intersystem crossing (ISC). If the intersystem crossing occurs, the excited electron in the CDs passes to a triplet state $T_1$. In the latter case, CDs can either donate or accept an electron or relax to give phosphorescence. If a sacrificial donor is employed it can fill the holes generated by the photoexcitation, leading to an increase in the lifetime of the excited states. The photosensitizer could transfer the electron from both $S_1$ and $T_1$ states to the substrate, leading to the deprotection reaction with the same pathways described in Figure 65. The CVs performed on substrates **5a**, **5b** and **5c**, demonstrate that the most reasonable pathway for photodeprotection is the electron transfer to the carbonyl group. Moreover, the analysis reveals a dependence of the feasibility of this process to the chemical structure of substrates explaining the different reactivity order observed in the photodeprotection reaction. Contextually, this mechanism could be affected by different features, such as the presence of the chromophore, the more or less graphitic core, defects and the quantum confinement effect resulting in a much more complicated but also intriguing phenomena.

# 8 Conclusions

In this work we investigated a library of CDs. For this aim we prepared three models of picolinum esters starting from of octanoic, p-nitrobenzoic and benzoic acid respectively. These substrates ware employed in the photodeprotection reaction in order to study the C-O cleavage reactivity. To identify by NMR the photocleavage product, 4-(hydroxymethyl)-1-methylpyridin-1-ium iodide and 1,4-dimethylpyridin-1-ium iodide were also prepared.

Different conditions were employed to optimize the photodeprotection such as different CDs, CDs and sacrificial donor concentration, light and oxygen. The reactivity of the best CDs was final compared to that of $Ru(bpy)_3^{2+}$.

Four CDs (g-CDs, g-N-CDs, a-CDs, a-N-CDs) was selected to investigate their electrochemical properties by voltammetry. From CVs results, HOMO-LUMO gap for each CDs was calculated proving that this gap affects the reactivity order of CDs towards **5a**.

The same voltammetric study was performed on substrates **5a**, **5b**, **5c** highlighting that the reactivity order with a-N-CDs depends on reduction potentials. The lower the reduction potential of substrates the higher was the C-O cleavage entity. These results are in accord with the reactivity order observed in the photocleavage test. From these experimental evidences, finally, a mechanism was proposed. In conclusion, the C-O photocleavage depends on CDs HOMO-LUMO gap and the LUMO energy of the picolinium esters. CDs, could be proposed as a new class of metal free nanomaterials for accomplish a green photocatalysis.

# 9 Acknowledgments

I would like to thank the research group Selva & Perosa for the opportunity to increase my cultural background in organic synthesis and photocatalysis and for the freedom that was granted to me in the proposed ideas. A special thanks goes to Dr. Emanuale Amadio and Cailotto Simone for the patience they showed despite my stubbornness. I also thank Professor Daniele Salvatore for allowing me to perform the measurements in his laboratory and to followed me for the electrochemical part very patiently. I also thank Rigo Davide, my laboratory friend with I shared the best moments of this period.

Finally, a thank you from the deeper of my heart goes to my family and friends, to my mother Oscarina and to my girlfriend Celeste who have supported me financially and morally in the most difficult moments of these five beautiful years. With this work I manifest all my gratitude.

# 10 Experimental part

## 10.1 Synthesis and characterization of substrates

### 10.1.1 Reagents

Table 18 shows the main reagents used in the synthesis.

| Reagent | Stockist | MW (gr/mole) | Density (gr/ml) | Boiling point (°C) |
|---|---|---|---|---|
| Octanoic acid | Sigma Aldrich | 144.21 | 0.910 | 237 |
| p-nitrobenzoic acid | Sigma Aldrich | 167.12 | - | - |
| Benzoic acid | Sigma Aldrich | 122.12 | - | - |
| Thionyl chloride | Sigma Aldrich | 118.97 | 1.64 | 79 |
| 4-(Hydroxymethyl)pyridine | Sigma Aldrich | 109.13 | - | - |
| 4-methylpyridine | Sigma Aldrich | 93.13 | - | 145 |
| Iodomethane | Sigma Aldrich | 141.94 | - | - |
| Silver perchlorate | Sigma Aldrich | 207.32 | - | - |

Table 18: main reagents used.

mQ-water, acetonitrile, methanol, toluene, ethyl acetate, hexane, also supplied by Sigma-Aldrich, were used as solvents. All the reagents used in the synthesis were used as received by Sigma-Aldrich. Deuterated solvents such as chloroform, water and acetonitrile and methanol were supplied by Sigma-Aldrich. For photodeprotection, CDs were synthesized by Perosa group. Details on their preparation can be found in the doctoral thesis of Dr. Cailotto Simone (in preparation). Ru $(bpy)_3^{2+}$ were supplied by Sigma-Aldrich and used as such.

### 10.1.2 Materials and instrumentation

TLC thin-layer chromatography was conducted on Silica gel 60 F254 (Merck KGaA)

Silica gel 60 M Merck KGaA (0.040-0.063 mm, 230-400 mesh ASTM) was used in flash chromatography.

The GC-MS spectra were registered with an Agilent Technologies 6890N Network GC System interfaced with an Agilent Technologies 5975 Inert Mass Selective Detector. He Carrier gas (1.2 mL / min), phase SPB-5, capillary column 30 m, I.D. 0.32 mm, film 0.25 µm.

Calibration curves for quantification were recorded with a GC Hp 5890 equipped with a capillary column Elite-624 (30 m x 0.32 mm, film width: 0.18 µm) coupled with FID detector.

For the acquisition of $^{1}H$, $^{13}C$ NMR spectra, a Bruker UltraShield 300'54 spectrometer was used ($^{1}H$: 300 MHz; $^{13}C$: 75.5 MHz;) and a Bruker Magnet System spectrometer 400'54 Ascend ($^{1}H$: 400 MHz; $^{13}C$: 100.6 MHz). The chemical shifts (δ) of the $^{1}H$ and $^{13}C$ NMR spectra have been reported in parts per million (ppm).

The following abbreviations were used to report multiplicities: s = singlet, d = doublet, t = triplet, q = quartet, m = multiplet.

For photocatalysis reactions, a LED UV lamp with a fixed wavelength of 370 nm, 400 mA, 25 mV was used.

The abbreviations used are GC-MS: gas chromatography coupled with mass spectrometry; NMR: nuclear magnetic resonance; TLC: thin layer chromatography

### 10.1.3 Synthesis and characterization of picolinium esters

The protection reaction of the corresponding acids follows the scheme shown in Figure 67.

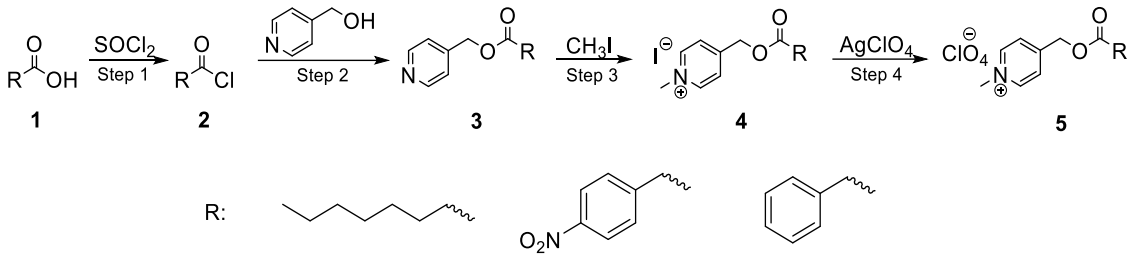


*Figure 67: general scheme for protection reaction.*

The reaction consists of four synthetic steps. Briefly, in the first step there is the chlorination of acid **1** by thionyl chloride forming acyl chloride **2**. In the second step the acyl chloride is reacted with 4-(Hydroxymethyl) pyridine to form the corresponding ester **3**. In the third step the ester is then methylated with methyl iodide to form the corresponding iodurate salt **4**. In the fourth step the iodide counterion is exchanged by silver perchlorate to form the corresponding perchlorate salt **5**. The following pages will describe each synthetic step in greater detail. All the $^{1}H$ and $^{13}C$ spectra can be found in the supporting information. The material used in the various synthetic steps is shown in Figure 68.

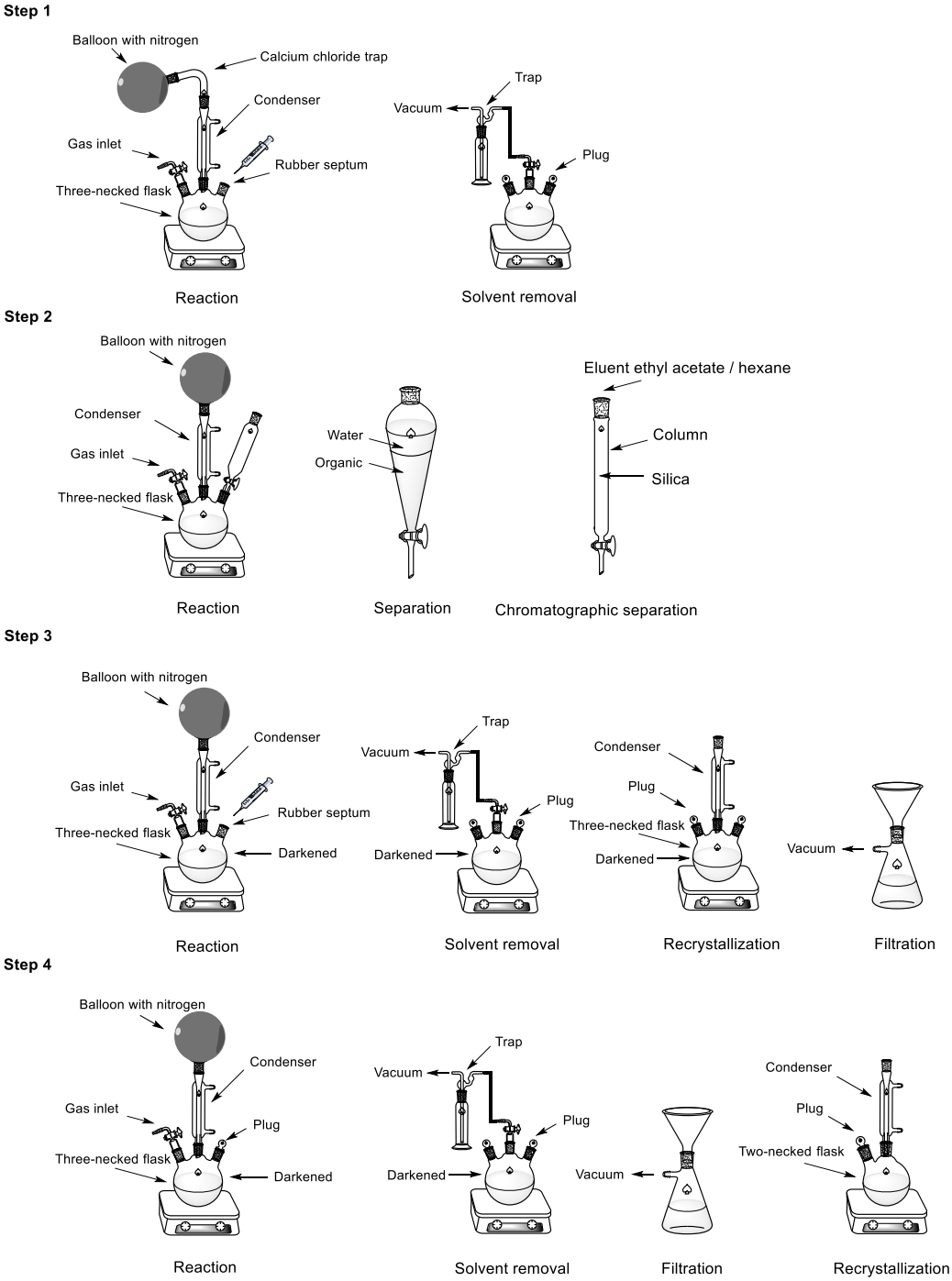


*Figure 68: Main phases of the various synthetic steps.*

### 10.1.4 Protection of octanoic acid

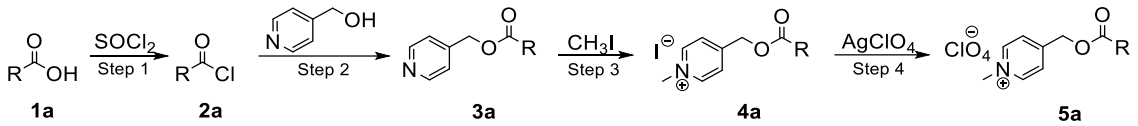


R:

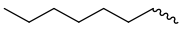

**Step 1**

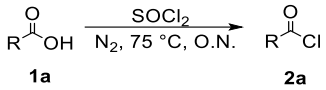


Octanoic acid **1a** (30.99 mmoli) and toluene (20 ml) was introduced into a three-necked flask equipped with a condenser, sodium bicarbonate and calcium chloride trap, rubber septum and tail. Then thionyl chloride (137.84 mmoli) was added and the mixture was refluxed overnight at 75°C. Then the the unreacted thionyl chloride and toluene was removed from the system by vacuum evaporation. The acyl chloride product **2a** was obtained in 89% yield.

**Step 2**

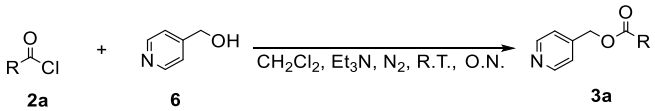


4-(Hydroxymethyl)pyridine **6** (18.97 mmoli), dichloromethane (20 ml) and triethylamine (32.92 mmoli) were introduced into a three-necked flask equipped with a condenser, dropping funnel and gas inlet. A solution of the corresponding acyl chloride **2a** (27,37 mmoli) in dichloromethane was then added dropwise and the reaction mixture was left under stirring overnight at room temperature and under nitrogen. Subsequently, the ester product **3a** was put into a separating funnel and washed with a solution of water and sodium bicarbonate (20ml), recovering the lower organic phase and repeating the operation three times. The organic phase was then dehydrated with sodium sulphate, filtered and the solvent was removed by rotary evaporation. The purified product **3a** was purified by column chromatography employing gradient elution with a mixture of hexane / ethyl acetate. The product **3a** was obtained in 53% yield.

**Step 3**

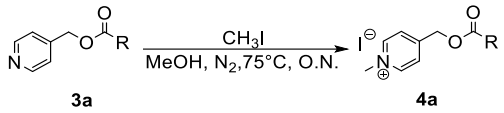


The corresponding ester **3a** (7.38 mmoli) and methanol (10 ml) were introduced into a three-necked darkened flask equipped with a condenser, rubber septum and tail. The system was put under nitrogen. The methyl iodide (11.29 mmoli) was then added with a syringe and the reaction mixture was refluxed and left under stirring at 75 °C overnight. Subsequently, the unreacted methyl iodide and methanol were removed by vacuum evaporation leading to a solid. The product was recrystalized in hot methanol. The solid was filtered and stored in the dark. The product **4a** has been obtained in 53% yield.

**Step 4**

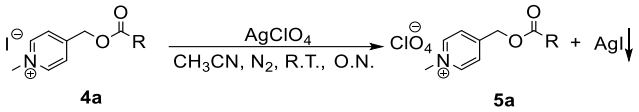


A solution of the corresponding ester **4a** (3.19 mmoli) in acetonitrile was added in a three-necked darkened flask with a tail and a plug. The silver perchlorate was then added in a stoichiometric amount. The system was placed under nitrogen and left under stirring at room temperature overnight. The reaction mixture was then filtered to remove the precipitated silver iodide and the filtrate was dried. The product was then recrystalized with hot methanol. The product **5a** was obtained in 72% yield.

Figure 69 and 70 show the $^{1}H$ and $^{13}C$ NMR spectra of the products obtained in each synthetic step. The assignment of the peaks for $^{1}H$ NMR and the $^{13}C$ NMR spectra are reported in the supporting information.

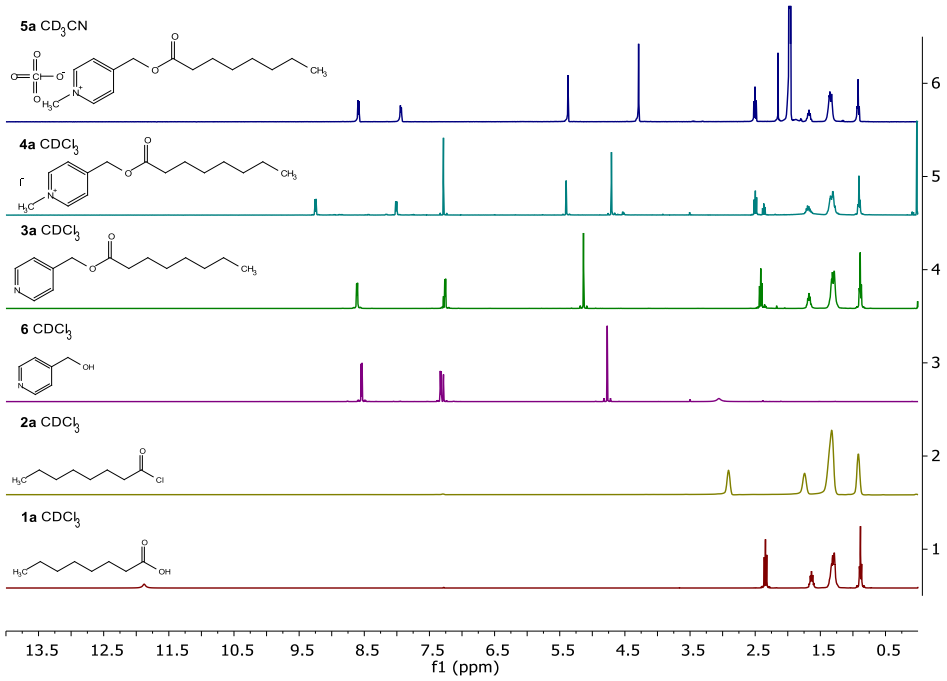


*Figure 69: $^{1}H$ NMR spectra for each product of synthetic steps.*

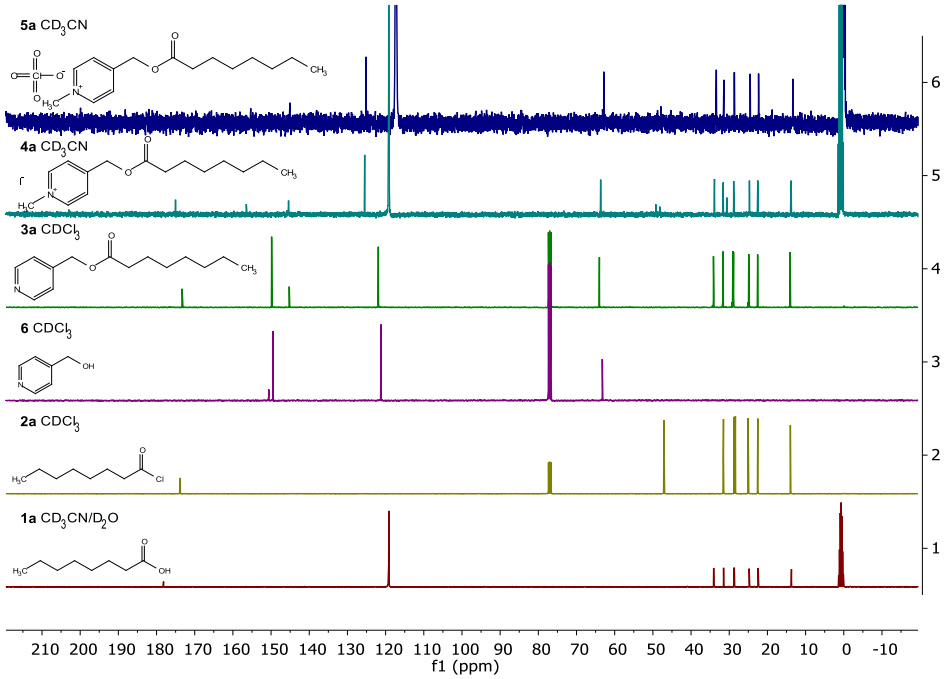


*Figure 70: $^{13}C$ NMR spectra for each product of synthetic steps.*

### 10.1.5 Protection of p-nitrobenzoic acid

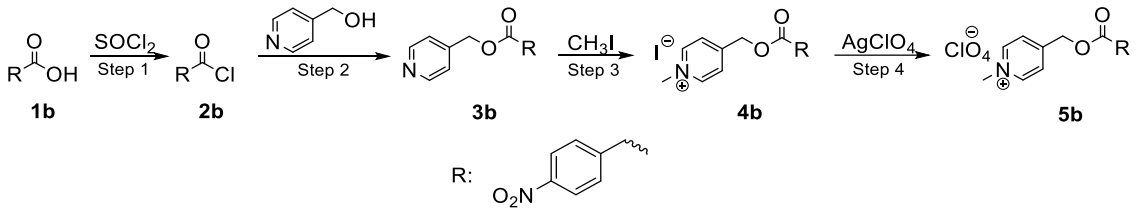


**Step 1**

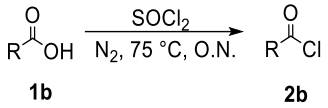


p-nirobenzoic acid **1b** (50.80 mmoli) and toluene (20 ml) were introduced into a three-necked flask equipped with a condenser, sodium bicarbonate and calcium chloride trap, rubber septum and tail. Then thionyl chloride (344.65 mmoli) was added and the mixture was refluxed overnight at 75°C. Then the the unreacted thionyl chloride and toluene was removed from the system by vacuum evaporation. The acyl chloride product **2b** was obtained in 86% yield.

**Step 2**

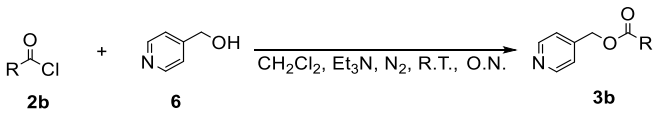


4-(Hydroxymethyl)pyridine **6** (23,24 mmoli), dichloromethane (50 ml) and triethylamine (71,94 mmoli) were introduced into a three-necked flask equipped with a condenser, dropping funnel and gas inlet. A solution of the corresponding acyl chloride **2b** (27,37 mmoli) in dichloromethane was then added dropwise and the reaction mixture was left under stirring overnight at room temperature and under nitrogen. Subsequently, the ester product **3a** was put into a separating funnel and washed with a solution of water and sodium bicarbonate (20ml), recovering the lower organic phase and repeating the operation three times. The organic phase was then dehydrated with sodium sulphate, filtered and the solvent was removed by rotary evaporation. The purified product **3b** was purified by column chromatography employing gradient elution with a mixture of hexane / ethyl acetate. The product **3b** was obtained in 35% yield.

**Step 3**

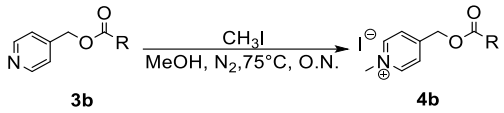


The corresponding ester **3b** (5,03 mmoli) and methanol (50 ml) are introduced into a three-necked darkened flask equipped with a coolant connected to a nitrogen ball, pierceable septum and tail. The system is put under nitrogen. The methyl iodide (8,03 mmoli) is then added with a syringe and the reaction mixture is refluxed and left under stirring at 75 °C overnight. Subsequently, the system is connected to the vacuum pump through a system of special traps to eliminate all the unreacted methyl iodide and methanol to obtain a solid. The product is then solubilized by adding the minimum amount of methanol and heating enough to solubilize. The solution is then left to rest overnight to allow crystallization. The solid was then filtered and stored in the dark. The product **4b** has been obtained with a yield of 40%.

**Step 4**

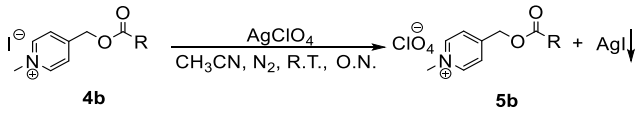


A solution of the corresponding ester **4a** (1.89 mmoli) in acetonitrile was added in a three-necked darkened flask with a tail and a plug. The silver perchlorate was then added in a stoichiometric amount. The system was placed under nitrogen and left under stirring at room temperature overnight. The reaction mixture was then filtered to remove the precipitated silver iodide and the filtrate was dried. The product was then recrystalized with hot methanol. The product **5b** was obtained in 53% yield.

Figure 71 and 72 show the $^{1}H$ and $^{13}C$ NMR spectra of the products obtained in each synthetic step. The assignment of the peaks for $^{1}H$ NMR and the $^{13}C$ NMR spectra are reported in the supporting information.

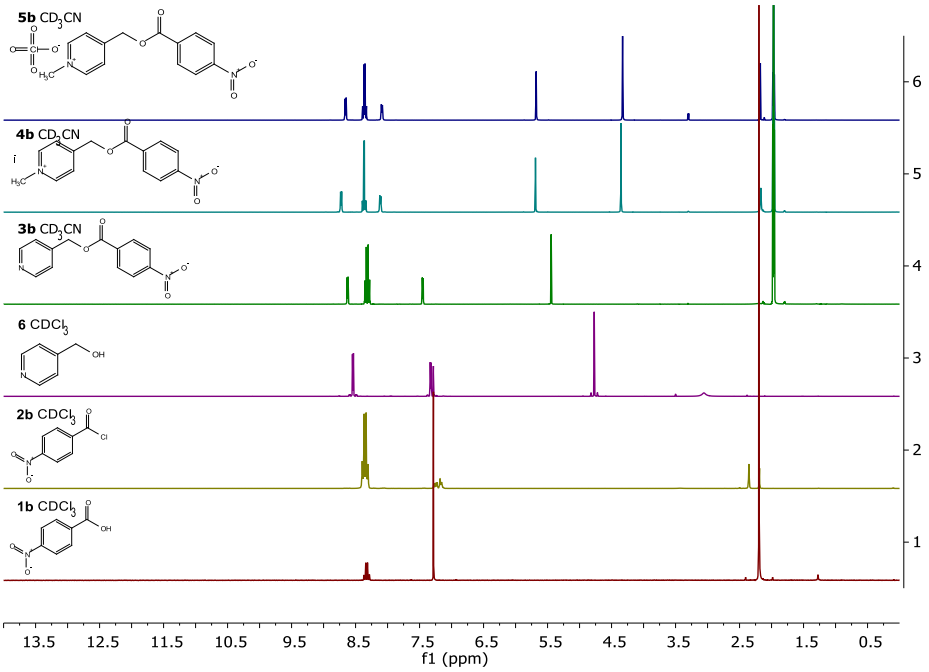


*Figure 71: $^{1}H$ NMR spectra for each product of synthetic steps.*

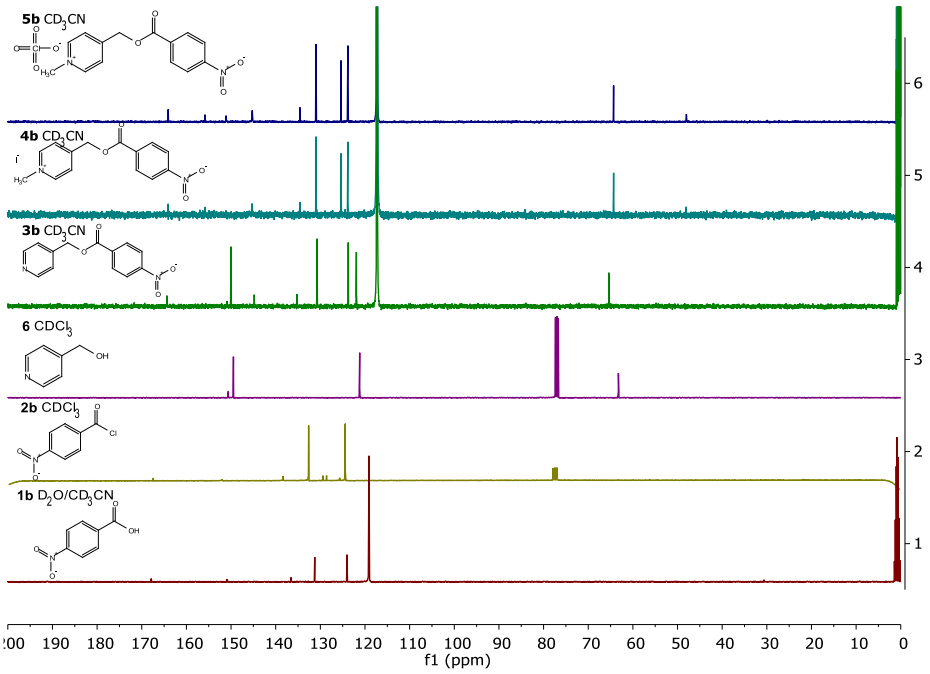


*Figure 72: $^{13}C$ NMR spectra for each product of synthetic steps.*

### 10.1.6 Protection of benzoic acid

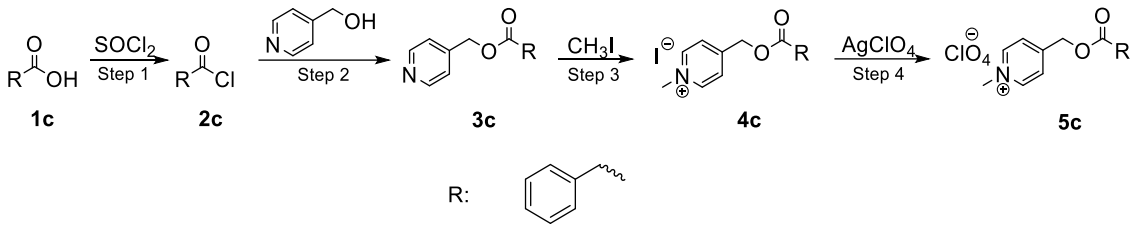


**Step 1**

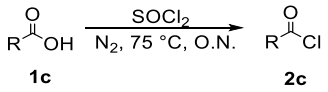


Benzoic acid **1c** (30.85 mmoli) and toluene (20 ml) was introduced into a three-necked flask equipped with a condenser, sodium bicarbonate and calcium chloride trap, rubber septum and tail. Then thionyl chloride (137.67 mmoli) was added and the mixture was refluxed overnight at 75°C. Then the the unreacted thionyl chloride and toluene was removed from the system by vacuum evaporation. The acyl chloride product **2c** was obtained in 85% yield.

**Step 2**

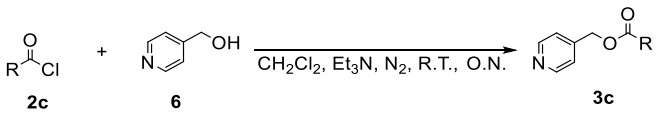


4-(Hydroxymethyl)pyridine **6** (23,26 mmoli), dichloromethane (35 ml) and triethylamine (41.99 mmoli) were introduced into a three-necked flask equipped with a condenser, dropping funnel and gas inlet. A solution of the corresponding acyl chloride **2c** (27,97 mmoli) in dichloromethane was then added dropwise and the reaction mixture was left under stirring overnight at room temperature and under nitrogen. Subsequently, the ester product **3c** was put into a separating funnel and washed with a solution of water and sodium bicarbonate (20ml), recovering the lower organic phase and repeating the operation three times. The organic phase was then dehydrated with sodium sulphate, filtered and the solvent was removed by rotary evaporation. The purified product **3c** was purified by column chromatography employing gradient elution with a mixture of hexane / ethyl acetate. The product **3c** was obtained in 54% yield.

**Step 3**

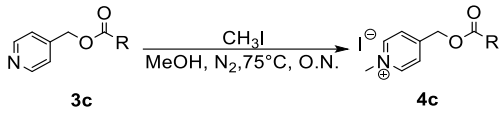


The corresponding ester **3c** (11.72 mmoli) and methanol (10 ml) were introduced into a three-necked darkened flask equipped with a condenser, rubber septum and tail. The system was put under nitrogen. The methyl iodide (19.44 mmoli) was then added with a syringe and the reaction mixture was refluxed and left under stirring at 75 °C overnight. Subsequently, the unreacted methyl iodide and methanol were removed by vacuum evaporation leading to a solid. The product was recrystalized in hot methanol. The solid was filtered and stored in the dark. The product **4c** has been obtained in 72% yield.

**Step 4**

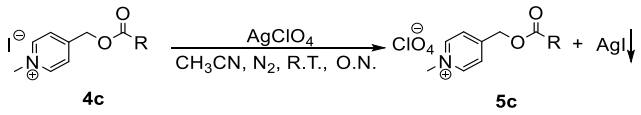


A solution of the corresponding ester **4c** (8.01 mmoli) in acetonitrile was added in a three-necked darkened flask with a tail and a plug. The silver perchlorate was then added in a stoichiometric amount. The system was placed under nitrogen and left under stirring at room temperature overnight. The reaction mixture was then filtered to remove the precipitated silver iodide and the filtrate was dried. The product was then recrystalized with hot methanol. The product **5c** was obtained in 72% yield.

Figure 73 and 74 show the $^{1}H$ and $^{13}C$ NMR spectra of the products obtained in each synthetic step. The assignment of the peaks for $^{1}H$ NMR and the $^{13}C$ NMR spectra are reported in the supporting information.

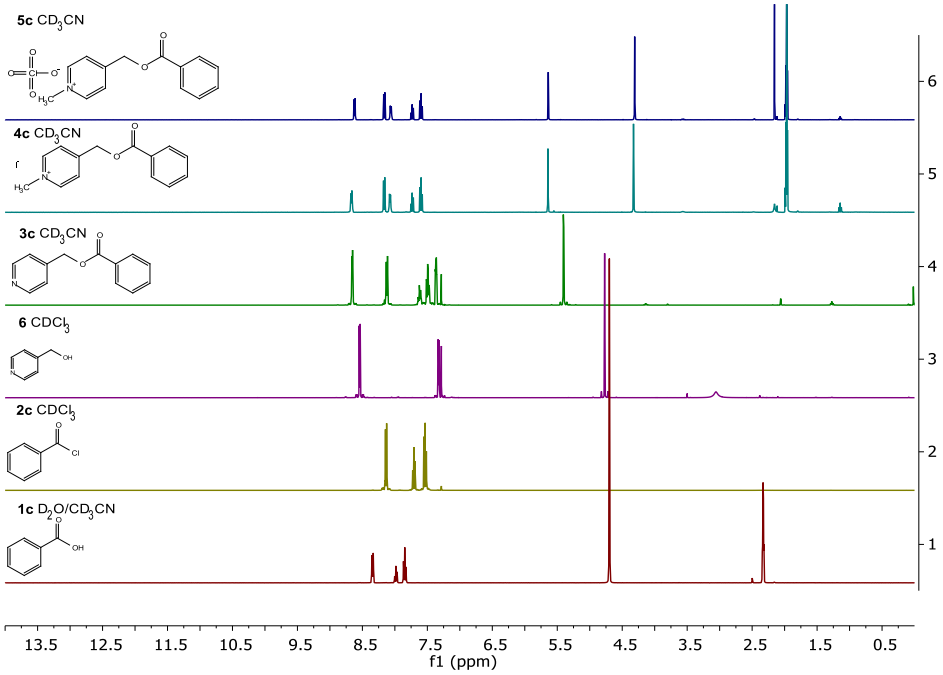


*Figure 73: $^{1}H$ NMR spectra for each product of synthetic steps.*

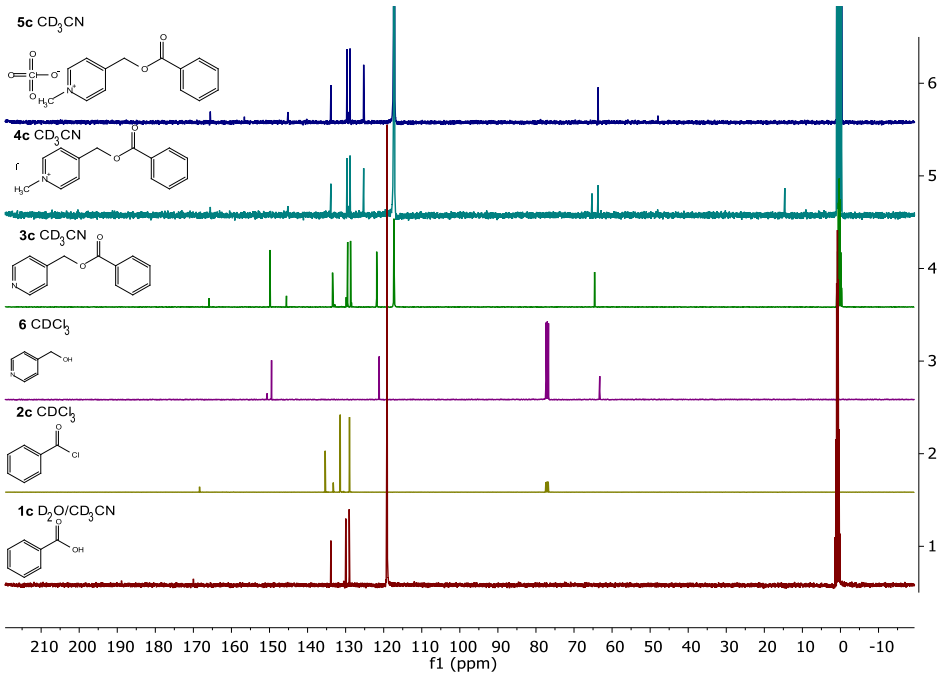


*Figure 74: $^{13}C$ NMR spectra for each product of synthetic steps*

### 10.1.7 4-(hydroxymethyl)-1-methylpyridin-1-ium iodide synthesis

**Step 3**

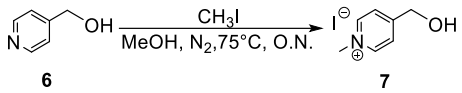


**6** **7**

4-(Hydroxymethyl)pyridine **6** (9.52 mmoli) and methanol (10 ml) were introduced into a three-necked darkened flask equipped with a condenser, rubber septum and tail. The system was put under nitrogen. The methyl iodide (23.80 mmoli) was then added with a syringe and the reaction mixture was refluxed and left under stirring at 75 °C overnight. Subsequently, the unreacted methyl iodide and methanol were removed by vacuum evaporation leading to a yellow solid. The product was recrystalized in hot methanol. The solid was filtered and stored in the dark. The product **7** has been obtained in 92% yield.

Figure 75 shows the $^{1}H$ spectra of the products obtained before and after methylation. The assignment of the peaks for $^{1}H$ NMR spectra and the $^{13}C$ NMR spectrum of **7** are reported in the supporting information.

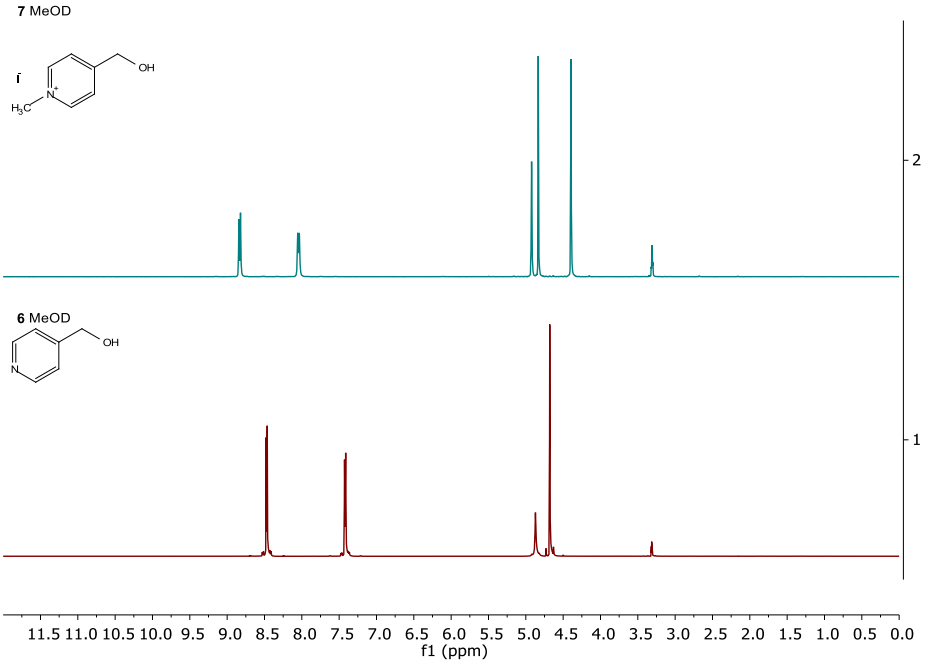


*Figure 75: $^{1}H$ NMR spectra for each product of synthetic step.*

### 10.1.8 1,4-dimethylpyridin-1-ium iodide synthesis

**Step 3**

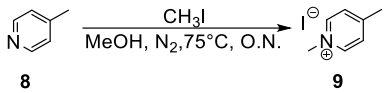


**8** **9**

The corresponding 4-methylpyridine **8** (9.52 mmoli) and methanol (10 ml) were introduced into a three-necked darkened flask equipped with a condenser, rubber septum and tail. The system was put under nitrogen. The methyl iodide (23.80 mmoli) was then added with a syringe and the reaction mixture was refluxed and left under stirring at 75 °C overnight. Subsequently, the unreacted methyl iodide and methanol were removed by vacuum evaporation leading to a yellow solid. The product was recrystalized in hot methanol. The solid was filtered and stored in the dark. The product **7** has been obtained in 89% yield.

Figure 76 shows the $^{1}H$ spectra of the products obtained before and after methylation. The assignment of the peaks for $^{1}H$ NMR spectra and the $^{13}C$ NMR spectrum of **9** are reported in the supporting information.

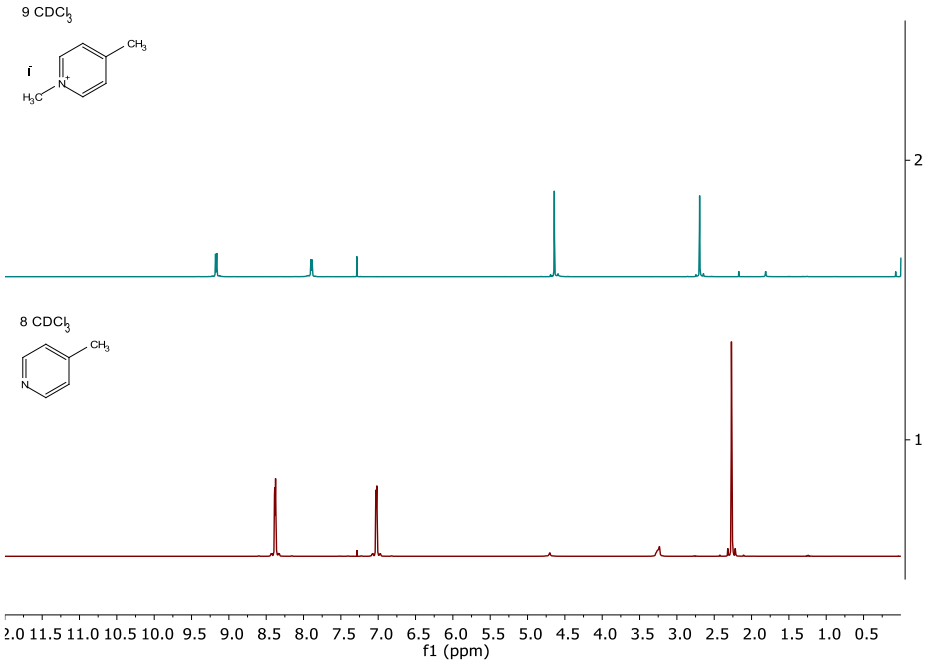


*Figure 76: $^{1}H$ NMR spectra for each product of synthetic step.*

## 10.2 Photodeprotection procedures

Photodeprotection reactions were conducted within an NMR tube. For each test an NMR tube was prepared containing the corresponding protected acid dissolved in a 60% water, 40% acetonitrile mixture. Depending on the test the CDs were added in variable quantities and the sacrificial donor EDTA in 0.1M concentration when present. The pH of the solution in this case because in a deuterated environment pD was corrected to 7 using hydrochloric acid. The mixture thus prepared was then degassed with nitrogen using a suitable system. The NMR tube was then exposed to the light of a UV lamp and NMR spectra were then recorded with different exposure times. In Figure 77 the procedure is illustrated.

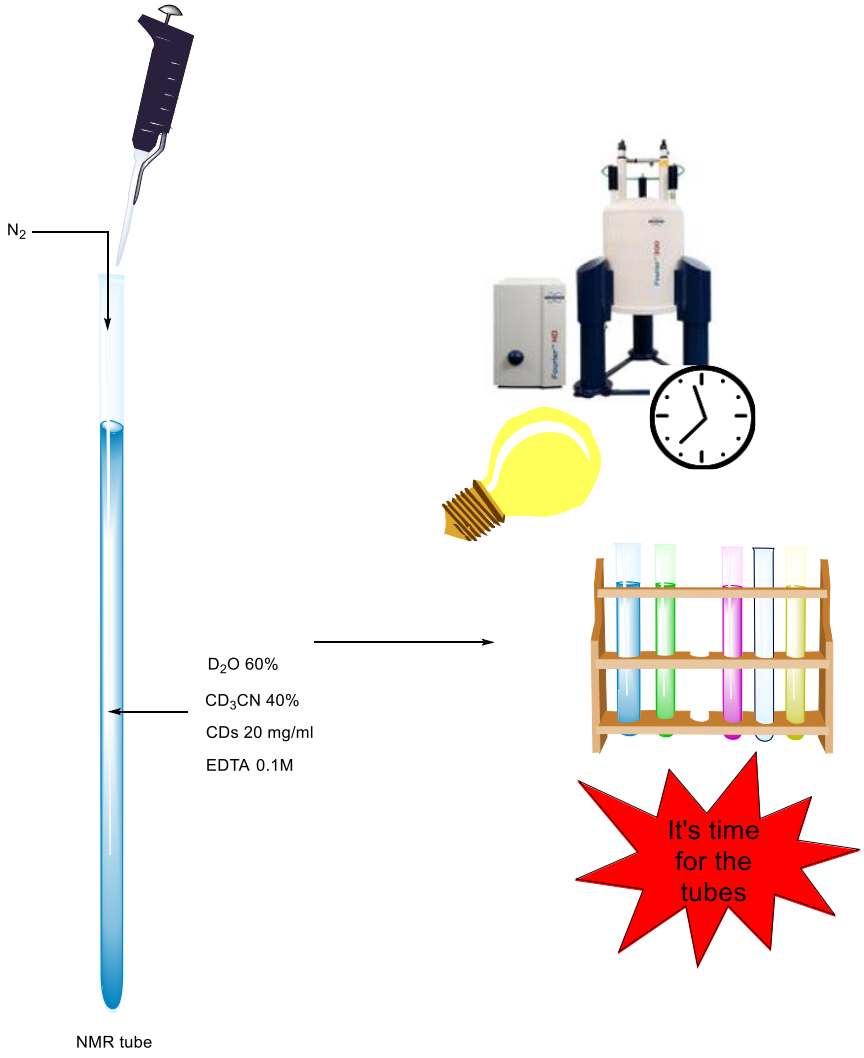


*Figure 77: illustration of how photodeprotection was conducted.*

## 10.3 Electrochemical procedures

This section describes how electrochemical measurements were performed.

### 10.3.1 Reagents

All reagents were analitycal grade and supplied by Sigma Aldrich, and unless otherwise stated, they used as receivd. Four different types of homemade CDs (g-CD, a-CD, g-N-CD, a-N-CD) were investigated. Details on their preparation can be found in the doctoral thesis of Dr. Cailotto Simone (in preparation). DMF was freshly distilled and for electrochemical measurements, tetrabutylammonium perchlorate (TBAP), was employed as supporting elctolyte. Milli-Q water was used when necessary. Ferrocene (Fc) was employed as internal reference system.

### 10.3.2 Instrumentations and electrodes for electrochemical experiments

All voltammetric measurement were perfomed using a CHI 820 potentiostat (CH instrument, USA), along with the CHI instrument software version 8.15. A the three-electrode cell was prepared to carry out voltammetric experiments. The working electrode was glassy carbon disc electrode (GSE), ϕ=3mm, A Platinum spiral was employed as counter electrode and a Ag/AgCl/KCl saturated as reference electrode. The latter was separated from the main solution by a porous septum in order to avoid contamination of DMF solutions with chloride ions leacing from the reference electrode. Figure 78 shows the system used.

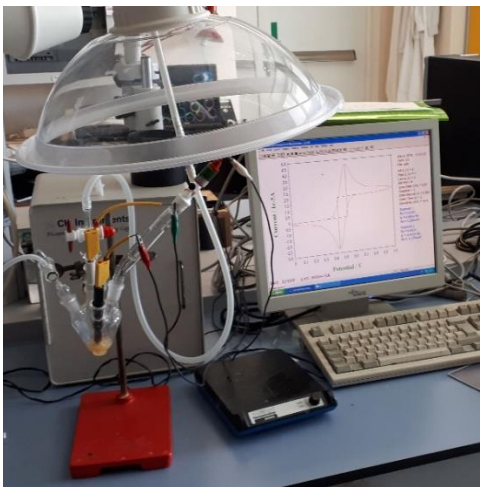

*Figure 78: electrochemical cell used in the measurements.*

### 10.3.4 Sample preparation

The DMF solutions containing CDs were prepared by adding the solvent (5ml) in 200 microliters of(L) water containing a weighted amount of CDs (typically 25mg). This procedure enseured the fully dispersion of CDs in the medium. All measurements were performed under nitrogen atmosphere.

# 11 References


(1) Clark, J. H. Green Chemistry : Challenges and Opportunities. *Green Chem.* **1999**, No. February, 1–8.

(2) Martindale, B. C. M.; Hutton, G. A. M.; Caputo, C. A.; Reisner, E. Solar Hydrogen Production Using Carbon Quantum Dots and a Molecular Nickel Catalyst. *J. Am. Chem. Soc.* **2015**, *137* (18), 6018–6025.

(3) Hutton, G. A. M.; Reuillard, B.; Martindale, B. C. M.; Caputo, C. A.; Lockwood, C. W. J.; Butt, J. N.; Reisner, E. Carbon Dots as Versatile Photosensitizers for Solar-Driven Catalysis with Redox Enzymes. *J. Am. Chem. Soc.* **2016**, *138* (51), 16722–16730.

(4) Cao, L.; Sahu, S.; Anilkumar, P.; Bunker, C. E.; Xu, J.; Fernando, K. A. S.; Wang, P.; Guliants, E. A.; Tackett, K. N.; Sun, Y. P. Carbon Nanoparticles as Visible-Light Photocatalysts for Efficient CO2conversion and Beyond. *J. Am. Chem. Soc.* **2011**, *133* (13), 4754–4757.

(5) Sahu, S.; Liu, Y.; Wang, P.; Bunker, C. E.; Shiral Fernando, K. A.; Lewis, W. K.; Guliants, E. A.; Yang, F.; Wang, J.; Sun, Y.-P. Visible-Light Photoconversion of Carbon Dioxide into Organic Acids in an Aqueous Solution of Carbon Dots. *Langmuir* **2014**, *30* (28), 8631–8636.

(6) Wang, Y.; Hu, A. Carbon Quantum Dots: Synthesis, Properties and Applications. *J. Mater. Chem. C* **2014**, *2* (34), 6921–6939.

(7) Georgakilas, V.; Perman, J. A.; Tucek, J.; Zboril, R. Broad Family of Carbon Nanoallotropes: Classification, Chemistry, and Applications of Fullerenes, Carbon Dots, Nanotubes, Graphene, Nanodiamonds, and Combined Superstructures. *Chem. Rev.* **2015**, *115* (11), 4744–4822.

(8) Cayuela, A.; Soriano, M. L.; Carrillo-Carrión, C.; Valcárcel, M. Semiconductor and Carbon-Based Fluorescent Nanodots: The Need for Consistency. *Chem. Commun.* **2016**, *52* (7), 1311–1326.

(9) Housecroft, C. E.; Sharpe, A. G. *INORGANIC CHEMISTRY*, Third edit.; Pearson Education Limited: London, 2008.

(10) Voznyy, O.; Sutherland, B. R.; Ip, A. H.; Zhitomirsky, D.; Sargent, E. H. Engineering Charge Transport by Heterostructuring Solution-Processed Semiconductors. *Nat. Rev. Mater.* **2017**, *2* (May), 1–10.

(11) Atkin, P.; Paula, J. *Physical Chemistry*, Eighth Edi.; W. H. Freeman and Company 41 Madison Avenue New York, N. 10010, Ed.; New york, 2006.

(12) Bera, D.; Qian, L.; Tseng, T. K.; Holloway, P. H. Quantum Dots and Their Multimodal Applications: A Review. *Materials (Basel).* **2010**, *3* (4), 2260–2345.

(13) Miyauchi, Y. Photoluminescence Studies on Exciton Photophysics in Carbon Nanotubes. *J. Mater. Chem. C* **2013**, *1* (40), 6499–6521.

(14) Hutton, G. A. M.; Martindale, B. C. M.; Reisner, E. Carbon Dots as Photosensitisers for Solar-Driven Catalysis. *Chem. Soc. Rev.* **2017**, *46* (20), 6111–6123.

(15) Song, Y.; Zhu, S.; Zhang, S.; Fu, Y.; Wang, L.; Zhao, X.; Yang, B. Investigation from Chemical Structure to Photoluminescent Mechanism: A Type of Carbon Dots from the Pyrolysis of Citric Acid and an Amine. *J. Mater. Chem. C* **2015**, *3* (23), 5976–5984.

(16) Jelinek, R. *Carbon Quantum Dots Synthesis, Properties and Applications*, First edit.; Springer, Ed.; Springer Nature: Switzerland, 2016.

(17) Zhang, F.; Liu, F.; Wang, C.; Xin, X.; Liu, J.; Guo, S.; Zhang, J. Effect of Lateral Size of Graphene Quantum Dots on Their Properties and Application. *ACS Appl. Mater. Interfaces* **2016**, *8* (3), 2104–2110.

(18) Ding, H.; Yu, S. B.; Wei, J. S.; Xiong, H. M. Full-Color Light-Emitting Carbon Dots with a Surface-State-Controlled Luminescence Mechanism. *ACS Nano* **2016**, *10* (1), 484–491.

(19) Fang, Q.; Dong, Y.; Chen, Y.; Lu, C. H.; Chi, Y.; Yang, H. H.; Yu, T. Luminescence Origin of Carbon Based Dots Obtained from Citric Acid and Amino Group-Containing Molecules. *Carbon N. Y.* **2017**, *118*, 319–326.

(20) Schultz, D. M.; Yoon, T. P. Solar Synthesis: Prospects in Visible Light Photocatalysis. *Science (80-. ).* **2014**, *343* (6174).

(21) Notes, S.; News, E.; Surface, M.; Articles, S. MODERN Civilization Is the Daughter of Coal, for This Offers to Mankind the Solar. *Science (80-. ).* **1912**, *XXXVI* (No), 926.

(22) Boyle, J. Lehninger Principles of Biochemistry (4th Ed.): Nelson, D., and Cox, M. *Biochem. Mol. Biol. Educ.* **2005**, *33* (1), 74–75.

(23) Willkomm, J.; Orchard, K. L.; Reynal, A.; Pastor, E.; Durrant, J. R.; Reisner, E. Dye-Sensitised Semiconductors Modified with Molecular Catalysts for Light-Driven H2production. *Chem. Soc. Rev.* **2016**, *45* (1), 9–23.

(24) Prier, C. K.; Rankic, D. A.; MacMillan, D. W. C. Visible Light Photoredox Catalysis with Transition Metal Complexes: Applications in Organic Synthesis. *Chem. Rev.* **2013**, *113* (7), 5322–5363.

(25) Martindale, B. C. M.; Hutton, G. A. M.; Caputo, C. A.; Prantl, S.; Godin, R.; Durrant, J. R.; Reisner, E. Enhancing Light Absorption and Charge Transfer Efficiency in Carbon Dots through Graphitization and Core Nitrogen Doping. *Angew. Chemie - Int. Ed.* **2017**, *56* (23), 6459–6463.

(26) Schelhaas, M.; Waldmann, H. Protecting Group Strategies in Organic Synthesis. *Angew. Chemie (International Ed. English)* **1996**, *35* (18), 2056–2083.

(27) Falvey, D. E.; Sundararajan, C. Photoremovable Protecting Groups Based on Electron Transfer Chemistry. **2004**, No. 2000, 831–838.

(28) Sundararajan, C.; Falvey, D. E. C-O Bond Fragmentation of 4-Picolyl- and N-Methyl-4-Picolinium Esters Triggered by Photochemical Electron Transfer. *J. Org. Chem.* **2004**, *69* (17), 5547–5554.

(29) Gagne, R. R.; Koval, C. A.; Lisensky, G. C. Ferrocene as an Internal Standard for Electrochemical Measurements. *Inorg. Chem.* **1980**, *19* (9), 2854–2855.

(30) Bard, A. J.; Faulkner. *ELECTROCHEMICAL METHODS Fundamentals and Applications*, Second Edi.; Sons, W. &, Ed.; New york, 1944.

(31) Webster, R. D.; Bond, A. M.; Compton, R. G. Voltammetric and EPR Spectroscopic Studies Associated with the Reduction of Pyridine- and Benzene-Substituted *n* -Alkyl Esters and Thioic *S* -Esters in Aprotic Solvents. *J. Phys. Chem.* **1996**, *100* (24), 10288–10297.

(32) Mattiello, L.; Rampazzo, L. Electrochemistry of a Spirolactone. *J. Electroanal. Chem.* **2001**, *507* (1–2), 118–123.

(33) Bonazza, G.; Tartaggia, S.; Toffoli, G.; Polo, F.; Daniele, S. Voltammetric Behaviour of the Anticancer Drug Irinotecan and Its Metabolites in Acetonitrile. Implications for Electrochemical Therapeutic Drug Monitoring. *Electrochim. Acta* **2018**, *289*, 483–493.

(34) C. K. Barnes, K. K. M. *Physical Chemistry of Organic Solvent Systems*, 1973rd ed.; Springer US: London, 1973.

(35) Mustroph, H.; Ernst, S.; Senns, B.; Towns, A. D. Molecular Electronic Spectroscopy: From Often Neglected Fundamental Principles to Limitations of State-of-the-Art Computational Methods. *Color. Technol.* **2015**, *131* (1), 9–26.

(36) Rigodanza, F.; Đorđević, L.; Arcudi, F.; Prato, M. Customizing the Electrochemical Properties of Carbon Nanodots by Using Quinones in Bottom-Up Synthesis. *Angew. Chemie - Int. Ed.* **2018**, *57* (18), 5062–5067.

(37) Bredas, J.-L. Mind the Gap! *Mater. Horiz.* **2014**, *1* (1), 17–19.

(38) Banerjee, A.; Falvey, D. E. Direct Photolysis of Phenacyl Protecting Groups Studied by Laser Flash Photolysis: An Excited State Hydrogen Atom Abstraction Pathway Leads to Formation of Carboxylic Acids and Acetophenone. *J. Am. Chem. Soc.* **1998**, *120* (12), 2965–2966.

(39) Romero, N. A.; Nicewicz, D. A. Organic Photoredox Catalysis. *Chem. Rev.* **2016**, *116* (17), 10075–10166.

(40) Atkins, P. W.; Friedman, R. *Molecular Quantum Mechanics*, Fourth Edi.; Press, O. university, Ed.; Oxford, 2011.

(41) Braslavsky, S. E.; Braun, A. M.; Cassano, A. E.; Emeline, A. V.; Litter, M. I.; Palmisano, L.; Parmon, V. N.; Serpone, N. Glossary of Terms Used in Photocatalysis and Radiation Catalysis (IUPAC Recommendations 2011). *Pure Appl. Chem.* **2011**, *83* (4), 931–1014.

(42) Tti, S. T. International Union of Pure and Applied Chemistry Commission on Electrochemistry * the Absolute Electrode Potential : An Explanatory Note. *Pure Appl. Chem.* **1986**, *58* (7), 955–966.

(43) Faulkner, L. R. Understanding Electrochemistry: Some Distinctive Concepts. *J. Chem. Educ.* **1983**, *60* (4), 262.

(44) Elgrishi, N.; Rountree, K. J.; McCarthy, B. D.; Rountree, E. S.; Eisenhart, T. T.; Dempsey, J. L. A Practical Beginner's Guide to Cyclic Voltammetry. *J. Chem. Educ.* **2018**, *95* (2), 197–206.

(45) Evans, D. H.; O'Connell, K. M.; Petersen, R. A.; Kelly, M. J. Cyclic Voltammetry. *J. Chem. Educ.* **1983**, *60* (4), 290.

(46) Cardona, C. M.; Li, W.; Kaifer, A. E.; Stockdale, D.; Bazan, G. C. Electrochemical Considerations for Determining Absolute Frontier Orbital Energy Levels of Conjugated

Polymers for Solar Cell Applications. *Adv. Mater.* **2011**, *23* (20), 2367–2371.

(47) Connelly, N. G.; Geiger, W. E. Chemical Redox Agents for Organometallic Chemistry. *Chem. Rev.* **1996**, *96* (2), 877–910.

*The end*